ON THE ROLE OF WIND DRIVEN OCEAN DYNAMICS IN TROPICAL ATLANTIC VARIABILITY

A Dissertation

by

MEYRE P. DA SILVA

Submitted to the Office of Graduate Studies of
Texas A&M University
in partial fulfillment of the requirements for the degree of

DOCTOR OF PHILOSOPHY

May 2005

Major Subject: Oceanography

ON THE ROLE OF WIND DRIVEN OCEAN DYNAMICS IN TROPICAL ATLANTIC VARIABILITY

A Dissertation

by

MEYRE P. DA SILVA

Submitted to Texas A&M University
in partial fulfillment of the requirements
for the degree of

DOCTOR OF PHILOSOPHY

Approved as to style and content by:

Ping Chang (Chair of Committee)	Benjamin S. Giese (Member)
Gerald R. North (Member)	Alejandro Orsi (Member)
Wilford Gardner (Head of Department)	

May 2005

Major Subject: Oceanography

ABSTRACT

On the Role of Wind Driven Ocean Dynamics
in Tropical Atlantic Variability. (May 2005)
Meyre P. Da Silva, B.S., Fundação Universidade do R. Grande, Brazil;
M.S., Universidade de São Paulo, Brazil
Chair of Advisory Committee: Dr. Ping Chang

The response of the tropical Atlantic Ocean to wind stress forcing on seasonal and interannual time scales is examined using an ocean data assimilation product from the Geophysical Fluid Dynamics Laboratory (GFDL), and an ocean general circulation model which incorporates a three dimensional flux correction technique to correct biases of the mean state of the ocean.

On a seasonal time scale, we investigated the impact of the annual migration of the ITCZ on the exchange pathways of the northern tropical Atlantic. The results indicate that seasonal variation of the zonal slope of the thermal ridge along the boundary between the north equatorial countercurrent and north equatorial current in response to changes in the ITCZ controls, to a large extent, the amount of water participating in the equatorial circulation. These changes can be explained in terms of a simple dynamical model where local Ekman pumping dominates thermocline variation in the western part of the basin, and Rossby wave adjustment comes into play in the eastern basin.

On an interannual time scale, we examined the upper heat budget of the equatorial Atlantic in order to identify the key mechanisms by which wind-driven ocean dynamics control SST variability during the onset and peak phases of the Atlantic zonal mode. It is found that, in contrast with Pacific ENSO, both Bjerknes and Ekman feedbacks act together to force the zonal mode, although their relative importance and dominance depend on season and location.

ACKNOWLEDGEMENTS

I would like to acknowledge the kind financial support I received from Brazil's Consellho Nacional de Desenvolvimento Científico e Técnologico of the Ministry for Science and Technology.

Sincere thanks to my advisor, Dr. Ping Chang, for his invaluable guidance throughout my years of graduate studies at Texas A&M University. I would also like to thank the rest of my committee members, Dr. Benjamin Giese, Dr. Alejandro Orsi, Dr. Gerald North, for their constructive comments and suggestions toward improving my dissertation. The technical assistance from Mark McCann and Dr. Hank Seidel is greatly appreciated.

Finally, I am deeply grateful to my Brazilian and German families for their constant and unconditional love that made my journey in Texas all possible.

TABLE OF CONTENTS

LIST OF FIGURES

FIGURE Page

FIGURE Page

FIGURE Page

LIST OF TABLES

CHAPTER I
INTRODUCTION

1. Current Challenges in Predicting Tropical Atlantic Climate Variability

Recent climate studies have focused on the tropical Pacific and El Ninõ Southern Oscillation (ENSO) related climate predictability due to their wide impact on global climate and also as a result of a more advanced ocean observing system developed during the Tropical Ocean-Global Atmosphere program (TOGA). The success of the TOGA program in the Pacific and the recognition by the Climate Variability and Predictability program (CLIVAR) as to the socio-economic importance of tropical Atlantic variability (TAV) for the surrounding continents have contributed to an increase of both modeling and observational (e.g. PIRATA) research activity in the tropical Atlantic after the end of TOGA in mid 1990s.

However, major aspects of the TAV are still not completely understood. One of the major challenges facing the climate research community is how to reduce large biases of current coupled climate models in order to realistically simulate the annual cycle and mean state of the ocean. Although these large systematic biases exist in both the tropical Pacific and Atlantic, the physical processes controlling seasonal and interannual variability in the tropical Pacific [*Köberle and Philander,* 1994] are quite different. The former is controlled by mixed layer processes, while the latter is controlled by the subsurface memory mechanism *[Neelin et al.,* 1998]. Therefore, ENSO forecasts have been quite successful in spite of existing biases in the annual cycle. Such a reasoning however does not necessarily apply to forecast of SST in the tropical Atlantic, where the SST dynamics controlling the annual cycle and interannual variability

---

This dissertation follows the style of *Journal of Geophysical Research*.

are more similar to each other than in the Pacific [*Philander,* 1990] and are less understood.

Atlantic SST anomalies, unlike those in the Pacific where only dynamic processes are dominant, are controlled by both thermodynamic and dynamic processes, as well as being influenced by other climatic fluctuations such as ENSO and Northern Atlantic Oscillation (NAO) [*Giannini et al.,* 2000; *Seager et al.,* 2000]. The interannual variability in the Atlantic is also much weaker than in the Pacific, and manifests itself as *two dominant modes* of variability with distinctive spatial structure, seasonality and time scale.

The equatorial mode or zonal mode is characterized by equatorial SST anomalies in the eastern Atlantic [e. g. *Zebiak,* 1993] which peaks during boreal summer. Warm/cold anomalies in the equatorial region shift the intertropical convergence zone (ITCZ) south/northward in the eastern part of the tropical Atlantic sector, affecting northern summer monsoon over western Africa. The meridional mode peaks during boreal spring on decadal time scales, and it is characterized by anomalous interhemispheric SST gradient along with a corresponding shift of the ITCZ towards the warmer hemisphere [*Nobre & Shukla,* 1996]. According to *Chang et al.* [2004], the phase locking of these modes to the annual cycle suggests that the processes involved in these modes are closely related to the processes that determine the coupled annual cycle. Thus, to improve the SST forecast in the tropical Atlantic, it seems fundamental to have a better understanding of the processes that control the seasonal cycle.

The seasonal cycle in the tropical Atlantic is characterized by asymmetric conditions relative to the equator in both ocean and atmosphere [*Chang and Philander,* 1994], whose features include: warmest SST to the north of the equator where the ITCZ is located; southerly winds that cross the equator; presence of eastward oceanic current — the North Equatorial Countercurrent (NECC) — between 4^{o}-10^{o} N, which has no counterpart in the Southern Hemisphere. The annual meridional migration of the ITCZ causes considerable

seasonal variation in the tropical Atlantic wind stress which in turn forces the ocean, changing the surface currents and oceanic heat transport [*Philander,* 1990]. On the other hand, the annual march of the ITCZ follows the SST distribution, which in part responds to variability in the regional upwelling [*Mitchell and Wallace,* 1992].

A key aspect of understanding SST variability in the tropical oceans has to do with the understanding of equatorial cold tongue dynamics. Within the upwelling regions along the equator and western coast of Africa mid latitudes thermocline waters return to the surface. They interact with the atmosphere and thus have the potential to affect tropical climate variability. The path followed by subducted waters determines if an anomalous subtropical signal will survive the journey to the equator and thus affect the tropical atmosphere. In turn, tropical variability in itself may affect the pathways of subtropical water. In the framework of the ventilated thermocline theory [*Luyten et al,* 1983] the subtropical/tropical pathways are entirely established by the subduction regions. However, the impact of Ekman suction induced by the ITCZ on the pathways of Northern Hemisphere waters is not addressed. A detailed analysis of the subtropics/tropics exchange pathways and its variability is promising to better understand the local ocean-atmosphere interaction.

The low skill of seasonal climate predictions in the tropical Atlantic is a reflection of our poor understanding of the complex processes controlling the meridional and zonal modes. Much of the previous studies on tropical Atlantic variability have focused on the meridional mode and the controversial role of the ocean in maintaining and/or setting the timescale of this variability. Some investigators argue for the importance of ocean dynamics through changes in heat content, heat transport and Ekman dynamics [*Huang and Shukla,* 1997; *Xie,* 1999; *Chang et al.,* 2001]. Others have dismissed any active role for the ocean *[Dommenget and Latif*, 2000; *Seager et al*., 2001].

There is no consensus about the mechanism responsible for generating the equatorial mode either. Traditionally, this mode is regarded as akin to ENSO in the sense that the air-sea feedbacks are governed by the Bjerknes mechanism [*Bjerknes,* 1969], in which the scale and amplitude of the SST anomalies are dependent upon thermocline displacement. Although both modeling [*Zebiak,* 1993; *Delecluse et al.,* 1994] and observational [*Servain and Arnault,* 1995, *Servain et al.,* 2000] studies support this notion, they also suggest that in the Atlantic the Bjerknes feedback is weaker than the Pacific counterpart and can not explain the total SST variability at the equator. Recent investigations based on in situ data [*Vauclair and Penhoat,* 2001] and model results [*Cabosnarvaez et al.,* 2002] suggest that interannual variability in the equatorial region might be generated with or without any subsurface ocean involvement.

The lack of understanding on the predictable dynamics of TAV hinder progress in current seasonal predictions of tropical Atlantic SST, that still rely on prediction given by persistence forecast. Thus, studying the processes that control the tropical Atlantic circulation and its variability at seasonal to interannual time scales is crucial to advance regional climate prediction.

2. Objectives

This investigation focuses on the adjustment processes of the tropical Atlantic Ocean in response to wind stress forcing. The first part addresses the response of the northern tropical Atlantic to seasonal changes of the wind stress; in the second part we study the dynamical mechanism by which surface winds regulate SST interannual variability in the equatorial region.

The specifics objectives are:

1. To diagnose the sensitivity of the relation between the tropical/subtropical pathways and seasonal changes in the wind stress caused

by seasonal variation in the ITCZ, in particular how the exchange process between the tropics and subtropics is affected by seasonality;

2. To determine the dominant processes that control SST variability in the equatorial Atlantic, with emphasis in establishing the dominant oceanic process at work during the onset and peak phases of the Atlantic zonal mode.

3. Methodology and Hypotheses

The spatial and temporal coverage of existing observations in the tropical Atlantic are inadequate to address these problems. Thus this study relies on output from OGCMs. Furthermore, to reduce deficiencies in the model physics we use in the first part of this study a global ocean data assimilation (ODA) product.

The combination of an ocean dynamical model with observational data is a relatively new procedure necessary to provide a more realistic estimation of the ocean state at any given time. As an example of model improvement by data assimilation procedure, Figure 1.1 shows an annual mean section of zonal velocity and temperature at 28^{o}W with (lower panel) and without data assimilation (upper panel). In general agreement with the observation [e. g. *Schott et. al.,* 1998], both simulation and data assimilation experiments present a well developed EUC with maximum eastward velocities higher than 70 cm/s. However, the EUC in the simulation run is clearly too shallow and the upper thermocline is too deep and diffuse. The data assimilation remedies these unrealistic features, making the modeled circulation and temperature structure more in line with observations. In Chapter III the performance of the ODA is further examined by validating against observations.

A realistic modeled circulation and thermal structure are important to address the first part of this study which deals with changes in thermocline circulation driven by the seasonal changes in the winds. Although it is well

known that the equatorial thermocline in the Atlantic Ocean is mostly supplied from the southern subtropics [*Metcalf and Stalcup,* 1967], this study focuses on the northern hemisphere because it is there that water pathways are likely to be strongly affected by seasonality [*Hazeleger, 2003*; *Lazar et al.,* 2002].

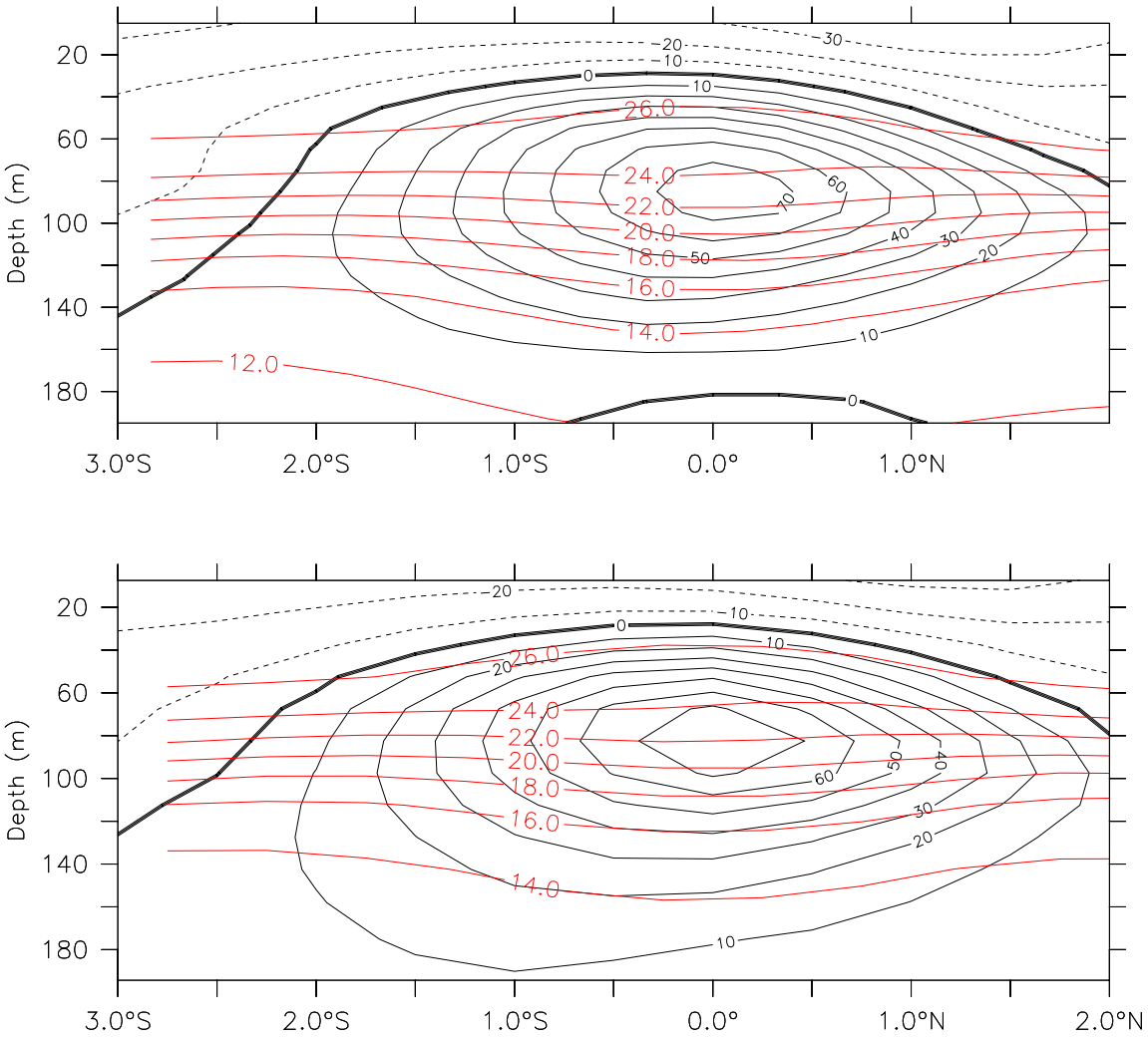

Fig. 1.1. Annual mean zonal velocity component (in cm/s) in black and temperature (in ^{o}C) in red at 28^{o}W with (lower panel) and without data assimilation (upper panel).

The working hypothesis is that in the northern tropical Atlantic the subtropical/tropical pathways are affected by seasonal variation in the circulation, which also affects the amount of subtropical water participating in the equatorial circulation. The problem is approached by first identifying the relevant seasonal changes in the circulation associated with changes in the winds. Second, a simple diagnostic model is used to study the physical mechanism involved in these changes. Finally, a Lagrangian analysis is applied to investigate how the seasonal changes in the circulation affect the subtropical/tropical pathways.

In the second part a three dimensional flux correction procedure developed by *Seidel et al.* [2005a] is used to correct biases of the mean state of the ocean, which is known to be flawed in the current generation of OGCMs. The flux corrected model can be regarded as an ``anomaly'' general circulation model which can be used to study fluctuations around a realistic annual cycle. This seems a reasonable choice to address the second objective of this study which deals with interannual variability

Atlantic interannual SST variability is most prominent in the equatorial region. The zonal mode has been regarded as El Niño like because of the apparent similarities between the Atlantic equatorial warming and the ENSO warm phase [*Merle,* 1980; *Hisard,* 1980]. However, there are also some fundamental differences between these two phenomena. Whereas the Pacific ENSO strongly relies on subsurface temperature changes induced by thermocline variability [e.g. *Philander,* 1990], not all events in the equatorial Atlantic are preceded by a subsurface signal [*Carton and Huang,* 1994]. There is also intriguing difference in seasonality between ENSO and the Atlantic zonal mode; the former is phase-locked to the boreal winter, whereas the latter is phase-locked to the summer boreal.

These differences make one wonder whether or not the Bjerknes feedback indeed is the main underlying mechanism responsible for the Atlantic zonal mode; or whether other mechanism may be involved. This issue is

explored by diagnosing the mixed layer heat budget of a set of model experiments, each with different surface forcing field. It will be argued that both mechanisms, Bjerknes and Ekman feedbacks, are important for the zonal mode of variability even though the relative importance of the two processes can be different in different regions.

We start by accessing the statistical characteristic of simulated zonal mode and comparing them with observation. Then, a detailed analysis of the upper ocean heat budget is performed in order to quantify the relative importance of the processes that determine the SST variation and how their relative magnitudes change with the season. In the region between ± 15^{o} the terms in the mixed layer temperature equation will be determined as outlined in Appendix A. Variance and regression analyses of monthly SST anomalies and the mixed layer heat flux terms will be performed to quantify the relative contribution of different processes to the SST variability. The same statistical analyses will be applied to the monthly anomalies of the mixed layer heat flux terms, SST divided into boreal spring (MAM) and summer (JJA), so that those processes dominant in each season can be identified. In order to explore the individual factors contributing to the changes in ocean heat transport the anomalous heat advection terms will be broken into its constituents and carefully analyzed.

CHAPTER II
MODEL AND DATASETS

The ocean general circulation model (OGCM) used in this study is based on the Geophysical Fluid Dynamics Laboratory (GFDL) Modular Ocean Model version 3 (MOM3) [*Pacanowski,* 1999]. Two configurations of this model is utilized. The first incorporates a data assimilation procedure, while the second is without assimilation but uses a three dimensional flux correction procedure developed by *Seidel et al.* [2005a].

1. The Ocean Assimilation System

The results presented in Chapter III are based on the ODA analysis carried out at the Geophysical Fluid Dynamics Laboratory [*Galanti et al.*, 2003]. The Ocean Data Assimilation system consists of three components: a quality controlled observational dataset, a statistical interpolation algorithm and a numerical ocean model.

Surface and subsurface temperature data incorporated into the ocean model were taken from the World Ocean data Bank-94 [*Levitus and Boyer* 1994], the Global Temperature and Salinity Profile Project and TOGA/TAO moorings. Additional data from Global SST datasets were provided by the National Center for Environmental Prediction (NCEP). Quality control checks included: a basin dependent range check for temperatures, standard deviation checks, and gravitational stability checks. The univariate variational optimal interpolation scheme developed by *Derber and Rosati* [1989] was used to assimilate the observed data into the numerical model.

The model domain covers the global ocean basin from 78^{o}S to 65^{o}N, with a uniform zonal resolution of 1^{o}. The meridional resolution is 1/3^{o} between 10^{o}S - 10^{o}N, and gradually increases to 1^{o} poleward of ±20^{o}. In the vertical, the model

has 40 levels with a constant 10 m resolution in the upper 210m. For horizontal mixing of momentum and tracers the model employed a *Smagorinsky* [1993] non-linear scheme and a *Gent and McWilliams* [1990] lateral tracer diffusivity scheme. In the vertical, a non-local K-Profile Parameterization (KPP) scheme was used together with a *Bryan and Lewis* [1979] tracer mixing scheme. The model was forced with climatological surface wind stresses derived from NASA/DAO/SSMI analysis superimposed on which were daily wind stress anomalies from the NCEP Reanalysis for the period from 1980 to 1999. Restoring boundary conditions to both weekly Reynolds OISST product and Levitus salinity were used at the ocean surface.

2. The 3-d Flux Corrected Model

The 3-d flux corrected model has the same integration domain than the assimilation model, except that it has a lower horizontal and vertical resolution in order to cope with high computational demands. The zonal resolution is 1.5^o and the meridional resolution is 0.5^o in the deep tropics ($\pm 10^o$) increasing to 1.5^o poleward of $\pm 20^o$. This model has 25 vertical layers with 15m resolution in the upper 150m. The parameterizations are kept the same as those used with the higher resolution version as well as the one hour time step.

The three dimensional flux-correction is applied to maintain the climatological temperature and salinity fields in the lower resolution model identical to the climatology of the ODA. It is implicit here that the climatology of the ODA is a good representation of the observed climatology. The method to calculate the correction is summarized in the following (for more detail see *Seidel et al.,* 2004). At every timestep and model grid point the correction is calculated as:

$$Q_T = \gamma (T_m - T_{am}),$$

$$Q_S = \gamma (S_m - S_{am}),$$

where Q_T and Q_S are the fluxes of temperature and salinity, respectively; T_m and S_m are the temperature and salinity fields from the model; T_{am} and S_{am} are the temperature and salinity fields from the seasonal cycle of the ODA; and γ is the damping time scale, a value of 30 days has been used. Then, the model is integrated again and the seasonally varying values of the above flux correction are applied to temperature and salinity equations as a specified flux forcing throughout the computational domain.

The results presented in Chapter IV are based on experiments carried out by Seidel at Texas A&M University using the lower resolution version of MOM3 with the 3-d flux correction method. Two experiments are analyzed: 1) The Control Experiment (CEXP) uses the same wind forcing as the ODA with a 30 days restoring timescale to the observed SST, which is longer than the 5 days used in the ODA; 2) in the second experiment the surface heat damping was set to zero, so the only forcing to the ocean is the wind stress, which is the same daily-wind product used in the CEXP. The wind only experiment (WEXP) is designed to examine the relative importance of the wind-driven ocean dynamics in generating SST interannual variability in the equatorial region.

3. Observational Datasets

The available observations in the tropical Atlantic are too scarce to readily compare with the simulated fields. In the future, the Pilot Research Moored Array in the Tropical Atlantic (PIRATA) project along with other observational programs will greatly improve the data coverage in the region. But at present, the available time series from the PIRATA buoys cover just the period from the end of 1997 up to the present. In order to evaluate the models performance over longer time periods, the PIRATA time series were combined with estimates and measurements from earlier observational studies (see page 16) and datasets.

In the first part of this work PIRATA time series and XBT data compiled by *White* [1995] are combined to evaluate the performance of the ODA product in simulating the tropical Atlantic circulation. In the second part the ODA is treated as quasi-observation against which the output fields from the CEXP and WEXP are verified.

CHAPTER III
SEASONAL CYCLE*

1. Introduction

In the Ekman convergence region in the mid latitudes surface waters are subducted into the thermocline. After subduction they move equatorward predominantly along isopycnals, and at the equator one part of these waters is incorporated into the Equatorial Undercurrent (EUC). The waters of the EUC are characterized by a salinity maximum, and are referred as the subtropical underwater (STUW) [*O'Connor*, 2002]. In the Atlantic the EUC is fed mainly by waters from the southern subtropics [*Metcalf and Stalcup*, 1967], an asymmetry caused by the interaction between the wind-driven gyres and the meridional overturning circulation (MOC) [*Jochum and Malanotte-Rizzoli*, 2001; *Fratantoni et al.,* 2000].

Bryden and Brady [1985] provided evidence that water returning to the surface in the equatorial region is also predominantly along isopycnals, implying that the density structure of the equatorial thermocline must be determined in analogy with the midlatitude thermocline. Inspired by this result *Pedlosky* [1987] extended the concept of ventilated thermocline of extratropics to tropics.

Following Pedlosky's work, numerical and analytical models have been used to study the processes that control the tropical/subtropical water exchange, and identify the pathways of this exchange. Focus has been given primarily to the Pacific Ocean [*McCreary and Lu,* 1994; *Liu,* 1994; *Liu et al.,* 1994; *Liu and Philander,* 1995; *Lu and McCreary,* 1995; *Rothstein et al.,* 1998 and recently to the Atlantic Ocean [e. g. *Harper,* 2000*; Malanotte-Rizzoli et al,* 2000]. The results of these studies emphasize the link between the Equatorial Undercurrent

(EUC) and the subtropical thermocline, providing basic support to Pedlosky's theory. However, the use of models with more complete dynamics and realistic wind forcing in more recent studies has produced conflicting results.

At the heart of the controversy is a subject not considered in Pedlosky's theoretical work, that is, the impact of Ekman suction induced by the ITCZ on the pathways of waters from the Northern Hemisphere. Does the ITCZ act as a barrier to interior exchange water between the equator and northern subtropics, as concluded by *Lu and McCreary* [1995]? Results from a high resolution general circulation model (GCM) [*Harper,* 2000] indicate that there is no total barrier, and ``the thermal structure under the ITCZ merely redirects the pathways of the thermocline ventilation''. Based on a reduced-gravity GCM of the Atlantic Ocean, *Inui et al.* [2002] suggested that on seasonal time scales the Ekman suction region permits interior flow towards the equatorial region during the winter (February) and prevents communication during the summer (August).

Traditionally, numerical studies of the tropical/subtropical pathways are based on annual-mean circulation fields, implying that the water pathways after subduction are not significantly affected by seasonal variation of the circulation. Even when dealing with seasonal variations, it is often assumed that the ocean is in equilibrium with the winds. These assumptions are under question for the northern tropical Atlantic because in this region the pronounced migration of the ITCZ causes considerable seasonal variation in the wind stress curl, and the oceanic adjustment to these wind fluctuations takes at least a few months. In addition to pumping the thermocline up and down, changes in the wind stress curl also cause changes in the thermocline slope and hence in the geostrophic meridional flow. In order to understand the extent to which the ITCZ can have an effect on the water pathways, it is necessary to take into consideration the oceanic response to seasonal changes in the wind stress. Furthermore, a realistic simulation of the thermal structure within the thermocline and its variability is imperative.

Although the equatorial thermocline is mostly supplied from the southern Atlantic, the water pathway in the northern hemisphere is likely to be affected strongly by seasonality [*Hazeleger et al.,* 2003; *Lazar et al.,* 2002]. Thus, in this study we will assess the seasonal variation of the northern tropical Atlantic circulation using a global ocean data assimilation (ODA) product. Our main objective is to diagnose the sensitivity of the relation between the tropical/subtropical pathways and seasonal changes of the wind stress caused by the annual migration of the ITCZ. A description of the ocean assimilation system is given in section 2. In section 3 simulated fields are compared with available observations. The main characteristics of simulated mean and seasonal circulation of the tropical Atlantic Ocean are presented in section 4, as well as details of the oceanic adjustment to fluctuations in the wind stress curl. In section 5 seasonal changes in the tropical/subtropical pathways are diagnosed using a Lagrangian trajectory analysis. Finally, section 6 summarizes the results.

2. Comparison with Observation

The equatorial current system and the low latitude western boundary play an important role in the tropical/subtropical exchange [e. g. *Blanke et al.,* 1989], thus we begin the model validation by examining the transports of the Equatorial Undercurrent (EUC), the North Equatorial Countercurrent (NECC) and the North Brazil Current (NBC). Table 3.1 provides monthly, seasonal and annual mean transport values from the model and available observation from 1980 to 1994, corresponding to the first 15 years of the assimilated experiment. To minimize the differences in sampling size and resolution between data and model, the comparison was performed using, whenever possible, the specific period, section and current definition as given by each observational work listed in Table 3.1.

Table 3.1. Observed and simulated transports of the EUC, the NECC and the NBC in Sverdrups.

Current	Section	Period	Obs.	Assim.
EUC (0m - 26.8σ_θ)	35°W	mean (1990-94)	22.3 Sv	23.0 Sv
		10/90	26.3 Sv	24.2 Sv
		06/91	43.6 Sv	28.7 Sv
		11/92	19.5 Sv	20.3 Sv
		03/94	21.2 Sv	18.8 Sv
NBC (0m - 26.8 σ_θ)	10°S	mean (1992-94)	11.1 Sv	10.1 Sv
		11/92	12.5 Sv	10.8 Sv
		03/94	9.6 Sv	9.5 Sv
	5°S	mean (1990-94)	14.6 Sv	19.3 Sv
		10/90	13.5 Sv	20.3 Sv
		06/91	21.6 Sv	20.2 Sv
		11/92	10.8 Sv	18.9 Sv
		03/94	13.2 Sv	18.0 Sv
Schott et al., 1998 (direct measurements)				
NBC(0 - 300m)	44°W	mean (1990-91)	23.8±4.6 Sv	19.2 Sv
	0° – 1.5°N	mean 12/90 - 02/91	22.0±3.2 Sv	20.6 Sv
		mean 06/90- 08/91	27.8±4.4 Sv	19.5 Sv
Schott et al., 1993 (direct measurements)				
NBC(0 - 800m)	4°N	mean (1989-91)	26.1 Sv	26.6 Sv
		04-05/89	13.0±6.0 Sv	15.1 Sv
Johns et al., 1998 (direct measurements)		07-08/89	36.0±6.0 Sv	40.7 Sv
EUC (≥ 20cm/s)	23°W	mean (1982-84)	15.0 Sv	15.2 Sv
		Std. dev.	7.0 Sv	4.1 Sv
Hisard and Henin, 1987 (direct measurements)				
NECC (≥ 5cm/s)	23°W	Summer 86	13.0 Sv	10.0 Sv
		Summer 87	6.0 Sv	8.4 Sv
	44°W	Fall 84	23.1 Sv	24.0 Sv
Chepurin and Carton, 1997 (indirect estimates)		Winter 91	18.0 Sv	17.4 Sv
NECC (4.5° – 10.5°N)	28°W	mean (1980-85)	9.0 Sv	9.2 Sv
		Fall	12.0 Sv	13.4 Sv
Richardson et al., 1992 (indirect estimates)		Spring	5.0 Sv	4.2 Sv

Overall, the simulated transport values for the EUC and the NECC are in reasonable agreement with observations. Since, in some cases, we are comparing instantaneous measurements with monthly mean output fields, simulated transport variations are weakened by time average. For instance, in

summer 1991 a maximum transport of 43.6Sv was measured at 35°W for the EUC [*Schott et al.,* 1998]. Even though the simulated transport is high (28.7Sv) in this period relative to the other period, it is about 34% lower than observation. This atypical transport value was not used for the mean EUC in Table 3.1.

The NBC transports at 10°S, 5°S, 4°N, and at the western equatorial region along 44°W were computed for comparison with transports estimates based on direct measurements by *Schott et al.,* [op cit.], *Johns et al.,* [1998] and *Schott et al.,* [1993], respectively. While the simulated transport compares well to the observed transport at 10°S and 4°N, the agreement is not completely satisfactory at 5°S and 44°W. The 5°S -simulated transports are up to 8Sv higher than the observed ones (see Table 3.1). Such an overestimate might be due to the additional inflow received by the western boundary current from the east through the South Equatorial Current (SEC), which causes its structure to change from an undercurrent at 10°S to a surface-intensified current at 5°S [*Schott et al.,* 1995]. Whereas the observation only reveals a mean inflow of 3.5Sv from the east between 5° and 10°S, the ODA renders mean SEC inflow of about 9Sv. At 44°W the NBC simulated seasonal cycle is slightly different from the observed cycle found by Schott et al. [1993].In the observation the NBC has high transports (> 26.0Sv) from June to August and two transport minima, one in January (< 20.0Sv) and another in May (≈ 20.0Sv). The simulated NBC shows maximum transports in August (24.6Sv) and one minimum in November (19.0Sv) and another in May (14.4Sv).

Since we are interested in the ocean adjustment to seasonal changes of the wind stress, it is necessary to assure that the variation of the thermocline depth is realistically simulated. The depth of the 20°C isotherm is used as a proxy of the thermocline depth. The simulated depth of the 20°C isotherm was evaluated against two independent datasets: For the period prior to 1994 we compared the model results with observed XBT data compiled by *White* [1995], while from 1997 to 2000 the PIRATA buoys at 15°N - 38°W, 0° - 35°W and 10°S

- 10°W were used. Due to the coarse resolution of the White dataset, a time series of thermocline depth averaged over 54.5°W - 22.5°W and 5°N - 20°N was used to represent the northern tropics. Correspondingly, the southern tropics were represented by a time series averaged over 38.5°W - 11.5°E and 15°S - 0°S.

Figures 3.1a to 3.1e display both observed and simulated time series of thermocline depth. The main difference identified between simulated and observed time series is a mean offset, with the simulated thermocline depth being too shallow in the north and too deep in the south. The agreement between simulated and observed thermocline depth is better in the northern tropics, where the correlation between the two series is 0.82 (Fig. 3.1a). In the southern tropics, the correlation has a lower value of 0.67 (Fig. 3.1b). The simulated and PIRATA time series also display a better agreement for those buoys located on and north of the equator (Figs. 3.1c and 3.1d). In both regions the correlations are higher than 0.80 which is at 99% significance level. By contrast, the 0.37 correlation value between the simulated and PIRATA time series at (10°S, 10°W) is slightly below the 99% significance level (Fig. 3.1e).

Taking into the consideration of the better quality of the observation in the Northern Atlantic, it is perhaps not surprising that the simulated thermocline depth in this region agrees better with observations than the southern Atlantic where the sparsity of data is a major concern. In sum, we conclude that the assimilated product gives a satisfactory overall description of the seasonal variation of the tropical Atlantic Ocean circulation. In the following, we focus on a more detailed analysis of important circulation features based on the assimilated data.

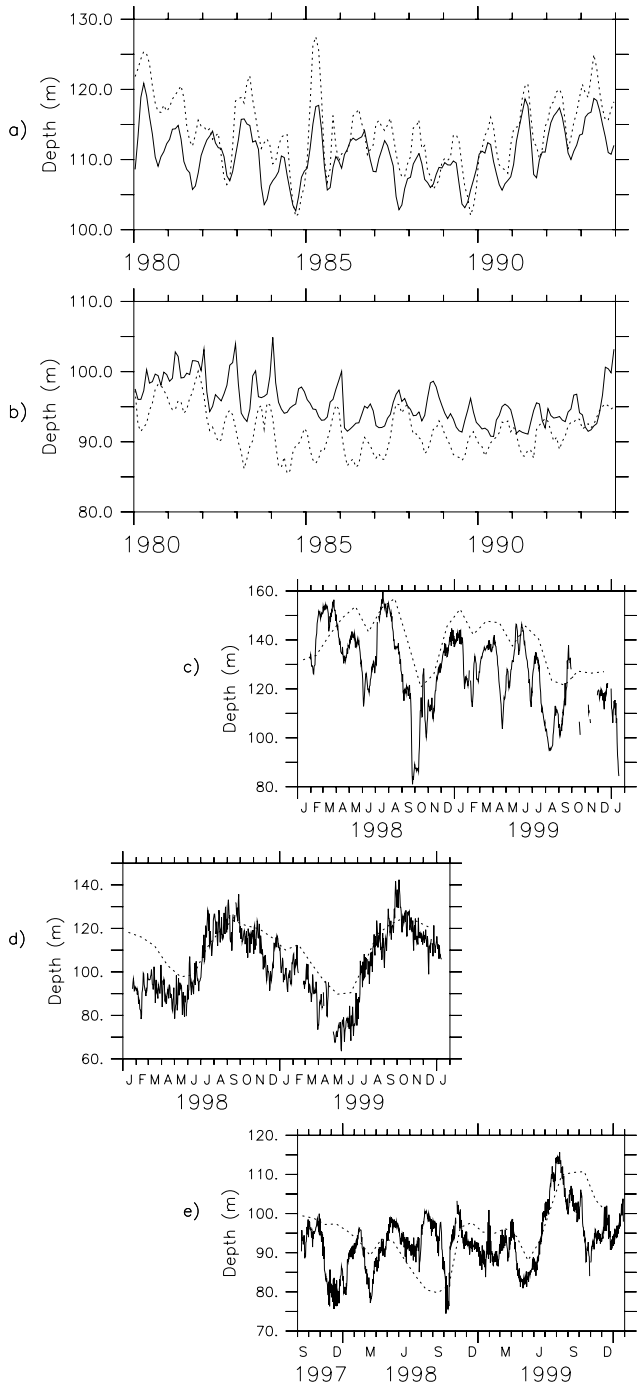

Fig. 3.1. Simulated (dotted) and observed (solid) thermocline depth: (a) northern tropics (54^{o} - 22^{o}W and 5^{o} - 20^{o}N); (b) southern tropics (38^{o} - 11^{o}E and 5^{o}S - 0^{o}N); (c) at 15^{o}N and 38^{o}W; (d) at 0^{o}N and 35^{o}W; (e) at 10^{o}S and 10^{o}W.

3. Simulated Circulation

a. Annual Mean

We first discuss some important features of the mean circulation represented by the ODA experiment. The analysis focuses on the flow below the mixed layer which in this study is defined as the depth at which the density difference from the sea surface is $0.125\sigma_\theta$ [*Monterey and Levitus,* 1997]. The flow in the thermocline will be described in terms of horizontal velocity vectors and streamlines of geostrophic currents projected onto an isopycnal surface which gives a good representation of the seasonal thermocline variation. This analysis provides a view of adiabatic circulation pattern (the cross isopycnal velocity is zero) so that the result can be compared to the theoretical picture of Pedlosky's analytical model. The superposition of streamlines of geostrophic currents to the total velocity, on the other hand, gives an indication of those regions in the model where the flow departs from geostrophy.

The streamlines of geostrophic currents Ψ on an isopycnal surface are given by

$$\Psi = \alpha' P + \Phi', \qquad (3.1)$$

where α' is the specific volume anomaly, P the pressure, and Φ' the geopotential anomaly. A computational method to derive Ψ using equation (3.1) is given in *Kessler* [1999]. The reference level to calculate Ψ was chosen at 500 m. For the tropical Atlantic region, this is approximately the depth of $27.15\sigma_\theta$, which is considered to be the transition layer between thermocline and intermediate waters [*Lux et al.,* 2000], and thus is a logical choice to represent the geostrophic flow within the thermocline.

The upper panel in Figure 3.2 shows contours of Ψ, and current vectors on the 25.0σ_θ surface. Shaded areas indicate the regions of positive Ekman pumping computed according to

$$W_e = curl(\frac{\tau}{f\rho}),$$

where τ is the wind stress used to force the model, f is the Coriolis parameter and ρ is density. The main features seen in the circulation on the 25.0σ_θ surface are representative of the flow in the thermocline. In the interior off-equatorial regions, the flow is predominantly geostrophic as indicated by Fig. 3.2a. In agreement with Pedlosky theory, three types of streamlines can be identified in both hemispheres: 1) streamlines connecting to the subtropical gyres, 2) western boundary streamlines feeding subducted waters to the EUC, and 3) interior streamlines linking the subduction zone directly to the EUC. The theory predicts the existence of bifurcation latitude, such that water reaching the western boundary poleward of it joins the subtropical gyre. If water strikes the western boundary equatorward of the bifurcation latitude, it proceeds to the equator. According to Figure 3.2a the bifurcations are located at about 10^{o}N and 14^{o}S for the northern and southern subtropics, respectively.

An additional type of streamline is seen in Figure 3.2a connecting one part of the outcrop zone to another part without interacting with either the western boundary or the equatorial region. This type of circulation is not considered in Pedlosky's theory, but appears in other recent modeling results [*Lazar et al.,* 2002; *Malanotte-Rizolli et al.,* 2000; *Inui et al.,* 2002]. They occupy the shadow zone described by the well known ventilated theory of *Luyten et al.* [1983], and form a region of closed geostrophic contours which is apparently caused by the upwelling and shoaling of the thermocline driven by Ekman suction. The shoaling of the thermocline results in higher potential vorticity, thus

no net southward flow can go over this potential vorticity barrier, and water can only reach the equator to the west of this region.

Figure 3.2b displays a zonal section of annual mean meridional velocity (cm/s) and potential density (σ_θ) at 10^{o}N. In this region the isopycnals present a dome-like shape which is associated with the cyclonic flow pattern. The isopycnals slope up to the east in the region of southward flow and in the opposite direction in the region of northward flow, consistent with geostrophy. However, there is some evidence of ageostrophic flow in the upper thermocline between 25^o and 20^o W and in the subthermocline close to the African coast. This feature which has been identified as the Guinea dome is in agreement with observation [*Siedler et al.,* 1992]: The vertical axis of the Guinea dome displays a westward deflection with increasing depth. The meridional velocities associated with both southward and northward branches reach values as large as 3cm/s. west of 40^{o}W, a relatively strong vertical shear occurs where the northward surface Ekman drift overlies the southward geostrophic flow. Even further west (at about 60^{o}W) the upper western boundary current, with velocities higher than 10cm/s, is fed largely by subtropical waters that impinge on to the coast of South America and deflect northward.

The total southward meridional transport of subtropical waters crossing 10^o N, between the base of mixed layer and 26.8σ_θ is about 8Sv. Among them, approximately 2.6Sv join the western boundary current and return back to the subtropics, while 3.8Sv are captured by the cyclonic gyre and return to the surface off the coast of West Africa. Thus, only 1.6Sv from the northern subtropics remain to eventually join the EUC. Net northward flows occur in the mixed layer (7.0Sv), and in the subthermocline (3.4Sv) and intermediate (5.6Sv) layers. Thus, the mean warm return flow of the MOC in the ODA is 16Sv which is consistent with values from the literature [e. g. *Schmitz and McCartney,* 1993].

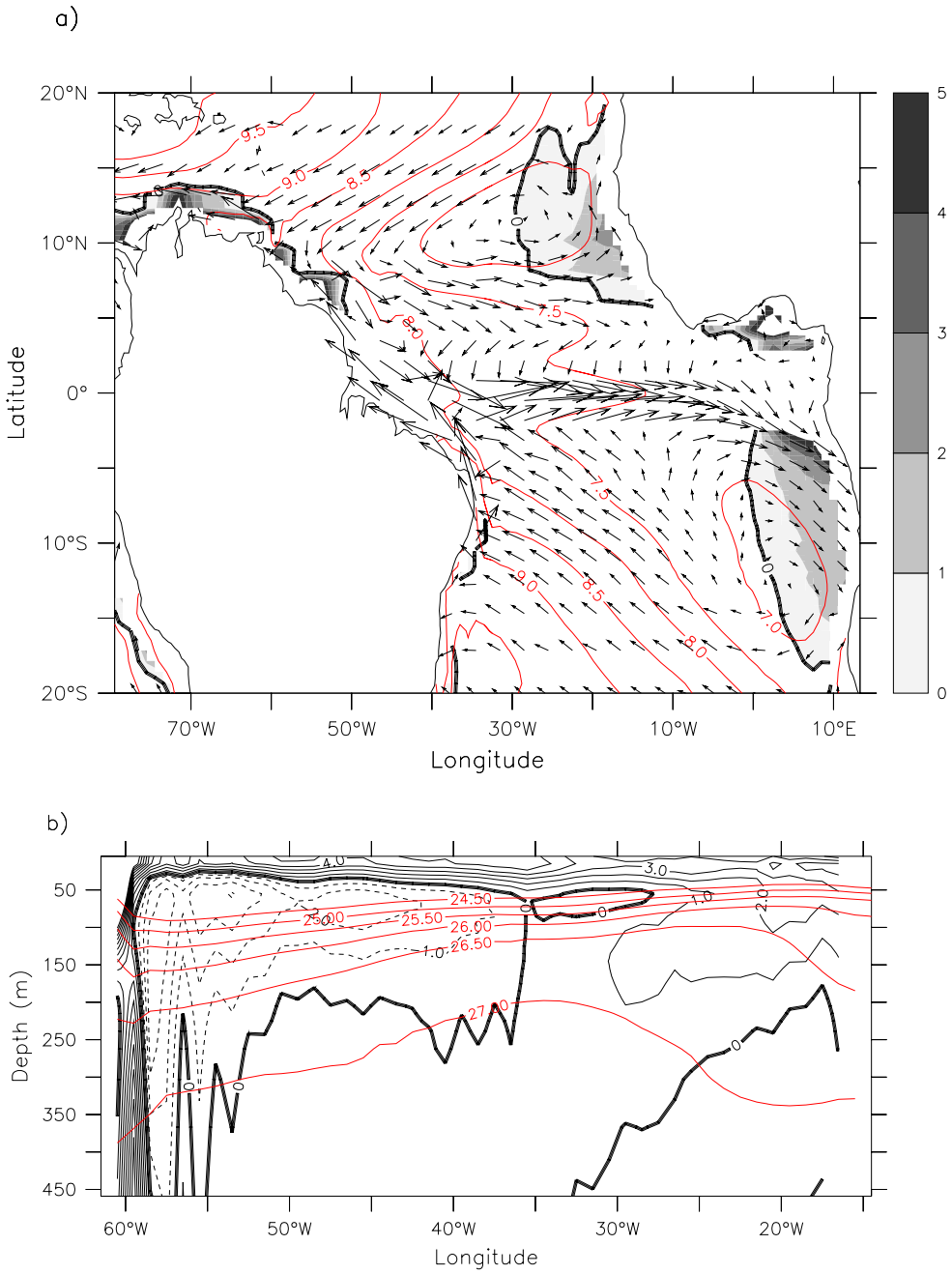

Fig. 3.2. a) Annual mean geostrophic streamlines (in m^2s^{-2}) in red and velocity vectors (in cm/s) on $25.0\sigma_\theta$. Shaded areas indicate regions of Ekman suction (in m/s scaled by 10^6). b) Zonal section of annual mean meridional velocity (in cm/s) and potential density along 10^oN. Solid contours represent northward flow and dashed contours southward flow.

b. Seasonal Circulation

The annual cycle of the Ekman pumping velocity in the northern tropics depends mainly on the location of the ITCZ. During the boreal spring, the ITCZ is situated close to the equator, while during the boreal fall it reaches its extreme northward position at about 10^{o} N. The wind stress curl associated with the annual migration of the ITCZ forces the thermocline to adjust, changing its meridional slope such that the strength of the NECC is altered. The simulated NECC is well developed during boreal fall and diminishes almost completely in the west during spring (see Fig. 3.3 and Table 3.1). This seasonal change in the meridional slope of the thermocline and in the NECC is one of the best examples of oceanic response to atmospheric forcing and has been well studied. In the following, we discuss the relevant oceanic dynamics in response to the ITCZ annual migration with a particular emphasis on the changes in the zonal extent of the Ekman and its effect on the change in the thickness and zonal slope of the thermocline.

Shown in Figure 3.3 is the annual cycle of horizontal velocity and geostrophic streamlines on $25.0\sigma_{\theta}$, shaded areas indicate the regions of positive Ekman suction. The cyclonic gyre in the northern tropics is present throughout the year. With the exception of fall, its center always is located northward of the region of Ekman suction. While the center of the gyre hardly moves meridionally, its western edge expands considerably, from near 38^{o}W in boreal spring to about 50^{o}W during fall and early winter. This implies that as the season progresses from spring to winter the exchange between tropics and northern subtropics becomes more and more confined to the western part of basin.

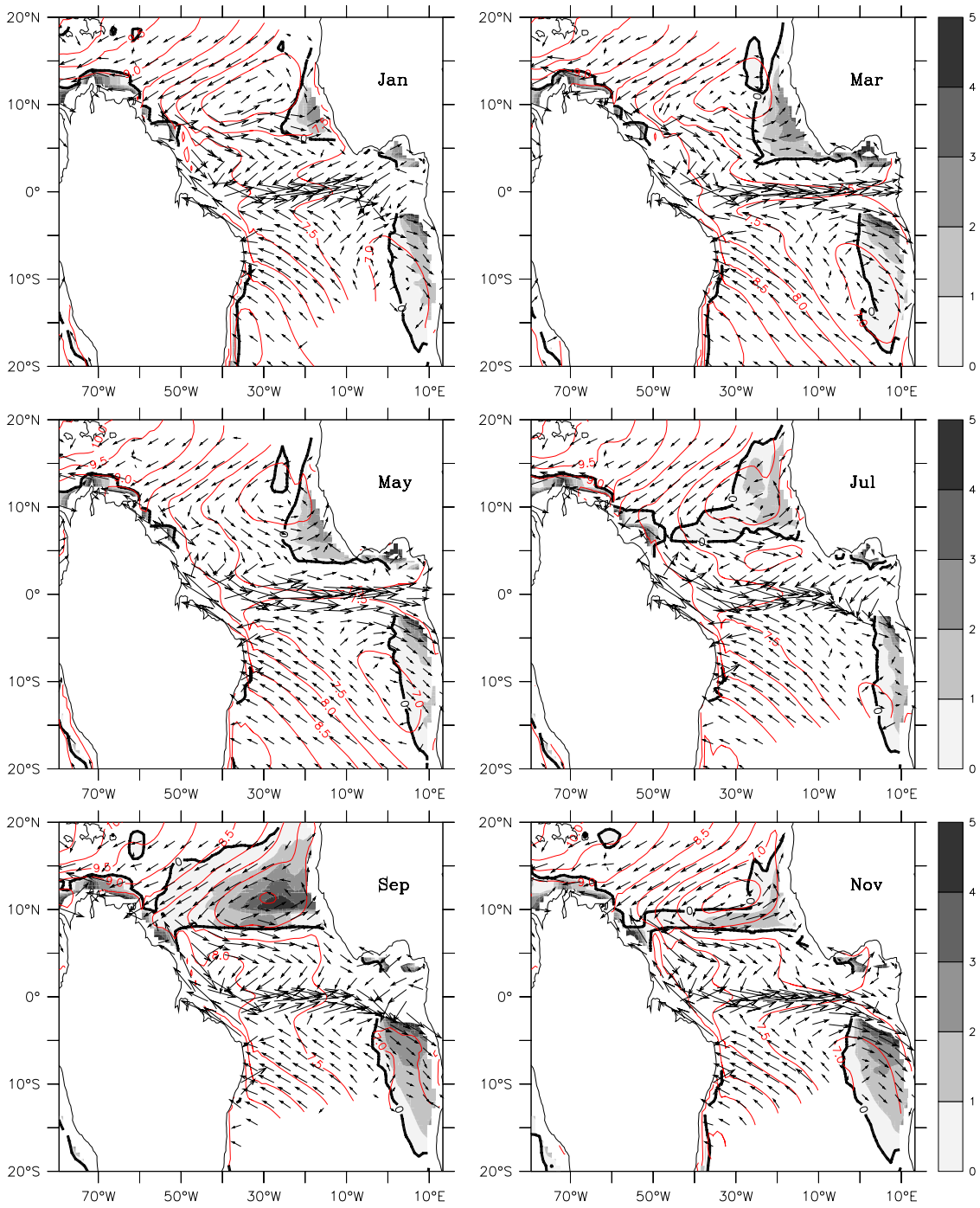

Fig. 3.3. Annual cycle of horizontal velocity vectors (in cm/s) and geostrophic streamlines contours (in $m^2 s^{-2}$) on $25.0\sigma_\theta$. Shaded areas indicate regions of Ekman suction (in m/s scaled by 10^6).

Figure 3.4a illustrates the seasonal changes in the zonal distribution of Ekman pumping velocity along 10^{o}N. The annual mean has been removed at each grid point. The meridional migration of the ITCZ results in changes in the wind stress curl and hence Ekman pumping velocity that are predominantly taking place in the zonal direction. For the first part of the year, Ekman pumping anomalies are positive in the far east (1.0 X 10^{-6}m/s) and negative in the west (< -2.0 X 10^{-6}m/s). After the boreal spring, as the ITCZ retreats to its northern latitudes, an area of positive anomalies appears over the whole basin and reaches its maximum (> 4.0 X 10^{-6}m/s) during boreal fall. A transitional phase can be seen from late boreal fall to early winter when the anomalous Ekman pumping velocities are negative (< -2.0 X 10^{-6}m/s) in the east and positive (≈ 1.0 X 10^{-6}m/s) in the west. Also worth noting is a semi-annual cycle of Ekman pumping close to the eastern boundary.

Simulated seasonal variations in the depth of the 20^{o}C isotherm at 10^{o}N after removing the annual mean are shown in Figure 3.4b. Just as with the Ekman pumping velocity, the displacement of the thermocline along 10^{o}N has a semiannual character in the east while in the central and western part of the basin is dominated by the annual signal. However, the simulated thermocline depth anomalies exhibit westward propagation that is not seen in the annual cycle of the Ekman pumping velocity (Fig. 3.4a). During the late boreal fall and early winter the thermocline is shallower than normal almost over the entire basin, except close to the African coast. At 40^{o}W the thermocline depth anomaly reaches minimum value (< -14m) in December, about three months after the positive Ekman pumping anomaly reaches its maximum. Towards boreal spring the thermocline gradually deepens in the center of the basin and rises in the east. The deepening progresses in the west until July when positive anomalies reach a maximum value of 14m.

Seasonal changes of the southward flow along 10^{o}N are associated with annual variations of the thermocline thickness in the interior of the basin. Figure

3.4c displays the annual cycle of thermocline thickness, defined as the height from the depth of the 20°C isotherm to the base of the mixed layer. Figure 3.5 shows the transport along 10°N which has been decomposed into four components: 1) total southward flow (from 62°W to 14°W), 2) interior southward flow (east of 50°W), 3) western boundary southward flow (west of 50°W), and 4) northward branch of recirculation (northward flow in the eastern part of basin). Each of these components was computed between the base of the mixed layer and $26.8\sigma_\theta$ layer.

The analysis of meridional transports along 10°N yields low transport values (≈ 6Sv) for the total southward flow from February to April and high transports of about 10Sv from July to November. The seasonality of western boundary transports is not very pronounced, and the interior flow takes into account most of the seasonal changes in the total southward flow. The northward flow in the eastern part of the basin which is a good indicator of the strength of the cyclonic gyre shows a low value of about 2Sv in February/March and a high value of almost 6Sv in November/December. Comparing Figs. 3.4c and 3.5, it is clear that, in the interior, the maximum transport corresponds with a period of strong thermocline thickness gradient and thick thermocline layer (about 75 m averaged between 50° and 25°W). The minimum transport is associated with small thermocline thickness (about 35 m averaged between 50° and 25°W) and a weak thermocline thickness gradient.

To examine how changes in the thermocline thickness affect the interior meridional flow, we selected three months that exhibit very distinctive characteristics: 1) March when both interior and western boundary southward flow are weak; 2) August when interior flow has maximum southward transport and the southward flow in the western boundary is relatively weak; and 3) December when the interior southward transport is weak and the western boundary is at its maximum.

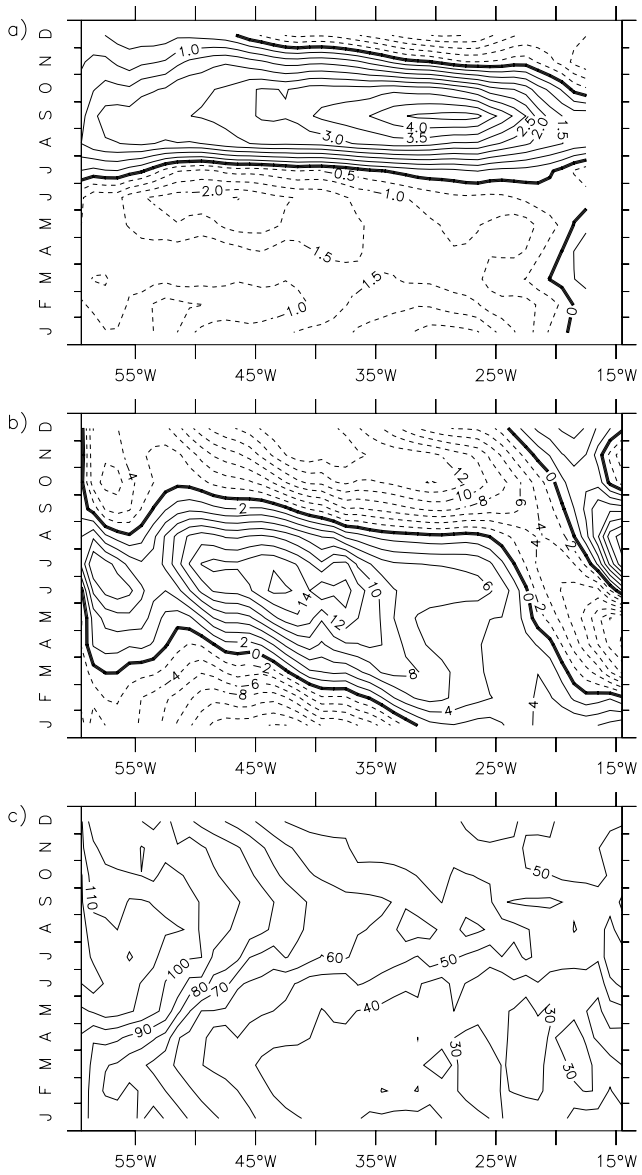

Fig. 3.4. a) Ekman pumping/suction velocity anomalies (in m/s, scaled by 10^6) along 10^oN. Solid contours indicate anomalous Ekman suction, dashed contours anomalous Ekman pumping. b) Thermocline depth anomalies (in m) at 10^oN. Solid contours indicate deep anomalies, dashed contours shallow anomalies. c) Thermocline thickness (in m) at 10^oN

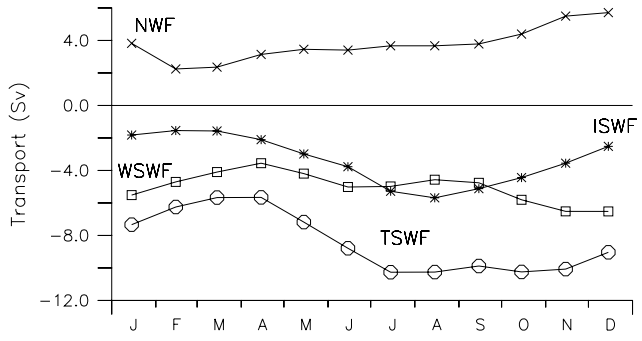

Fig. 3.5. Meridional transport (in Sv) at 10°N decomposed into 4 components: total southward flow (TSWF), interior southward flow (ISWF), northward flow (NWF), and western boundary southward flow (WSWF).

In March (Fig. 3.6a) the mixed layer reaches its maximum depth, and although during this period the thermocline is also deep (Fig. 3.4b); the thickness between the base of the mixed layer and thermocline is more affected by the mixed layer depth, resulting in a relatively thin thermocline layer. Two weak cores of southward flow are seen in the interior, and the northward branch of the recirculation is relatively weak and confined to the east in the upper thermocline.

In August (Fig. 3.6b) the mixed layer is shallow while the thermocline is still deep in the interior of the basin (Fig. 3.4b), the combined effect of these two processes results in a maximum thermocline thickness. The southward flow in the interior intensifies and extends eastward. An eastern boundary current with velocities higher than 5cm/s develops in the upper thermocline.

In December (Fig. 3.6c) the mixed layer begins to deepen, while the thermocline is being upwelled in most part of the basin (Fig. 3.4b). Since the upwelling is not homogeneous across the basin, the thermocline thickness tends to be thinner in the eastern part of basin. The southward flow with maximum

velocities up to 5cm/s is confined to the region west of 40^{o}W, extending westward to the Brazilian coast and forming a southward western boundary current from about 100 to below 300m depth. A diffused and weak (< 3cm/s) northward flow is observed in the eastern half of the basin.

The thermocline thickness as defined here is dependent on both mixed layer and thermocline depth. Thinking in terms of potential vorticity barrier as outlined in *Lu and McCreary* [1995], thickening/thinning of the layer bounded by the base of the mixed layer and the thermocline would permit/restrict interior southward flow. However, an inspection of Figs. 3.6 and 3.4c indicates that the strength of the interior southward flow is controlled by changes in the gradient of the thermocline thickness (pressure gradient) and not by the absolute value of the thermocline thickness. For instance, during August the southward flow extends almost over the entire basin (Fig. 3.6b) which corresponds to a strong zonal pressure gradient in the interior (Fig. 3.4c). In contrast, during March, the zonal gradient is considerably weakened in the interior, which results in a weak southward flow. From Fig. 3.6, it is clear that the seasonal changes in the mixed layer is almost uniform across the interior of the basin, therefore changes in the zonal slope of the thermocline are basically responsible for changes in the pressure gradient and thus the magnitude of the southward flow and westward extension of the cyclonic gyre.

c. Adjustment of Thermocline to Seasonal Winds

The above analysis shows that seasonal variations in the southward flow are directly related to changes in the zonal slope of the thermocline in the interior of the basin. To better understand the processes that control the displacement of the northern tropical thermocline, we use in this section a simple model of thermocline response to the changes in winds based on the quasi-geostrophic approximation:

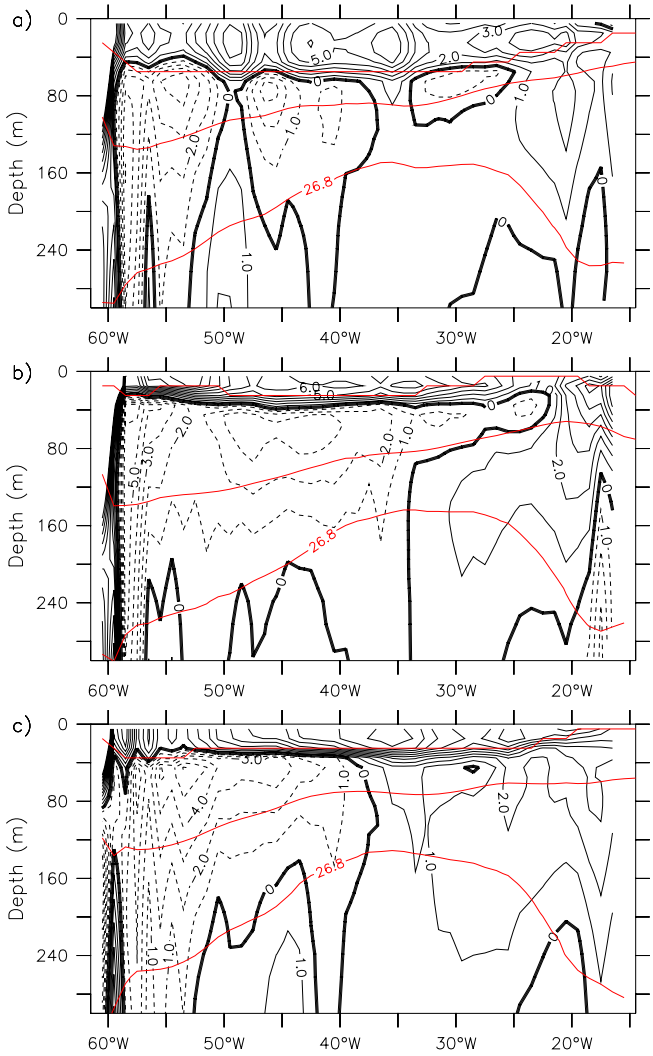

Fig. 3.6. Zonal section of meridional velocity (in cm/s) at 10°N: a) March, b) August, c) December. Red lines indicate the mixed layer depth, the thermocline depth, and the 26.8σ_θ. Dashed lines indicate southward flow.

A B C D

$$\frac{\partial h}{\partial t} - C_r \frac{\partial h}{\partial x} + \gamma h = W_e, \qquad (3.2)$$

where $C_r=\beta g' H_0/f^2$ is the phase speed propagation for non-dispersive long Rossby wave, h and H_0 are the depth and mean depth of the thermocline, β is the derivative of the Coriolis parameter f, γ damping rate, W_e is the Ekman pumping/suction velocity. Solutions to (3.2) consist of a local oceanic response to the Ekman pumping (balance between A and D) and a remote response through non-dispersive long Rossby waves (balance between B + C and D).

Similar or modified versions of the equation (3.2) have commonly been used in observational studies for the Pacific [*Meyers,* 1979*; Kessler and McCreary,* 1990] and for the Atlantic [*Garzoli and Katz,* 1983; *Katz* 1987], as well as for analyzing model output [*Busalachi and Picaut,* 1983]. The results of these earlier studies suggest that in the southern boundary of the NECC, Rossby waves contribute dominantly to the annual cycle of thermocline. Near 10°N, local response to Ekman pumping is the primary source for annual thermocline depth variations.

Following the approach by *Kessler and McCreary* [1990] and *Meyers* [1979], displacements of the thermocline (h) were first calculated using only the Ekman pumping velocity by neglecting the β-effect (remote response) with the boundary condition that $h_b(t) = \int -W_e dt$. The solutions are then compared to those calculated according to (3.2) using Rossby wave speeds (C_r) that give the best fit in phase to the simulated annual cycle of 20°C isotherm at each latitude. A maximum correlation value of 0.9 between the simple model hindcast and the ODA were found at 10°N for C_r value of 16.0cm/s. This best-fit value is higher than the theoretical phase speed of 7.0cm/s given by $C_r=\beta g' H_0/f^2$.

Observational studies also indicate that linear theory underestimates the phase speed of baroclinic Rossby waves [e. g. *Chelton and Schlax,* 1996]. However, for a latitude as low as 10^oN the discrepancy between the theoretical and observation estimated wave speeds is normally much less than a factor of 2. Limitations of the simple approach used here may be responsible for such large difference. When finding a best-fit value for C_r, it was assumed that a single Rossby wave propagates exactly westward along given latitude. In reality, this assumption may not be accurate because the waves that affect the oceanic adjustment at 10^oN may consist of many wave modes of different propagating speed and have a significant meridional group velocity depending on frequency and wavelength [*Philander,* 1990]. In addition, as shown in the previous section (see Fig. 3.3), the forcing has also westward propagation which can contribute to the high value of C_r found by the fitting process.

The thermocline depth at the eastern boundary h_e was taken from the ODA product and used as a boundary condition to (3.2) $h_b(t)=h_e(t)$. In order to reproduce amplitudes comparable with simulation, a simple Newtonian damping term (γh) was added to the vorticity equation (3.2) to take into consideration effect of dissipation. For each latitude, solutions to (3.2) using a damping rate varying from 1/2 to $3year^{-1}$ were calculated. Along 10^oN a decay rate of about $1year^{-1}$ gives the best agreement with simulation. The vorticity equation (3.2) was solved numerically using a leap-frog scheme with a time step Δt=8days and spatial resolution $\Delta x=1^o$. The annual cycle of the Ekman pumping W_e and thermocline displacement at the eastern boundary h_e were represented by six Fourier harmonics.

Figure 3.7 shows thermocline displacements at 10^oN from the assimilated experiment (Fig. 3.7a), and the hindcasted solutions based on (3.2) with all dynamical processes (Fig. 3.7b) and with only Ekman pumping (Fig. 3.7c). The results suggest that the oceanic response at 10^oN can be divided into three parts: western part, interior and eastern part. For the region west of 45^oW, the

local Ekman response closely follows the fully assimilated response, indicating that local Ekman dynamics are most important. In the interior, between 45^{o} and 25^{o}W, solution to (3.2) agrees better with the assimilated thermocline variation. In particular, the westward propagation of the thermocline depth anomalies which dominate in the eastern part of the basin is successfully reproduced. This indicates that long Rossby waves play an essential role in the oceanic adjustment in this region.

East of 25^{o}W the thermocline displacements are also better described by solution to (3.2), which is not a surprise when taking into account the boundary condition imposed. However, whereas in the interior the oceanic response is dominated by seasonal changes in the zonal gradient of the Ekman pumping velocity which is predominantly an annual cycle, in the eastern boundary the response has a semiannual component. This semiannual signal is in part related with the semiannual changes in the wind stress curl near the African coast, and in part with semiannual fluctuations of the thermocline depth at the eastern boundary which can be traced back to the equatorial region. *Yamagata and Iizuka* [1995] found a similar propagation in their model results, which they attributed to intrusion of coastal Kelvin waves excited in the equator due to the semiannual relaxation of the trade winds east of 30^{o}W [*Philander and Pacanowski*, 1986].

Thus the zonal slope of the thermocline at 10^{o}N results from the response to local Ekman pumping in the western part of the basin and wave adjustment in the east. In particular, the thermocline response in the region of meridional southward flow is mainly governed by local process. Since in this region the time rate of change of the thermocline depth is given by the local wind stress curl, the response of the thermocline depth lags the local winds by a quarter of the forcing period [*Philander,* 1990]. As the wind stress curl at 10^{o}N has a strong annual signal, it will take approximately three months for the thermocline depth to respond to the seasonal changes of the wind, which is in

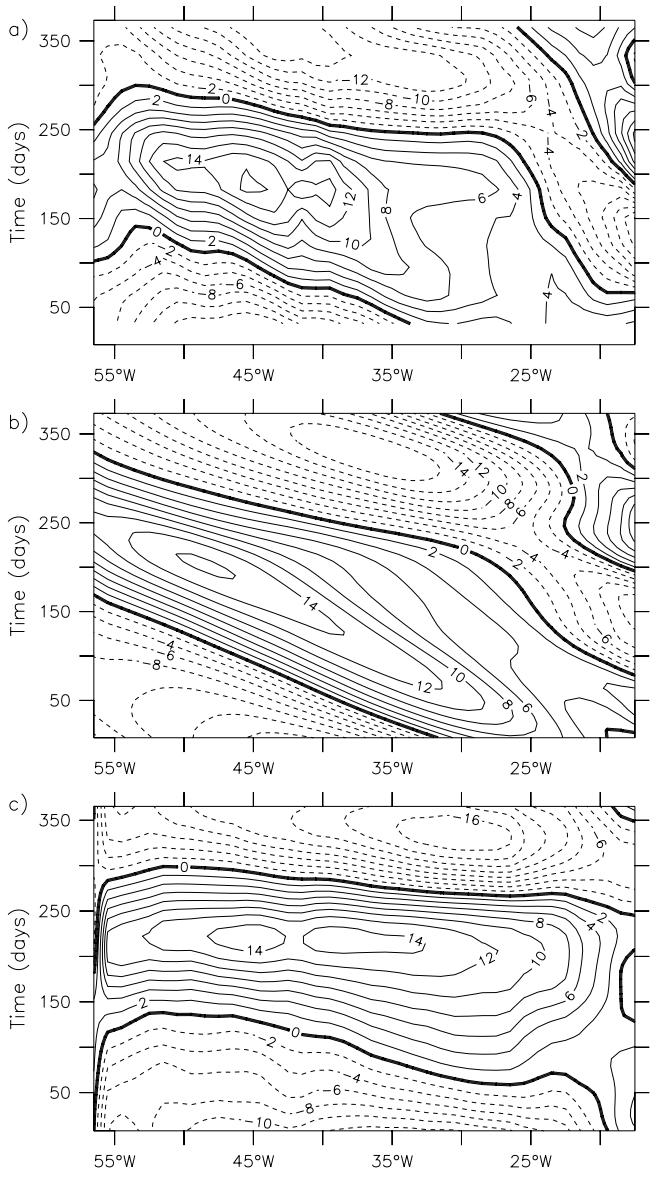

Fig. 3.7. a) Simulated variations in the thermocline depth (in m) at 10^{o}N. Hindcasted thermocline depth anomalies at 10^{o}N using b) equation (3.2), c) Ekman pumping alone.

agreement with the results of the previous section. The absence of Rossby waves in this region may be attributed to the fact that the waves have a significant meridional group velocity due to the existence of the NECC, which

causes wave energy to propagate equatorward and be absorbed by critical layer [*Chang and Philander,* 1988]. Thus, waves excited in the east are difficult to reach the western part of basin.

4. Lagrangian Analysis

The tropical/subtropical water exchange is not modulated only by the strength of the southward meridional transport in the ITCZ region, seasonal variation in the northern cyclonic gyre and the NECC also play an important role. In this section we explore how these changes in the circulation affect the water exchange and pathways between tropics and subtropics by using a Lagrangian trajectory analysis. To track water particle movement along representative isopycnal surfaces under adiabatic assumption, horizontal velocities were projected on the 24.5, 25.0, and 26.0 isopycnal layers. The flow within the mixed layer, where diabatic processes are important, is masked out. For each isopycnal surface particles were released along 12^{o}N and from 60^{o} to 20^{o}W and integrated forward in time using the seasonally varying velocity fields, which were decomposed into the six Fourier harmonics in time to provide continuous time series.

Figures 3.8a, 3.8b and 3.8c display trajectories for particles deployed on the 25.0 isopycnal in March, August and December over 3 years period. In these plots the trajectories color are coded such that the color changes every half year. The Lagrangian diagnostics reveals that the fate and pathway of the trajectories not only depend on the condition when they are released, but also on the development of the tropical circulation in the following months.

In March, the meridional velocity in the interior is weak (Fig. 3.6a), the cyclonic gyre is also weak and confined to the region east of 42^{o}W, retracting further east in the next 2 months (Fig. 3.3). Figure 3.8a illustrates that the flow in the western part of the basin has a southwest component and hence particles

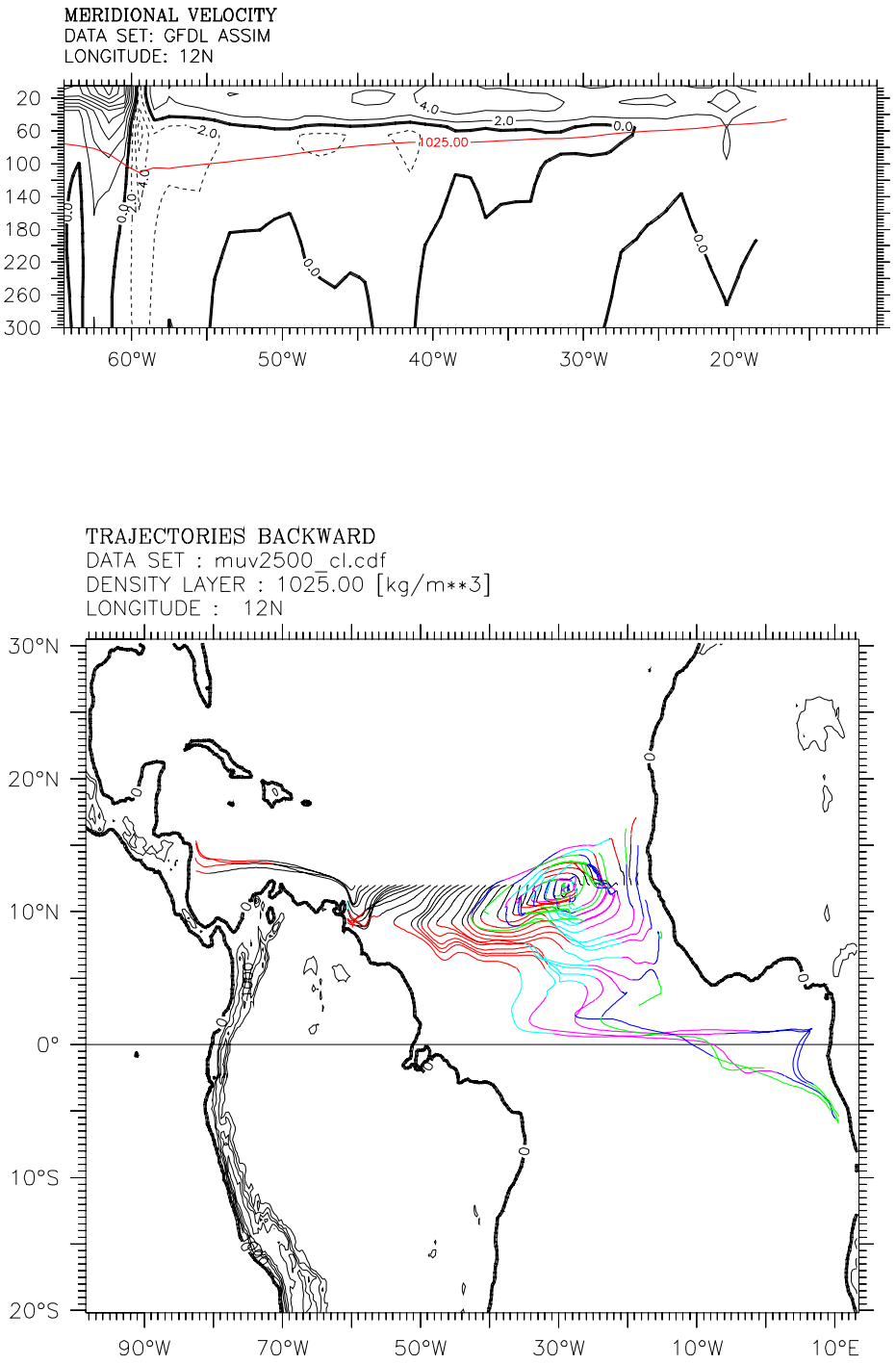

Fig. 3.8a. Lagrangian trajectories for particles released on the 25.0σ_0 along 12°N and from 60° to 20°W over 3-year period. Particles released in March. Trajectory color is coded such that the color changes every half year.

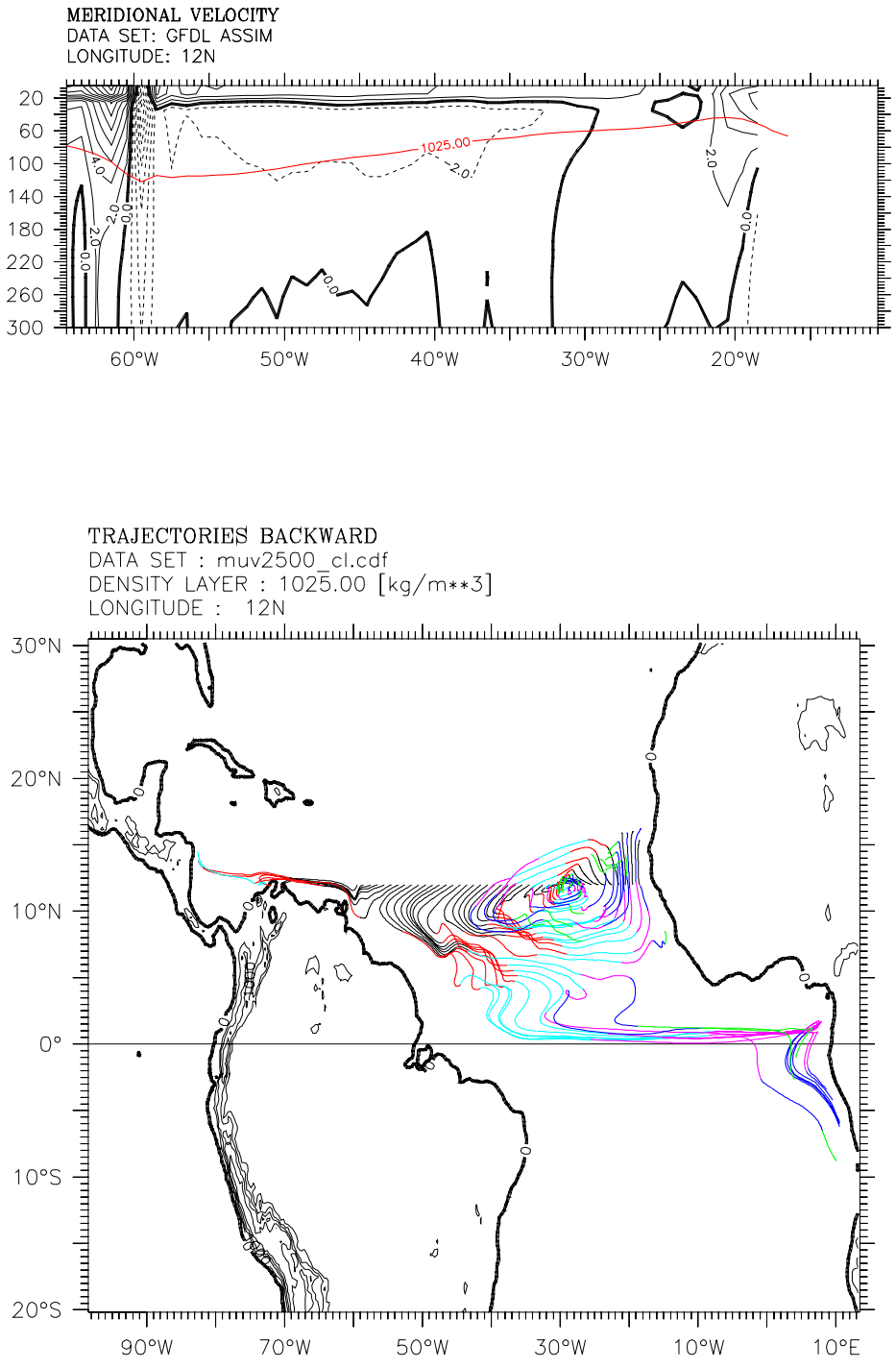

Fig. 3.8b. Same as Figure 3.8a except for particles released in August.

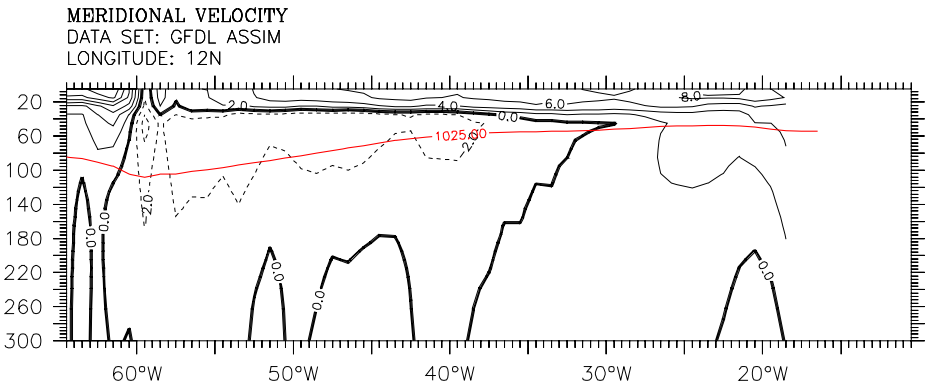

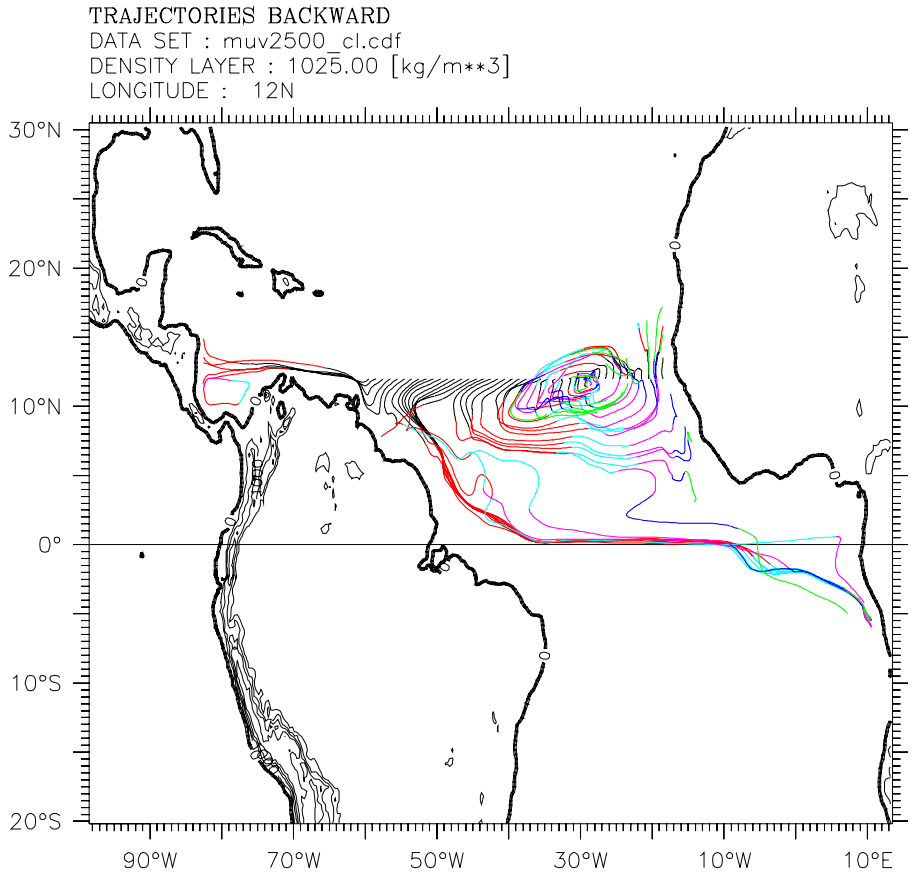

Fig. 3.8c. Same as Figure 3.8a except for particles released in December.

released west of 49°W flow towards the western boundary and deflect north. Particles released in the interior of the basin take 5-6 months to reach 9°N, arriving just when the gyre starts to strengthen and shifts westwards. Thus, in the following 4 months these particles are carried eastward until the gyre weakens again and particles in the southern limit of the gyre escape southward joining the EUC. Only those particles released between 48° and 43°W are able to reach the equator, taking about 15 months to up to 3 years.

The condition of the tropical circulation in August is almost opposite to that in March. The southward flow in the interior of basin strengthens (Fig. 3.6b) and the cyclonic gyre is expanding westward (Fig. 3.3). With the intensification of the gyre from July to December the interior flow south of 10°N has a more pronounced southeasterly component and particles that do not make it to the western boundary are brought eastward (Fig. 3.8b). After 7 months, particles released between 52° and 44°W reach the northern boundary of the NECC (≈ 8°N) just as both the NECC and the cyclonic gyre start to weaken. Thus, they move equatorward along trajectories that have a more southward component, while particles arriving to the same latitudes 6-8 months later are carried further east before joining the EUC. Most of particles reach the equatorial region in about 15 months and only a few take more than 2 years.

Figure 3.8c shows that particles released in December favor the western boundary pathway to reach the equator. This is a result of several factors: First, during the time when the particles are released, the western edge of the cyclonic gyre is in its westernmost position (Fig. 3.3). As a consequence, southward flow is confined to the western part of the basin and has considerable strength close to the western boundary (Fig. 3.6c). Thus particles tend to move very fast southwestward in the beginning. Then just 2 months later the gyre weakens and starts shrinking eastward, which causes the particles released between 54° and 44°W to assume a more southward trajectory. Finally, when these particles arrive at about 7°N, six months later, the NECC is still weak and the cyclonic

gyre is confined to the east, thereby favoring the particles to continue traveling close along the western boundary until they reach the equatorial region. Most particles arrive at the equator in a record time of only 9 months.

The expression ``exchange window'' is used here to indicate the longitudinal band along 12^{o}N where particles released eventually join the equatorial circulation. It is included in the above definition the initial longitude of those particles that after years following the recirculation pathway, when the conditions are favorable, are able to escape and move equatorward. In general, the exchange window has a large longitudinal extension from late boreal summer through winter, reaching its maximum in November when extends from 54^{o} to 43^{o}W. By contrast, the exchange window is restricted to the region between 48^{o} and 43^{o}W in boreal spring.

Flow patterns on different isopycnals may vary along their pathways. Comparison between the 24.5 and 25.0σ_θ (not shown) yields similarity throughout the year for the pathways and the exchange window, except during boreal winter, when the particles released on the 24.5σ_θ take the interior rather than the west boundary pathway to reach the EUC. This difference is related to the fact that the 24.5σ_θ is located above of the southward western boundary current prevalent from late fall to winter, which is responsible for those particles released at 25.0 and 26.0σ_θ to follow the western boundary pathway. With increasing depth the cyclonic gyre extends westward, the NECC disappears, and meridional and zonal velocities weaken. Only a few particles that make it to the equator on the 26.0σ_θ were released in the western edge of the exchange window, favoring more the western boundary pathway to move equatorward and taking a longer time than those released in the layers above.

5. Summary and Conclusions

Based on a state-of-the-art assimilated GFDL run from 1980 - 2000, the seasonal variability of the Northern Tropical Atlantic circulation is investigated. Most of the circulation features revealed by our analysis agrees qualitatively and quantitatively with previous observational and modeling works, except for a few noted differences. Among these differences is the importance of seasonal variation of the circulation in mediating meridional exchange process between the subtropics and equatorial zone in the Northern Tropical Atlantic. While some of the previous modeling studies suggest that the exchange process is determined mainly by the mean circulation and is not affected strongly by its annual cycle, our results suggest that the seasonal change in the Northern Tropical Atlantic Circulation not only can affect the amount of water participating in the equatorial circulation, but also the pathways taken by the subtropical water toward the equator.

The annual migration of the ITCZ causes changes in the wind stress curl that are not homogeneous across the basin and neither is the oceanic response to these changes. The oceanic response to the seasonal changes in wind stress curl can be explained in terms of a simple dynamical model. It is shown that the thermocline displacement along 10^{o}N is mainly controlled by local Ekman pumping in the western part of the basin, while in the east Rossby wave adjustment is also an important part of the oceanic response. This difference between the oceanic responses in the eastern and western sets the thermocline slope in the interior of the basin, which controls, to a large extent the seasonal variation of the southward meridional transport toward the equator. The total southward flow has high transport of more than 9Sv from boreal summer to late fall, when the thermocline slope is well developed. A low transport of less than 6Sv is observed from February to April when the thermocline slope relaxes in the central part of the basin.

According to the Lagrangian analysis, more particles tend to join the EUC when released during the period when the total southward flow is strong. However, the fate of the subducted water depends also on the seasonal variation of the tropical circulation in the period following the release of particles. In particular, seasonal changes in the NECC and in the cyclonic gyre affect directly the destination of a subducted water parcel. These variations also allow exchanges between the cyclonic gyre and interior pathway which are not observed when the time-mean flow is used, and thus the pathways taken by the particles in the seasonal varying field are not only dependent of the subduction region.

While the northern cyclonic gyre is present all year around, both its zonal extent and strength undergo a well noted seasonal variation. In February/March, the gyre is weak (≈2Sv) and confined to the region east of 38^{o}W. In November, with a transport value of about 5Sv, its western edge shifts to approximately 50^{o}W, following the seasonal change in the zonal slope of the thermocline. However, there appears to be no significant meridional movements in the gyre location. During most part of year the gyre is located north of the region of Ekman suction. Although the center of this gyre coincides with the observed cyclonic circulation feature related to the Guinea Dome, its dimension appears to be much larger and more related with counterclockwise flow fields composed of the eastward NECC (upper thermocline) and the westward NEC (see Fig. 4 and 5 *Stramma and Schott,* 1999).

Our results indicate that the role of the cyclonic gyre in the tropical/subtropical pathways is twofold. On the one hand, it prevents particles released east of 42^{o}W from influencing in the equatorial circulation. Although the western edge of gyre moves to east of 38^{o}W during the boreal spring, the meridional velocities in the interior of basin are so weak that particles are not able to move away from the sphere of action of the gyre before it strengthens again. On the other hand, for particles released west of 42^{o}W, the cyclonic gyre

acts to reinforce the communication between tropic/subtropics. When the gyre is strong the flow in its southwest edge is predominantly eastward, hence particles under its area of influence tend to move towards the interior of basin, instead of reaching the western boundary and deflecting north. The subsequent relaxation of the gyre occurs when the particles has entered the NECC. Once entrained into the NECC, the likehood of water particles being recaptured by the recirculation is low. Therefore, an interior pathway will be favored only when particles are released during the strengthening of the gyre (June/July), and a western boundary pathway is favored when the gyre is well developed (November/December).

CHAPTER IV
INTERANNUAL VARIABILITY

1. Introduction

The ocean and atmosphere interact at the interface on a large variety of time scales and thus a large fraction of tropical variability may be attributed to air-sea interaction. The atmosphere forces the upper ocean through thermodynamic and dynamical wind-induced mechanisms. The ocean in turn forces the tropical atmospheric circulation through SST changes. In the equatorial Atlantic, SST changes are caused mainly as a response of the ocean to wind changes [e. g. *Carton et al.,* 1996; *Carton and Zhou,* 1997]. The amplitude and spatial scale of the resultant SST anomalies determine whether and how the atmosphere can feed back onto the ocean.

Two types of ocean-atmosphere coupling may be important in the equatorial region. The first involves interactions between zonal winds stress driven by convection and SST anomalies caused by thermocline displacement. It was first proposed by *Bjerknes* [1969] to explain the Southern Oscillation, and can be described as follow: a relaxation of the westward winds along the equator weaken the eastward slope of thermocline, weakening upwelling in the cold tongue region and generating a warm SST anomaly in the eastern part of the basin. The warm SST anomaly in turn can cause a further relaxation of the winds and further warming. Thus, the ocean dynamics driving the SST anomaly is mean upwelling acting on the anomalous vertical temperature gradient.

The second mechanism, similar to the Bjerknes feedback, is associated with changes in the upwelling induced by the winds. However, in this case it is the anomalous upwelling driven by local Ekman divergence acting on the mean stratification that forces the SST anomalies. This mechanism, referred as Ekman feedback [*Chang and Philander,* 1994], has been used in TAV context as a

possible feedback mechanism for the meridional mode. Appearance of a northward cross-equatorial SST anomaly gradient would develop a northward wind anomaly, since winds tend to converge over the warm SSTs (low pressure anomaly). The cross-equatorial wind anomaly in turn causes surface Ekman divergence and upwelling south of the equator, further intensifying the northward SST anomaly gradient and in turn the northward wind anomaly.

The first well recorded event in the Equatorial Atlantic was the 1963 warm event [*Merle,* 1980; *Hisard,* 1980], whose evolution apparently followed pattern similar to ENSO in the Pacific. The appearance of a warm SST anomaly in the eastern basin during the summer of 1963 was accompanied by relaxation of the trade winds in the western Atlantic. Thus, this phenomenon was named by the above authors as the "Atlantic Niño", and most of the following studies in the tropical Atlantic have regarded the zonal mode as similar to ENSO. Indeed some modeling studies [*Carton and Huang,* 1994; *Delecluse et al.,* 1994; *Chang et al.,* 2000] suggest that the Bjerknes feedback does operate in the equatorial region.

However, *Zebiak's study* [1993], based on observational data of winds and SST for the period 1967-1988 in the Atlantic and 1970-1991 in the Pacific found some noticeable differences between ENSO and the zonal mode. These differences include 1) the correlation between the zonal wind and equatorial SST anomaly is considerably lower and the spatial correlation structure is narrower and displaced further west in the tropical Atlantic than in the Pacific (0.4 vs. 0.7); 2) in the Pacific, the ENSO related SST anomalies in the eastern basin tend to vary out of phase with those in the western basin, the SST anomalies associated with the Atlantic zonal mode tend vary together in all longitudes with nearly equal amplitude; 3) extreme values tend to occur at different times in the two basins: during midyear for the Atlantic, and near the end of the year for the Pacific; 4) east Pacific warm SST anomalies are generally preceded by weak positive anomalies in the western region which sometimes show eastward migration at other times the anomalies appear to migrate westward, contrary to

the Pacific, there is little evidence of systematic anomaly migration in the Atlantic; 5) in the Pacific, the zonal wind anomaly appears to migrate eastward during an ENSO event, there is no migratory component to Atlantic zonal wind stress anomaly.

Zebiak's results further indicate that in central and eastern equatorial Atlantic the anomalous upwelling acting on mean stratification is the dominant forcing of SST, providing a hint for another possible mechanism operating in the zonal mode. However, just recently the Ekman feedback has been considered to explain SST variability on the equator. In a recent study by *Barreiro* [2003], Ekman feedback involving the coupling between surface winds, ocean currents and SST is suggested to be an important mechanism controlling the evolution of SST anomalies in the equatorial and cold tongue regions.

Both Bjerknes and Ekman feedbacks are likely to operate in the equatorial Atlantic. However, the relative importance of these feedbacks for the zonal mode has not been elucidated. In this chapter, we address this issue by diagnosing the mixed layer heat budget in two OGCM experiments, one driven by heat flux and winds and the other forced only by winds. The major oceanic processes controlling SST variability in the equatorial region are identified in light that Ekman and Bjerknes feedbacks involve different dynamical response of the ocean to the winds. This chapter is organized as follows. Section 2 analyzes the characteristics of zonal mode in the model and compares them with those derived from the assimilation experiment. In Section 3 the results of the heat budget analysis are presented and discussed, and Section 4 a summary of main results and conclusions are presented.

2. Comparison of Datasets

In this section we revisit some of Zebiak's dynamically motivated analyses not only as a way to access the characteristics of the zonal mode in

the model and compare with the assimilation, but also as a way to infer if those statistical relationships hold for the period and datasets analyzed here.

Figure 4.1 shows correlation of ATL3-index as defined by Zebiak – the area averaged SST anomaly over 3N-3S, 20W-0 – with SST, and zonal wind stress for ODA, CEXP and WEXP. The correlation patterns in the ODA are similar to those displayed in Zebiak's Figure 2. The SST structure extends across the entire basin and is asymmetric with higher correlation values in the Southern Hemisphere, while the zonal wind stress presents a higher correlation with ATL3 in the western part of the basin. Although the general correlation patterns in the CEXP and WEXP are somewhat similar to the ODA, the SST structure is much more confined to the equatorial zone, being almost symmetric to the equator, and the zonal wind stress structure is displaced more to the center of the basin. The latter two characteristics make the zonal mode in the CEXP and WEXP more similar to the ENSO pattern. Note also that the SST coherence between the central equatorial region and the eastern and western boundaries is lower in the CEXP and WEXP than in the ODA.

Another interesting contrast between equatorial Pacific and Atlantic, as pointed out by *Carton et al.* [1996], is that in the Pacific fluctuations in the depth of the thermocline are strongly correlated with anomalies of SST, while in the Atlantic the correlation is weaker and areas of significant correlation between anomalous thermocline depth and SST are limited to the eastern equatorial zone. In the ODA this difference between the two basins is well reproduced (Fig. 4.2a). Correlation between thermocline depth and SST reaches values higher than 0.6 in the central and 0.8 in the eastern equatorial Pacific, while in the Atlantic the maximum value of 0.4 is basically confined to the eastern basin south of the equator.

In both CEXP and WEXP (Fig. 4.2b left panel) the coupling between surface and subsurface is much stronger than in the ODA. Correlation values higher than 0.6 are found in the eastern as well in the western basin. Here once

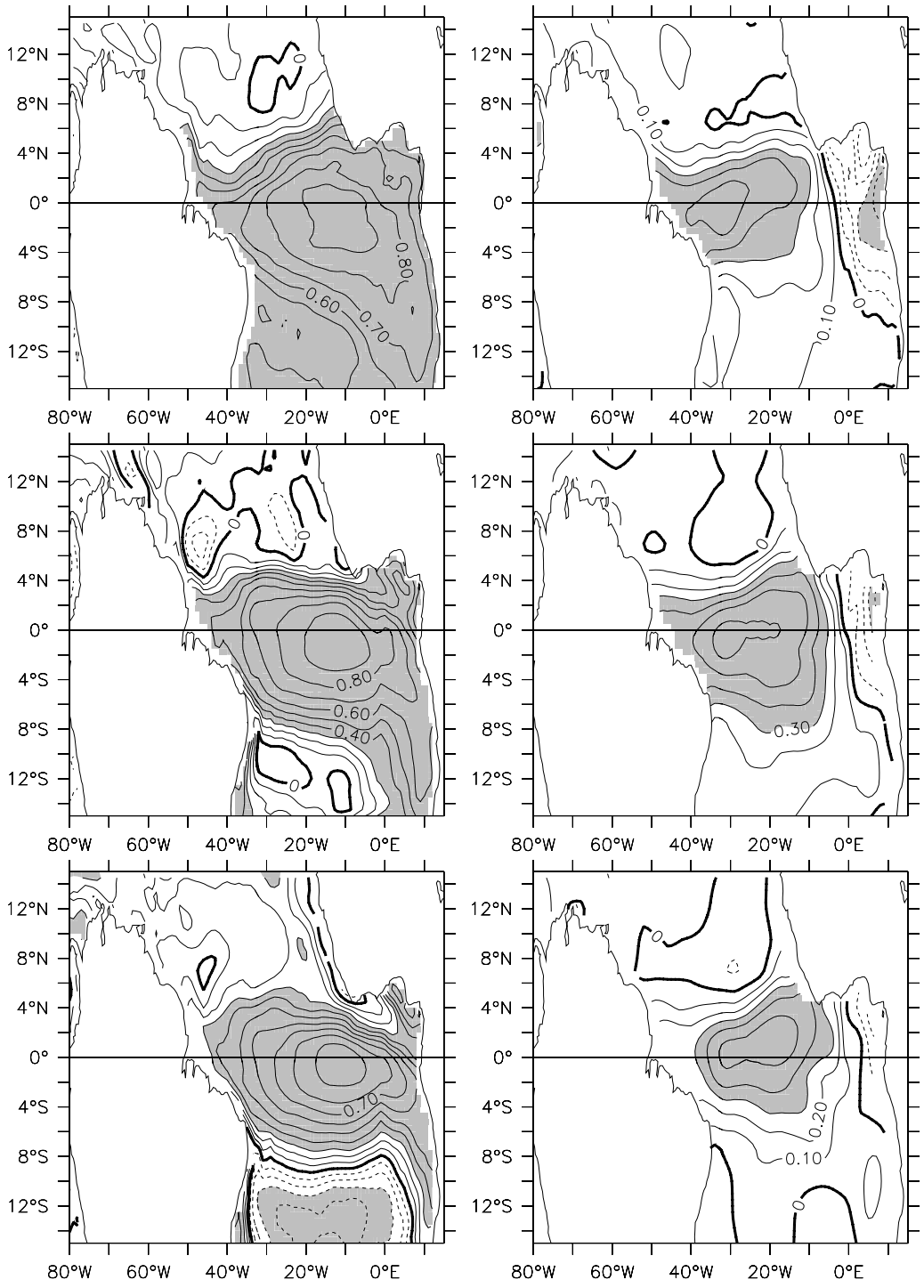

Fig 4.1. Correlation between ATL3 index and SST (left panel) and zonal wind stress (right panel), for ODA (upper panel), CEXP (mid panel) and WEXP (lower panel). Shaded areas denote the 95% significance level.

more the correlation pattern shows greater symmetry about the equator than that in the ODA, and thus tends to resemble more ENSO. However, in all three datasets analyzed here the maximum correlation between Atlantic SST and thermocline depth anomalies occurs at zero lag in the ATL3 region, contrary to the NINO3 region in the Pacific where SST anomalies lag thermocline depth anomalies by 1-3 months (Figs. 4.2a upper panel).

In the ODA as well CEXP and WEXP there are some overall similarities in the SST-wind relationship that agree with the results of Zebiak; this can be interpreted as evidence that Bjerknes feedback does operate in the tropical Atlantic. In the following, correlation between SST and Ekman pumping anomalies at each grid point is used to examine the influence of local Ekman dynamics on the evolution of SST anomalies.

By mass conservation, divergence and convergence of the horizontal Ekman transport, $V_{E,}$ can produce vertical velocity, $W_{E,}$ at the base of the Ekman layer, which can be written as $W_E = \nabla \cdot V_E$. The Ekman transport is calculated from the wind stresses following *Zebiak and Cane* [1987]

$$\rho u_E H = \frac{f\tau_y + \gamma\tau_x}{f^2 + \gamma^2}, \qquad \rho v_E H = \frac{-(f\tau_x + \gamma\tau_y)}{f^2 + \gamma^2}, \tag{4.1}$$

where the subscript E refers to Ekman layer velocities; τ_x and τ_y are the zonal and meridional wind stress components; γ is the damping coefficient set to 0.5day^{-1} as in *Barreiro* [2003] and *Hazeleger* [2003]; f is the Coriolis parameter; ρ is the density; and H is the Ekman layer depth.

Figure 4.3a shows correlation maps of SST and Ekman pumping anomalies (left) and lag-correlation histograms of the same variables averaged

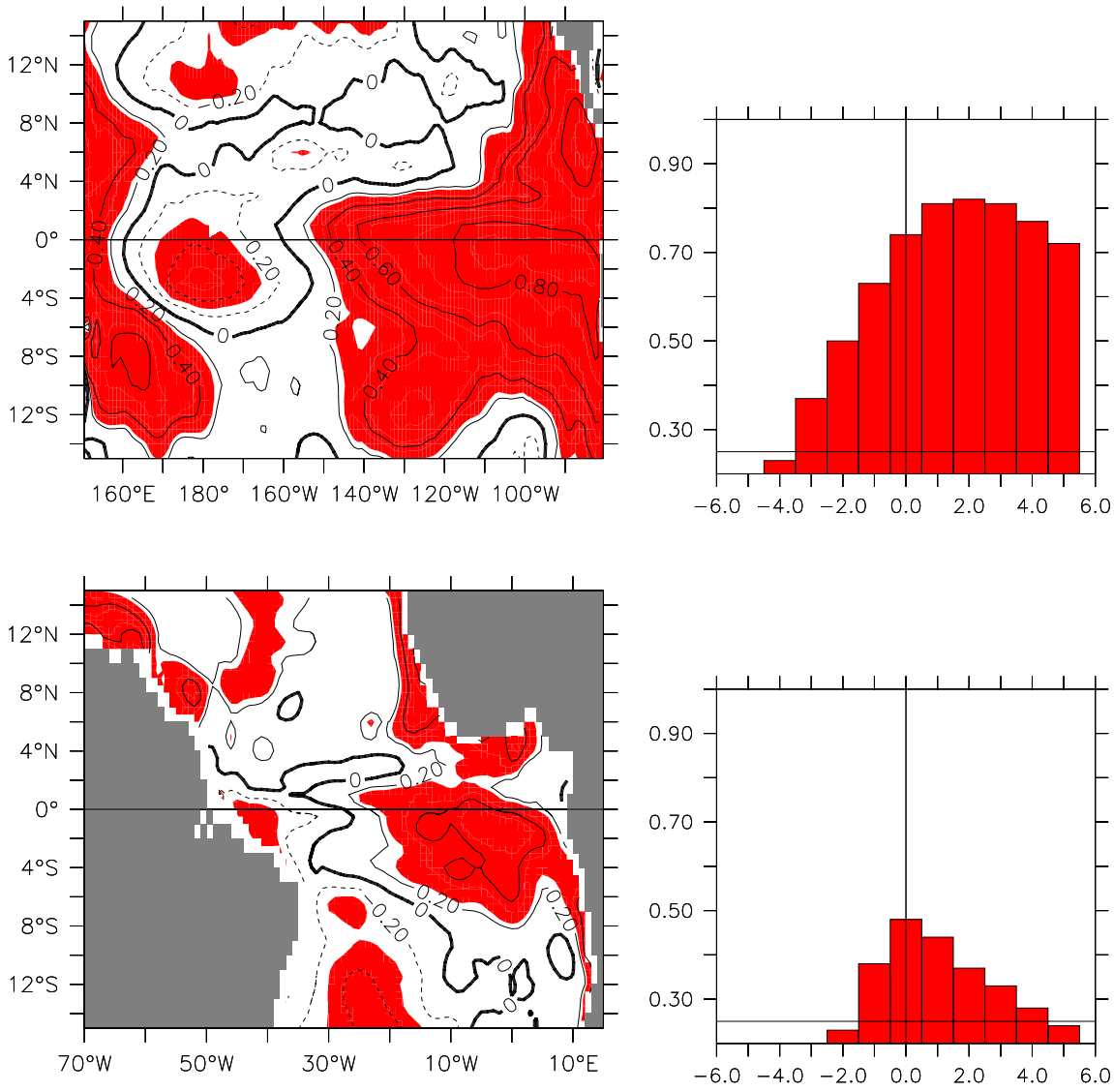

Fig 4.2a. Point to point correlation between thermocline depth and SST anomalies for the Pacific (upper panel) and Atlantic (lower panel) basins based on the ODA. Shaded areas denote the 95% significance level. The right panel presents lag-correlation histograms of the same variables averaged over the ATL3 region. In all histograms, positive lags indicate that thermocline depth anomalies lead SST.

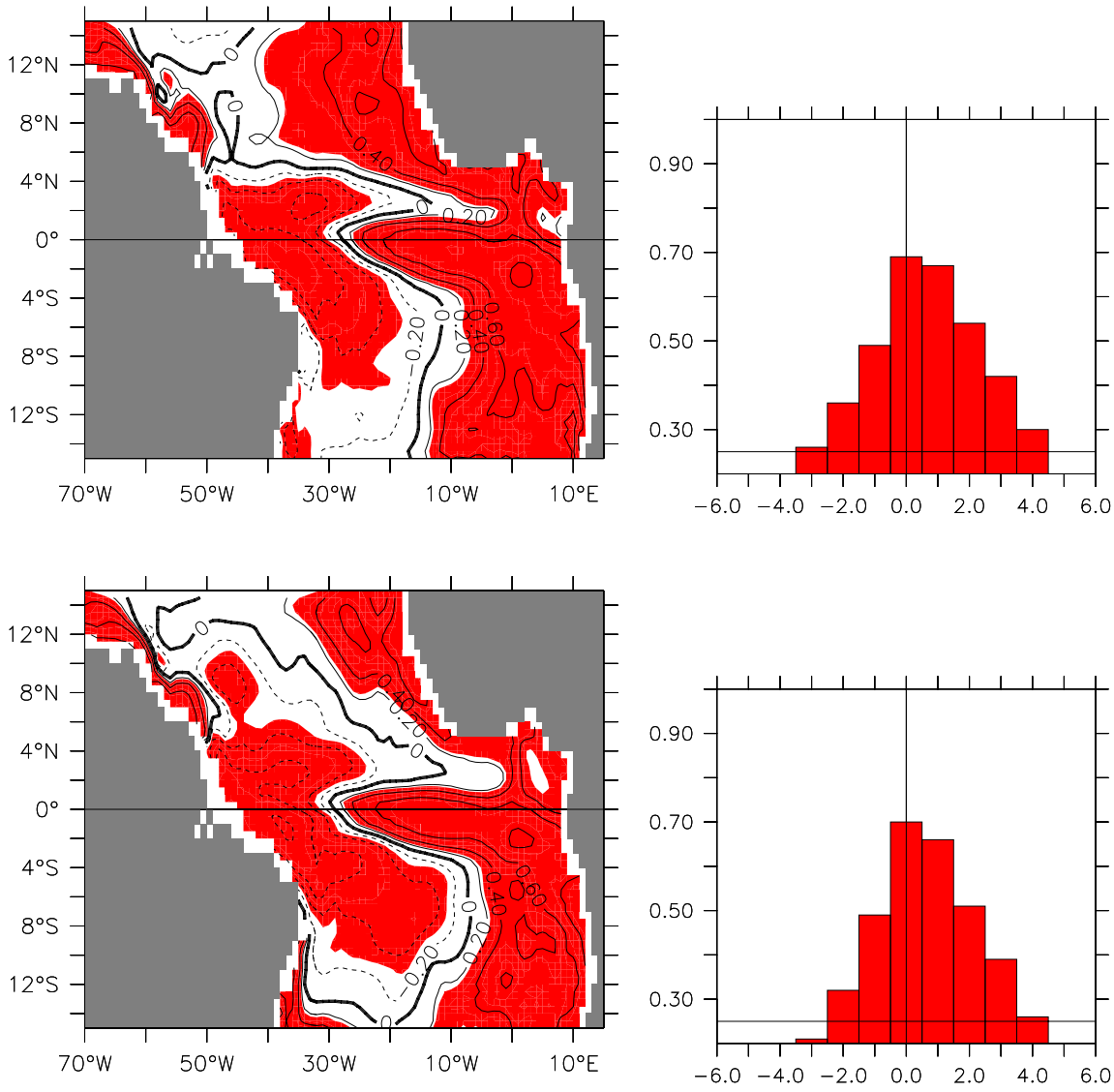

Fig 4.2b. Same as Figure 4.2a except for CEXP (upper panel) and WEXP (lower panel).

over the ATL3 region (right) for ODA, CEXP and WEXP, respectively. In all three datasets SST anomalies display significant (< -0.25) negative correlation with Ekman pumping velocities in the equatorial region, implying that anomalous Ekman upwelling is associated with anomalously cold SST. However, in both CEXP and WEXP the areas of significant correlation extend further east than in

the ODA. The lag-correlation histograms show that Ekman pumping leads SST anomalies by one month in the CEXP and WEXP. Although in the ODA maximum correlation values are found with Ekman pumping anomalies leading SST by 1-2 months, they are below the 95% significance level in the ATL3 region.

In order to investigate the contribution of the zonal wind stress in generating Ekman pumping anomalies, similar maps and plots shown in Fig. 4.3a are reproduced but this time the divergence of the Ekman transport was calculated by neglecting the meridional wind stress. The resulting figure (Fig. 4.3b) suggests that convergence/divergence driven by zonal wind stress anomalies is dominant in generating Ekman pumping anomalies in the equatorial region, in particular for the central equatorial Atlantic.

The results of the previous analyses indicate that in the ODA, CEXP, and WEXP both local and remote processes may play a role controlling SST changes in the equatorial region. However, they also show that there are differences in how these processes operate in each dataset. Some of the differences seem to be model dependent, since CEXP and WEXP deviate from ODA in a similar fashion. It should also be taken into account the fact that ODA SST is strongly constrained by the observation which may obscure the role played by different physical processes. Thus we next examine to what extent CEXP and WEXP can reproduce the SST tropical variability of the ODA.

Figure 4.4a displays correlation maps of SST anomalies from ODA with CEXP (left), and with WEXP (right) for the 20-year time period. This Figure shows that there is a good agreement between CEXP and ODA, with correlation values ranging from 0.6 to 0.9 over most of the domain. Significant correlation values (> 0.25) between SST anomalies from the WEXP and ODA are basically found in the interior of the basin between 3^{o}N and 12^{o}S, indicating the importance of ocean dynamics in determining the SST variability. Similar results

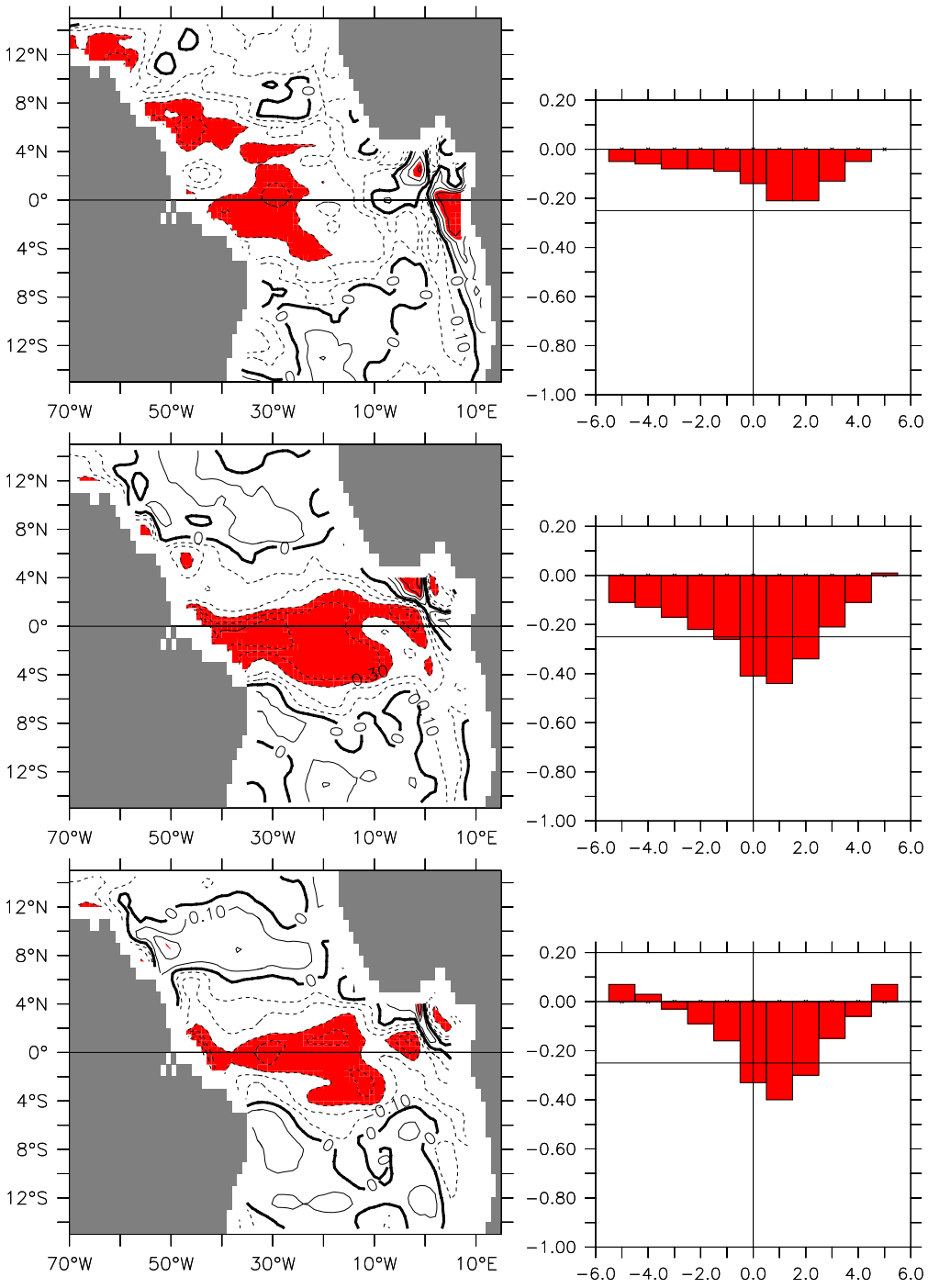

Fig 4.3a. Point to point correlation between Ekman pumping and SST anomalies for ODA (upper panel), CEXP (mid panel) and WEXP (lower panel). The right panel presents lag-correlation histograms of the same variables averaged over the ATL3 region. Shaded areas denote the 95% significance level. In all histograms, positive lags indicate that Ekman pumping anomalies lead SST.

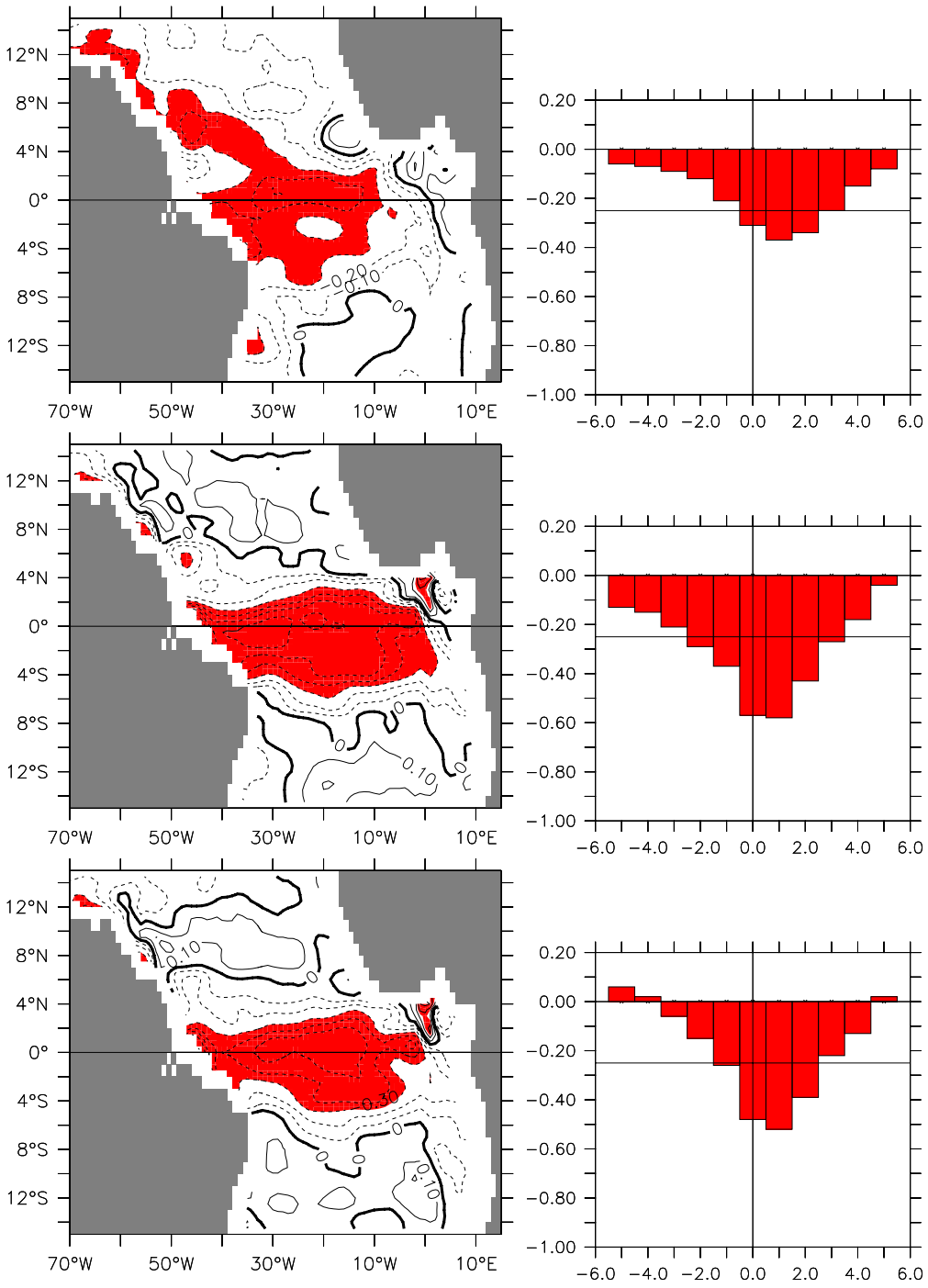

Fig 4.3b. Same as Figure 4.3a except Ekman pumping anomalies are calculated neglecting the meridional wind stress.

were found by *Carton and Zhou* [1997] when examining the annual cycle of SST in the tropical Atlantic.

The relatively poor performance of the WEXP in the eastern, western, and northern equatorial region does not necessary imply that ocean dynamics are not important. One should note that the correlation values between CEXP and ODA are also relative low in these areas, indicating the possibility of deficient model physics or insufficient model resolution to simulate the complex processes controlling the SST variability in these regions.

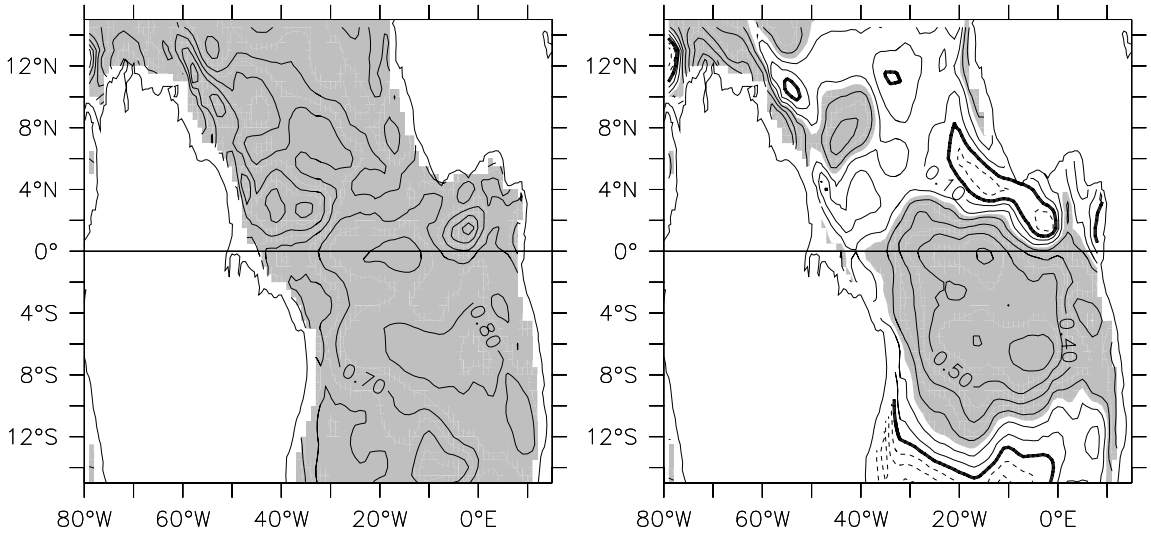

Fig 4.4a. Correlation between SST anomalies from ODA with CEXP (left panel) and WEXP (right panel). Shaded areas denote the 95% significance level.

Correlation between SST anomalies from CEXP (left panel) and WEXP (right panel) with ODA for different months reveals that summer (Fig. 4.4b) is the season when the assimilated SST anomaly variability is reproduced best by CEXP and WEXP. In particular from May to July the correlation coefficients are higher than 0.7 in the equatorial region. In August, the correlation values drop below the significance level in the region where the two main off equatorial zonal

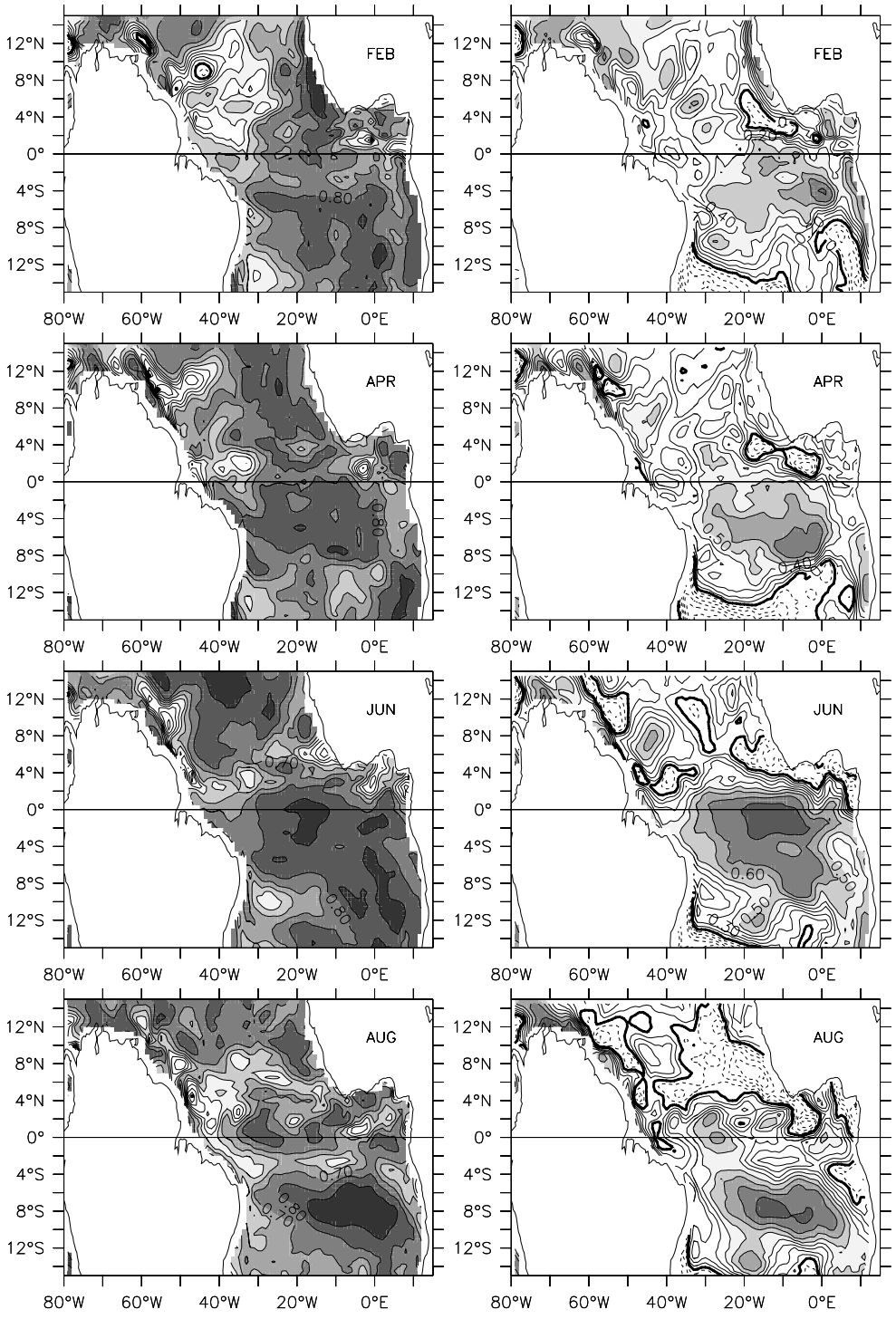

Fig 4.4b Same as Figure 4.4a except for different months.

currents are situated, but are still higher than 0.7 in the deep tropics. In the WEXP, correlation values are also below the significance level in the northern tropics.

Figure 4.5a shows the leading EOFs of SST of the ODA based on the whole 20-year period (upper panel), only boreal spring months – MAM (mid panel), and only boreal summer months – JJA (lower panel) with respective principal components (PC) time-series. These EOFs explain 73%, 49% and 59% of the total variance, respectively. It should be noted that the EOF of the 20-year period is generally similar to the summer EOF; both are characterized by negative anomalies largely confined south of 4^{o}N with more weight in the eastern part of the basin. This similarity is not coincidental. Boreal summer is the period when the zonal mode is dominant, and due to the fact that the EOF analysis is confined to the tropical region (15^{o}N and 15^{o}S) were ocean dynamics play an important role controlling SST changes, the spatial pattern associated with the zonal mode explains a larger portion of the total variance.

The spring EOF, on the other hand, displays the characteristic pattern associated with the meridional mode. A cross-equatorial SST gradient with a band of warm anomalies centered around 10^{o}N and cold anomalies confined to the south of the equator. The meridional mode is believed to be primarily controlled by heat flux changes [e.g. *Carton et al.,* 1996] and is dominant during boreal spring when the seasonal entrainment is weak and the mixed layer is shallow, making the SST more sensitive to changes in the heat flux.

The leading EOFs of CEXP and WEXP for the same period and seasons are shown in Figs. 4.5b and 4.5c, respectively. The variance explained by the CEXP (WEXP) EOFs is about 54 %(36%) in spring, 57 %(40%) in summer, and 44 %(29%) in the whole 20-year period. Similar to the ODA (Fig. 4.5a lower panel), the spatial patterns associated with the 20-year and boreal summer EOFs in both CEXP and WEXP are characterized by a tongue of negative anomalies asymmetric to the equator. However, in the CEXP the anomalies in

the equatorial region are slightly displaced to the southwest relative to the ODA. This feature is more pronounced in the WEXP, which presents the largest amplitudes in the western instead of eastern part of the basin. The associated PC1 time series from both CEXP and WEXP are correlated with those of ODA at 95% significance level (see Table 4.1).

The boreal spring EOF of CEXP (Fig. 4.5b mid panel) is characterized by dipole pattern whose PC1 is highly correlated (0.9) with that of ODA. But different from the ODA (Fig. 4.5a mid panel), the amplitude of anomalies in the southern equatorial region are more pronounced than those in the northern hemisphere. The spring EOF of WEXP (Fig. 4.5c mid panel) does not exhibit the traditional north/south dipole that characterizes the meridional mode. However, the correlation between the associated PC1 and the ODA counterpart is higher than 0.5 (see Table 4.1) which is significant at 95% level.

The EOF patterns and PCs from CEXP have a better agreement with the assimilation than those from WEXP. This result was expected since the WEXP accounts only for the dynamical effects of wind stress in driving SST changes, while the CEXP also includes a Newtonian damping as a parameterization for heat flux. It seems that in the western equatorial region heat fluxes are necessary to counteract ocean dynamics which tend to enhance SST anomalies in this region especially during boreal summer. The above results also indicate that a 30-day SST restoring is not sufficient to reproduce the observed spatial structure associated with the meridional mode, but appears sufficient to capture the temporal variability. The WEXP is even able, to some degree, to reproduce the ODA spring temporal variability, suggesting that the first EOF of the ODA for boreal spring may be partly forced by ocean dynamics, in particular in the southern tropics.

Table 4.1. Correlation values between ODA, CEXP and WEXP SST principal components (PC1) for whole 20-year period, spring, and summer. Asterisk indicates correlation value that is not significant ($p < 0.025$).

	ODA-20yrs		
CEXP-20yrs	0.87		
WEXP-20yrs	0.40		
	ODA-MAM		
CEXP-MAM	0.90		
WEXP-MAM	0.54		
	ODA-JJA		
CEXP-JJA	0.89		
WEXP-JJA	0.57		
	ODA-MAM	CEXP-MAM	WEXP-MAM
ODA-JJA	0.71	0.70	0.32*
CEXP-JJA	0.83	0.82	0.50
WEXP-JJA	0.66	0.70	0.75

Another very interesting result displayed in Table 4.1 is that in the ODA as well as in CEXP and WEXP the spring EOFs are well correlated with the summer EOFs, which could be interpreted as an evidence that the spring condition evolves into the summer condition. A connection between the zonal and meridional mode has been noted in earlier studies by *Servain et al.* [2000]. However, their conclusion is based on a correlation analysis between the cross-equatorial SST gradient and variations of the equatorial thermocline slope during 1980-1997.

The above results indicate that CEXP and WEXP are generally able to capture the SST variability in the equatorial region and southern tropics, in particular during the onset and peak phases of the zonal mode. Encouraged by

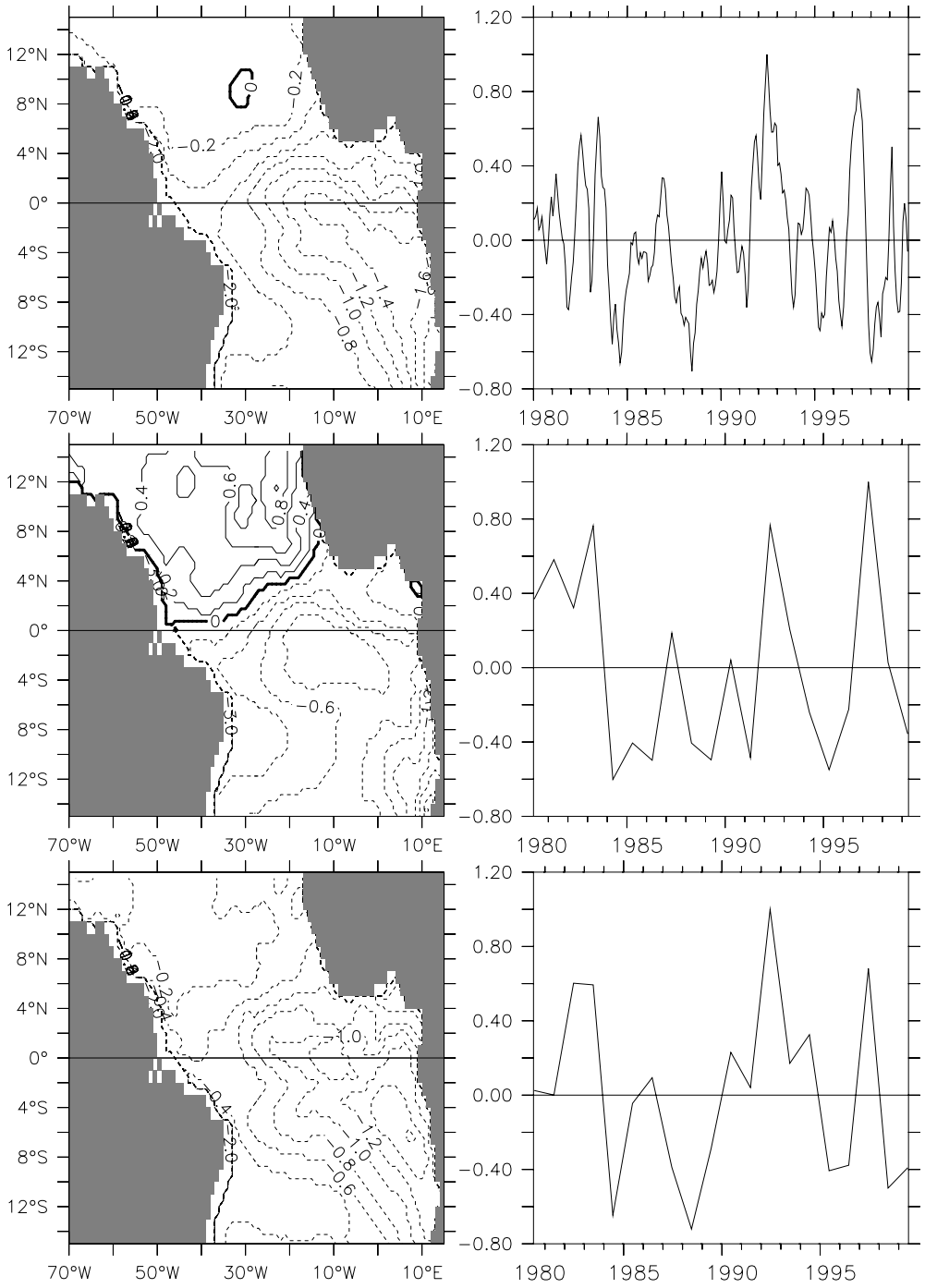

Fig 4.5a. Leading EOFs of SST anomalies based on ODA during the whole 20-year period (upper panel), only boreal spring months – MAM (mid panel), and only boreal summer months – JJA (lower panel). The right panel presents the associated PC1 time series.

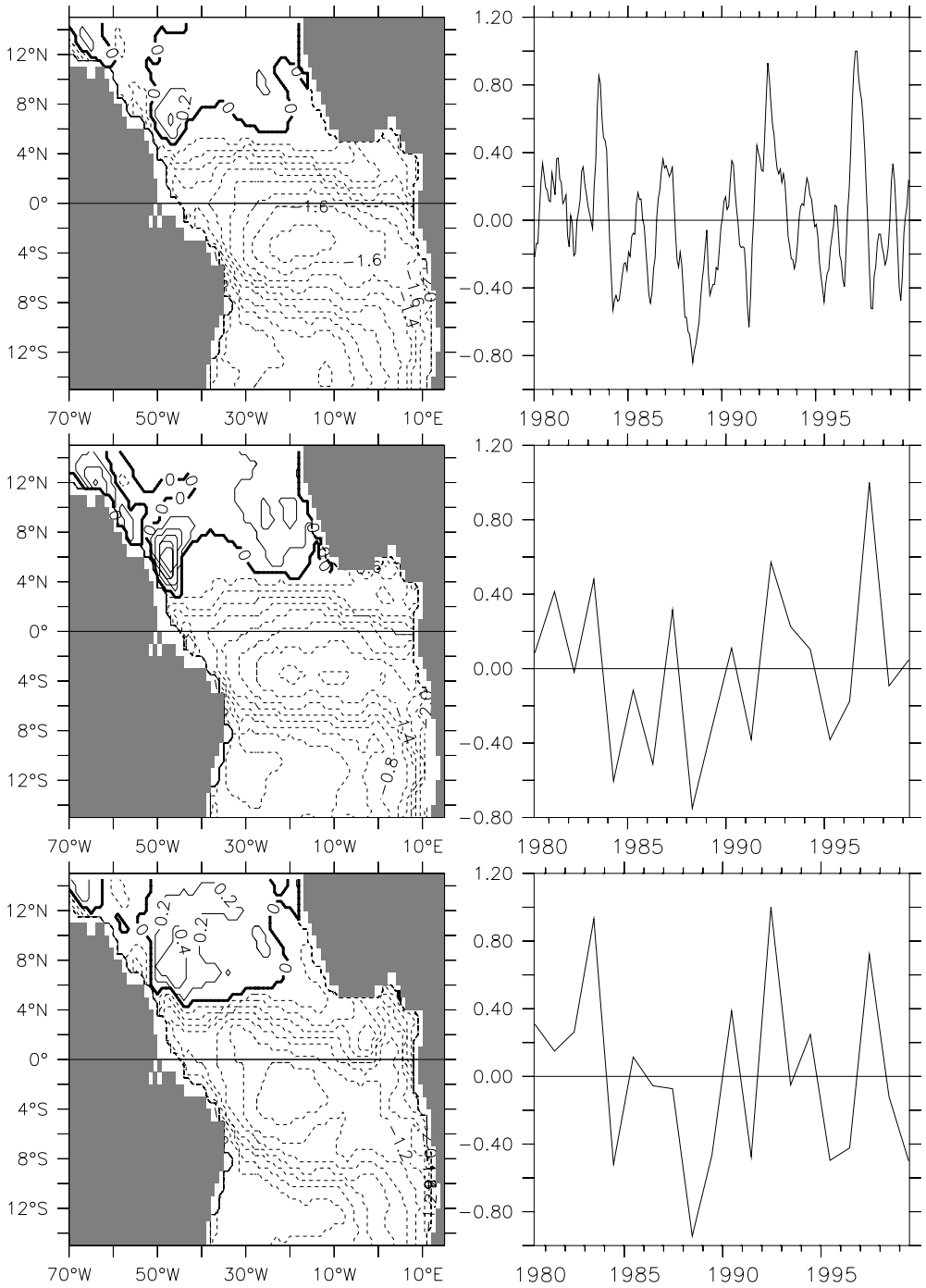

Fig 4.5b. Same as Figure 4.5a except for CEXP.

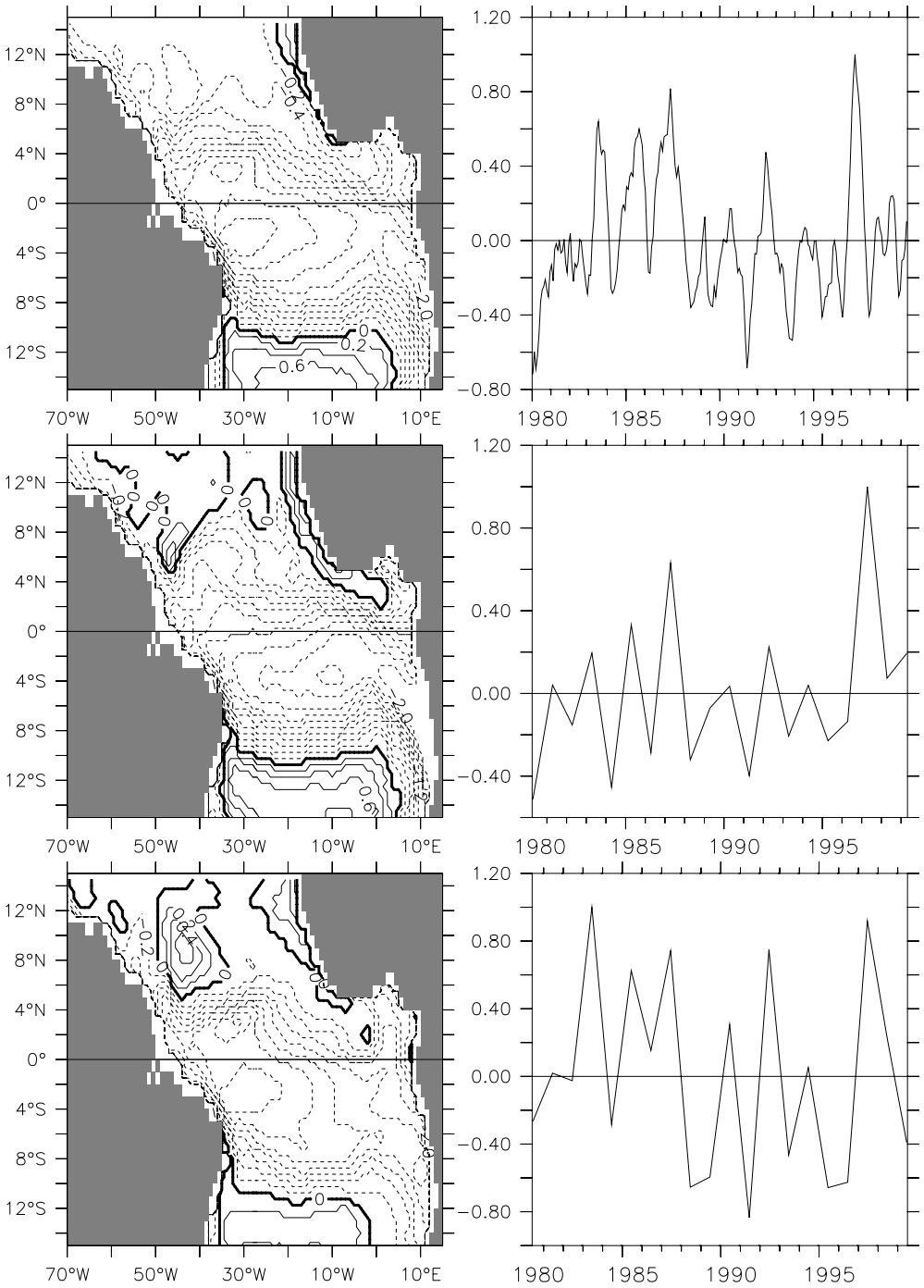

Fig 4.5c. Same as Figure 4.5a except for WEXP.

these results, a heat budget analysis is performed on the CEXP and WEXP following the outline given in the Chapter II and the results are presented next.

3. Mixed Layer Heat Budget Analysis

The vertically integrated temperature equation within the mixed layer is given by

$$\frac{\partial T}{\partial t} + \frac{\partial}{\partial x}(uT) + \frac{\partial}{\partial y}(vT) - w_e H(w_e)\frac{T - T_{sub}}{h_{mix}} = \frac{Q}{\rho_0 C_p h_{mix}} + h_{mix} K \nabla^2 T \ . \quad (4.2)$$

Equation (4.2) represents, from left to right, the balance of the following terms: SST tendency, horizontal advection, vertical entrainment into the mixed layer, net surface heat flux, and horizontal dissipation. Details of the experiments' heat budget analyses are described in Appendix A. Consistent with Chapter III, the experiments' mixed-layer depth, h_{mix}, is determined using formulation by *Monterey and Levitus* [1997]. The temperature below the base of the mixed layer was used as subsurface temperature (T_{sub}).

Horizontal and vertical velocities associated with the advective terms in equation (4.2) can be decomposed into a geostrophic part and an Ekman part. Although, both parts involve a response of the ocean to the wind forcing, the Ekman currents represent a response directly related with the local winds, while the geostrophic currents are resultant of large-scale ocean adjustment that takes longer and may not be directly correlated to the local winds. Thus, two different ways of computing the vertical entrainment (w_e) were examined in this study. The first type, following *Stevenson and Niiler* [1983], is determined as divergence of the mixed layer, i.e.,

$$w_e = \frac{\partial h_{mix}}{\partial t} + \nabla \cdot h_{mix} V \ , \quad (4.3)$$

where V is the total horizontal velocity which includes both geostrophic and Ekman components. The second approach computes the entrainment velocity directly from the wind stress using equation (4.1) and therefore is a way to quantify how much of w_e is due to Ekman dynamics.

The model described by equation (4.2) was integrated using u, v, w_e, h_{mix}, T_{sub} and Q from CEXP and WEXP as input, December climatology from the 5-year spin up is used as initial condition, and the eddy diffusivity K is assigned a value of $1\times10^{8}s^{-1}$. Figure 4.6 shows correlation maps of temperature hindcasted by (4.2) and SST from CEXP (upper panel) and WEXP (lower panel). The left panel shows results computed using w_e according to eq. (4.1) and the right panel shows results according to eq. (4.3).

The results indicate that for most part of the basin the two approaches yield similar findings, suggesting that the entrainment velocity is mainly determined by Ekman dynamics in both CEXP and WEXP. Some large differences are found along the eastern boundary north of the equator. In the equatorial region and southern tropics w_e computed according to (4.1) is slightly better than that computed from the divergence of the mixed layer. Since the objective of this chapter is to determine how much of the SST variability is due to the coupling between local winds and SST, the results presented and discussed next are based on the simple model response using (4.1) as a way to compute w_e.

a. Results from Simplified Mixed Layer Model

In this section, we present results from the simplified mixed layer model based on w_e computed from (4.1). We compare the simple model response forced with CEXP variables (hereafter referred as SM_CEXP) and with WEXP

variables (hereafter referred as SM_WEXP). Emphasis will be given to the equatorial region where the 3-d flux corrected model seems to capture better the assimilated SST evolution, defined as EQA (3^oN – 6^oS and 35^oW – 0^oW). This area includes the ATL3 region as defined by *Zebiak* [1993]. We first show that the simple model is capable of reproducing the full model results, and then proceed to further dissect the ocean dynamics contributing to SST variability in the framework of the simple model.

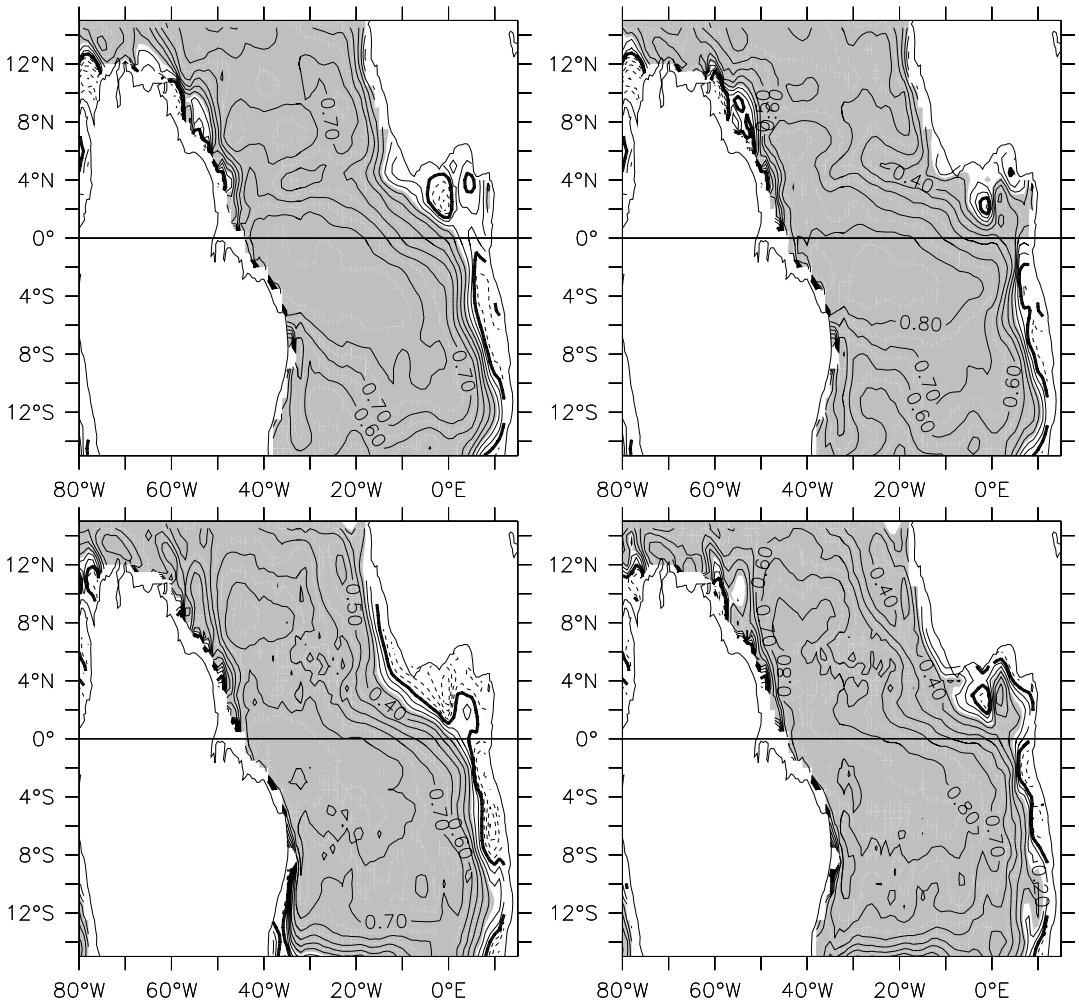

Fig 4.6. Correlation between temperature hindcasted by equation (4.2) and SST from CEXP (upper panel) and WEXP (lower panel). The left panel shows results computed using w_e according to equation (4.1) and the right panel shows results according to equation (4.3). Shaded areas denote the 95% significance level.

Time series of SST averaged over the EQA region for ODA (black), CEXP (red) and SM_CEXP (green) are shown in the upper panel of Fig. 4.7. The lower panel displays the same plot but for WEXP (red) and SM_WEXP (green). The simple model responses reproduce well the SST variability of the original experiments with a correlation of about 0.9 between the two time series in both CEXP and WEXP. However, the amplitude of the SST anomalies is somewhat underestimated by the simple model and tends to be closer to the assimilation than CEXP and WEXP. The correlation between ODA and CEXP time series is the same as that between ODA and SM_CEXP, with value of about 0.8. On the other hand, the 0.6 value for the correlation of ODA with SM_WEXP is slightly higher than the 0.5 value for ODA with WEXP.

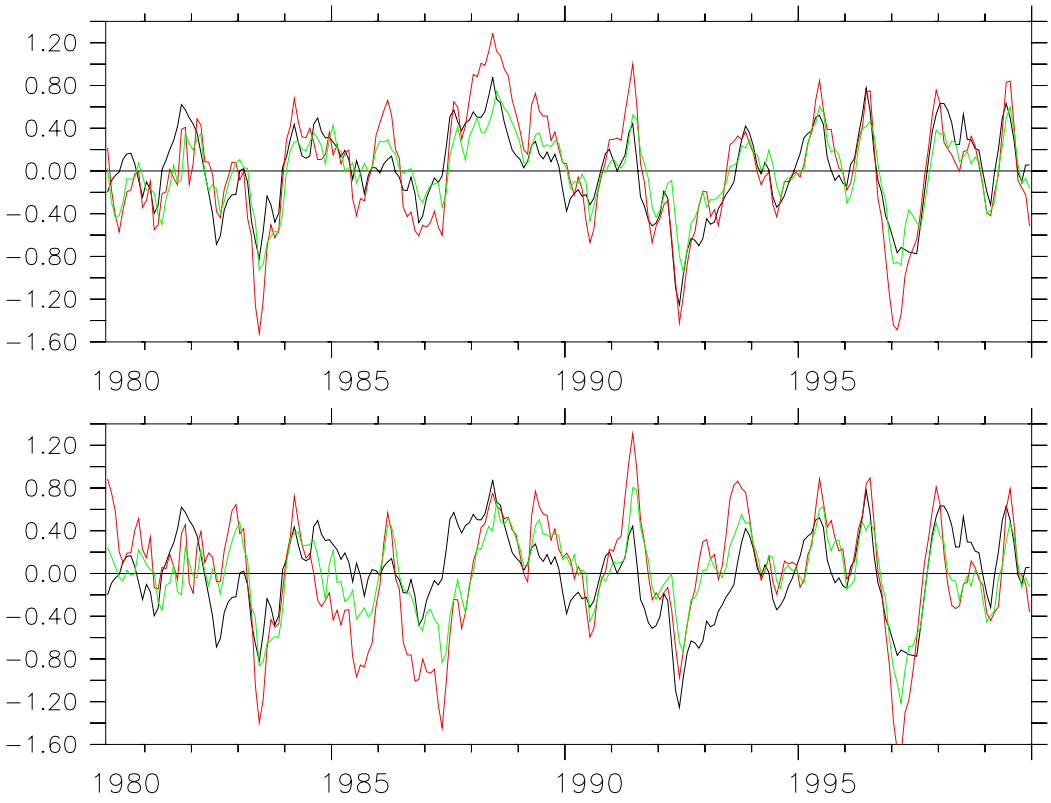

Fig. 4.7. Time series of SST anomaly averaged over the EQA region (upper panel) for ODA (black), CEXP (red) and SM_CEXP (green). The lower panel presents the same plot except for SM_WEXP.

The tendency terms for vertical entrainment (black), net heat flux (red), meridional advection (green), zonal advection (blue) averaged over the EQA region and the sum of these terms plotted against the SST anomaly tendency are shown in Figs. 4.8a and 4.8b respectively for SM_CEXP, and in Figs. 4.8c and 4.8d for SM_WEXP. A 3-months running mean has been applied to the time series to eliminate high frequency fluctuations. In agreement with previous studies on interannual [*Zebiak,* 1993] and seasonal [*Carton and Zhou,* 1997; *Foltz et al.,* 2003] time scales, the vertical entrainment term is the dominant term in this region, which is balanced by the net surface heat flux in the SM_CEXP. Note that the surface heat flux in the SM_WEXP includes only the Newtonian damping to the annual mean to correct for drift in the simple model. The horizontal advective terms are secondary and have a comparable order of magnitude. The horizontal diffusion term (not shown in Fig. 4.8), although more important in the SM_WEXP than in the SM_CEXP, has a minor contribution to the SST tendency.

b. Dissecting Ocean Dynamics

To further dissect the oceanic processes controlling the evolution of the SST variability, the advective terms in (4.2) are decomposed into climatological mean and departures from the climatology:

$$
\begin{aligned}
u\frac{\partial T}{\partial x} &= \underset{1a}{-u\frac{\partial \overline{T}}{\partial x}} + \underset{1b}{-u\frac{\partial T'}{\partial x}} + \underset{1c}{u'\frac{\partial \overline{T}}{\partial x}} + \underset{1d}{u'\frac{\partial T'}{\partial x}}, \\
v\frac{\partial T}{\partial y} &= \underset{2a}{-v\frac{\partial \overline{T}}{\partial y}} + \underset{2b}{-v\frac{\partial T'}{\partial y}} + \underset{2c}{v'\frac{\partial \overline{T}}{\partial y}} + \underset{2d}{v'\frac{\partial T'}{\partial y}}, \\
w\frac{\partial T}{\partial z} &= \underset{3a}{-w\frac{\partial \overline{T}}{\partial z}} + \underset{3b}{-w\frac{\partial T'}{\partial z}} + \underset{3c}{w'\frac{\partial \overline{T}}{\partial z}} + \underset{3d}{w'\frac{\partial T'}{\partial z}},
\end{aligned}
\qquad (4.4)
$$

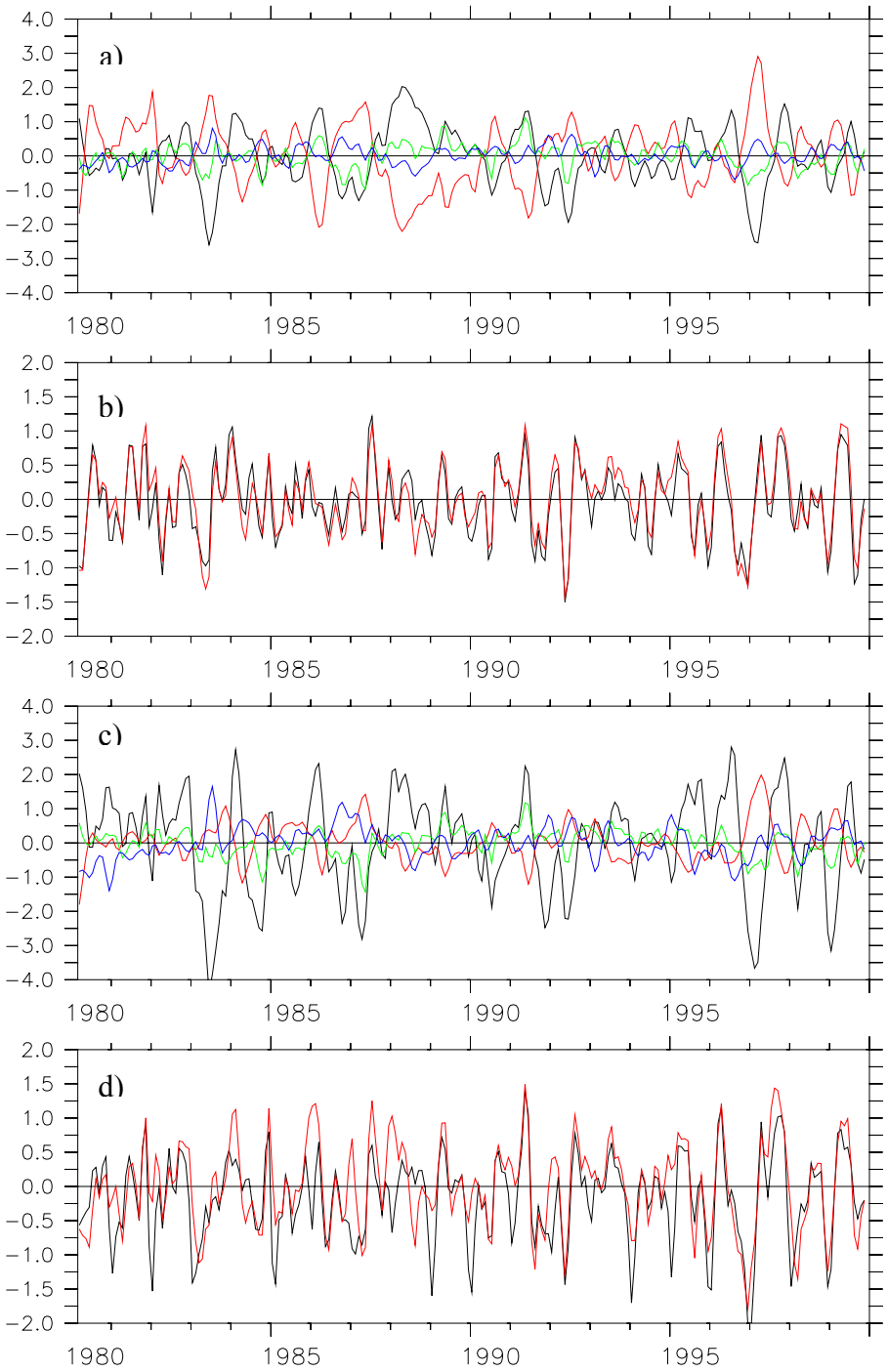

Fig. 4.8. a) The tendency terms for vertical entrainment (black), net heat flux (red), meridional advection (green), zonal advection (blue) averaged over the EQA region for SM_CEXP and b) the sum of these terms plotted against the SST anomaly tendency. c) The same tendency terms for SM_WEXP and d) the sum of these terms plotted against the SST anomaly tendency.

where the terms 1a, 2a, and 3a are climatology; 1d, 2d, and 3d are nonlinear terms (usually small); 1b (2b) represents anomalous temperature advection by mean zonal (meridional) currents; 1c (2c) represents mean temperature advection by anomalous zonal (meridional) currents; 3b and 3c represent mean upwelling against anomalous vertical stratification and anomalous upwelling against mean vertical stratification, respectively. A composite of the linear tendency terms above is constructed for the extreme years of the ODA summer PC1 which both CEXP and WEXP are able to reproduce. Thus, three cold events (83, 92, and 97) and four warm events (88, 95, 96, and 99) were selected.

Figure 4.9 shows the composite of cold events (upper panel), warm events (mid panel), and the difference between cold and warm events (lower panel) for SM_CEXP (left panel) and SM_WEXP (right panel). Looking first at the composite of SM_CEXP one sees that the SST tendency anomalies (black) amplify from February to June, after June they start to decay, and in August have switched sign. During March April and May the main terms forcing SST changes are anomalous upwelling, mean upwelling (cold events) and advection by anomalous meridional current. Note that mean upwelling is the largest term, but its contribution is more important during June, July and August. Although in a smaller degree, advection by anomalous zonal currents and advection by mean meridional currents also acts to force SST anomaly, in particular in June. The terms responsible for the change of sign in the SST tendency anomalies towards the end of summer are advection by mean zonal currents, anomalous upwelling, and advection by anomalous meridional currents.

Thus, advection by anomalous meridional currents and anomalous upwelling contribute to the onset of the events, mean upwelling has a more important role in the persistence of SST anomalies, and the decay is caused by advection by mean zonal currents, anomalous upwelling, and advection by anomalous meridional currents. The SM_WEXP composites yield basically the

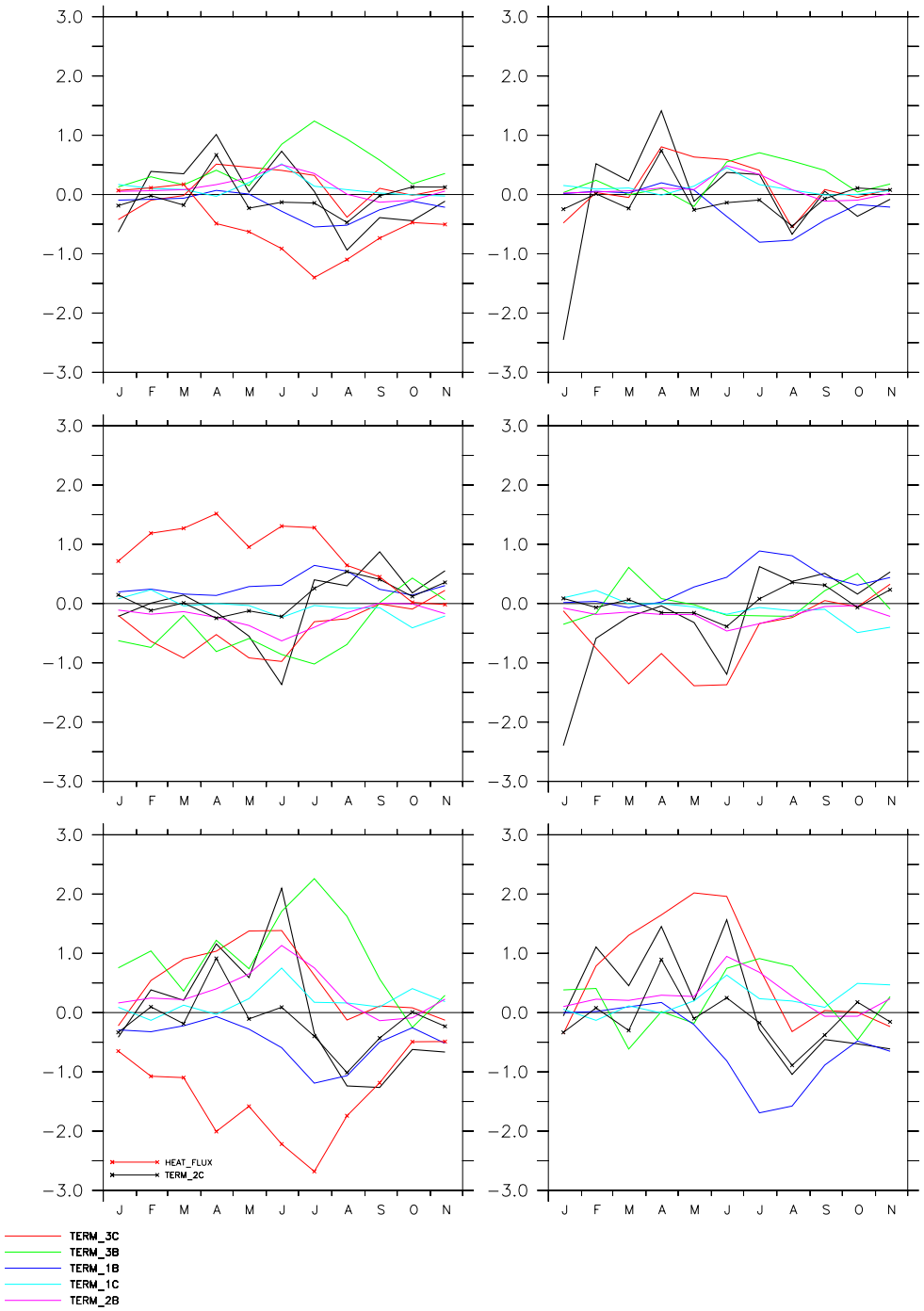

Fig. 4.9. Composites of the temperature tendency terms in equation (4.4) for cold events (upper panel), warm events (mid panel), and the difference between cold and warm events (lower panel). The left panel shows the composites for SM_CEXP and the right panel for SM_WEXP.

same results with only one difference. That is the mean upwelling term is comparatively smaller than the SM_CEXP counterpart, and anomalous upwelling, and advection by anomalous meridional currents are larger. This implies that, overall, the events in the WEXP are shorter lived than in the CEXP. The autocorrelation plot of the ATL3 index for ODA, CEXP and WEXP (Fig. 4.10) indicates that indeed this may be the case. In the ODA SST anomaly in June is still correlated with September anomaly at 95% significance level. In the CEXP June anomaly persists after August, while in the WEXP after July the autocorrelation tend to fall below the significance level.

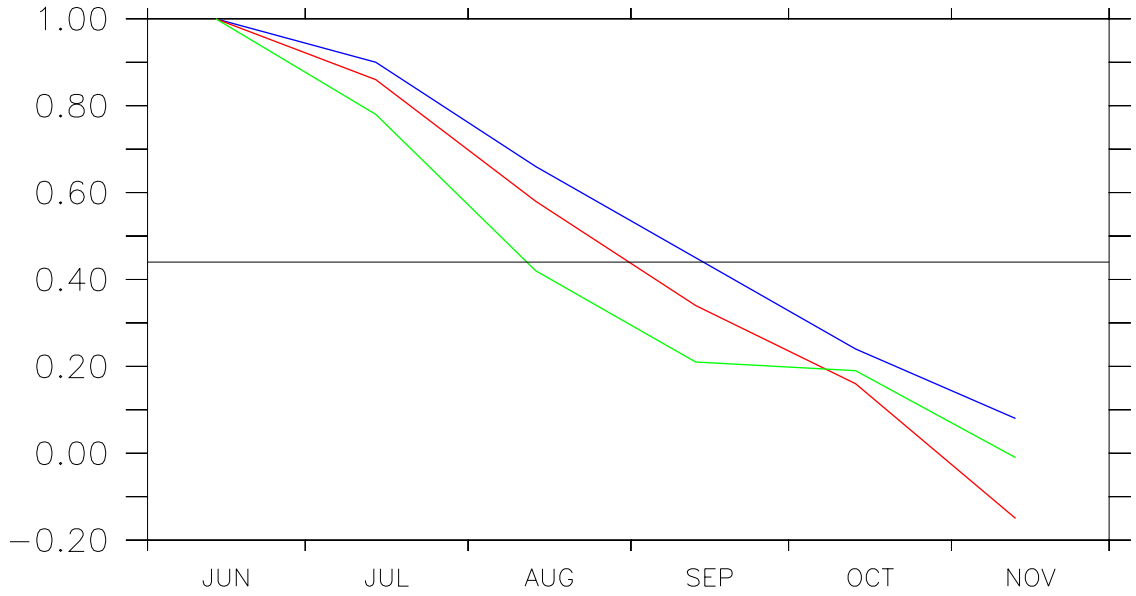

Fig. 4.10. Autocorrelation plot of the ATL3 index starting from June for ODA (blue), CEXP (red) and WEXP (green). The horizontal line denotes the 95% significance level.

The SST variability is the time integral of the SST tendency and therefore SST anomalies lag the terms of the tendency equation. From the above tendency analysis is difficult to determine with precision whether each term is lagging or leading the SST anomaly. Furthermore, it represents the heat budget for the EQA in the averaged sense and does not explore the fact that the relative

importance of the oceanic processes may be different in different regions. Thus, to further test the hypotheses raised by the tendency analysis, the SST evolution given by each of the linear advective terms in (4.4) is computed separately, i.e.:

$$
\begin{aligned}
T_{1b} &= T_0 - \int_0^t \bar{u}\frac{\partial T'}{\partial x}dt\,, \\
T_{1c} &= T_0 - \int_0^t u'\frac{\partial \bar{T}}{\partial x}dt\,, \\
&\vdots \qquad\qquad \vdots \\
T_{3c} &= T_0 - \int_0^t w'\frac{\partial \bar{T}}{\partial x}dt\,, \\
T &= T_{1b} + T_{1c} + \ldots + T_{3c} \qquad (4.5)
\end{aligned}
$$

and then regressed onto the time series associated with the leading summer EOF of the ODA (Fig. 4.5a lower panel). This procedure is expected to quantify not only the relative contribution of the advective terms to the summer SST variability, but also identify the areas of maximum covariance. Since the SST variability in the summer may have evolved from the previous season, ODA PC1 is regressed onto temperature fields from March to August.

Before we present the results of the regression analysis, a covariance analysis is performed to estimate how much of the covariance of the total temperature T with ODA EOFs can be explained by each of the temperature terms in (4.5). The covariance of a particular term in (4.5) with ODA PC1 $\langle T_{i,} PC1\rangle$ is computed and normalized by the covariance of the total temperature with ODA PC1 $\left\langle \sum_{i=1}^{6} T_i, PC\,1 \right\rangle$. The $w'\frac{\partial \bar{T}}{\partial z}$, $\bar{w}\frac{\partial T'}{\partial z}$, $\bar{u}\frac{\partial T'}{\partial x}$, $u'\frac{\partial \bar{T}}{\partial x}$, $\bar{v}\frac{\partial T'}{\partial y}$, and $v'\frac{\partial \bar{T}}{\partial y}$ temperature terms account for 44%, 28%, 7%, 2%, 6%, and 11% of the covariance of T with ODA spring PC1, and 24%, 49%, 6%, 3%, 5% and 5% of

the covariance of T with ODA summer PC1, respectively. The above results confirm the dominance of anomalous upwelling in the control of SST variability during spring, and mean upwelling during summer.

Regression maps of the temperature terms in (4.5) onto ODA summer PC1 are shown in Figs. 4.11a to 4.11e. Overall, the lagged regression maps tend to confirm the previous results in showing that anomalous upwelling (Fig. 4.11a) contributes in forcing SST variability during the onset of the zonal mode, particularly in the ATL3 region. April and May are the months when the SST anomalies generated by this term are largest in the central equatorial region. From June to August the negative anomalies tend to gradually decrease and shift towards the western part of the basin, while in the eastern part they switch sign. This result is consistent with coupled model results by *Barreiro* [2003], who suggests that anomalous upwelling is particularly important for the observed evolution of the equatorial SST during MAM.

The dynamical process can be explained as a local coupled feedback between the surface wind stress (mainly zonal) and the SST. Easterly wind stress anomaly causes anomalous eastward equatorial current and Ekman divergence which enhances the climatological Ekman upwelling, cooling the surface. This cooling then amplifies the easterly wind anomaly, closing the feedback loop. The propagation characteristic of the anomalies generated by the anomalous upwelling term may be indicative of the so-called fast mode [*Jin et al*., 2003] that has been found in the Pacific. In the Atlantic a similar mode has been described to operate at seasonal time scales [*Chang and Philander,* 1994] and may be responsible for westward propagating features in the annual cycle of zonal winds and SST.

The mean upwelling term is related to coupled ocean-atmosphere interactions in which SST changes are determined by thermocline displacement as those involved in ENSO. Figure 4.11b shows that, similar to the anomalous upwelling, this term is also important in generating the SST anomaly in the

equatorial region associated with summer PC1. However, the maximum amplitudes are observed in a different area and season. The center of action of this term is localized in the southern tropics just off the equator, about the same region where the surface and subsurface are coupled in the ODA (Fig. 4.2 lower panel). The SST anomalies generated by this term tend to strengthen from May to August mainly in the central and western part of the basin and have a more stationary character than those forced by the anomalous upwelling. Note that this term is the one mainly responsible for the large (unrealistic) anomalies in the western equatorial region seen in the leading summer EOF of the WEXP (Fig. 4.9 lower panel).

All the previous results indicate that the contribution of advection by anomalous zonal currents to the summer SST variability is almost negligible. Therefore, only the lag regression maps for the other three horizontal advective terms will be presented. The mean zonal currents term (Fig. 4.11c) forces the SST anomalies in the western equatorial region and damps in the eastern. Thus, this term mainly contributes to the western propagation rather than a strengthening of the SST anomalies, in agreement with results of *Barreiro* [2003]. Advection by mean meridional currents (Fig. 4.11d) contributes in forcing SST off the equator, with larger contribution in the boreal summer months. The influence of the anomalous meridional currents (Fig. 4.11e) term is confined to a small area north of the equator between 20^{o} and 0^{o}W and mainly in July.

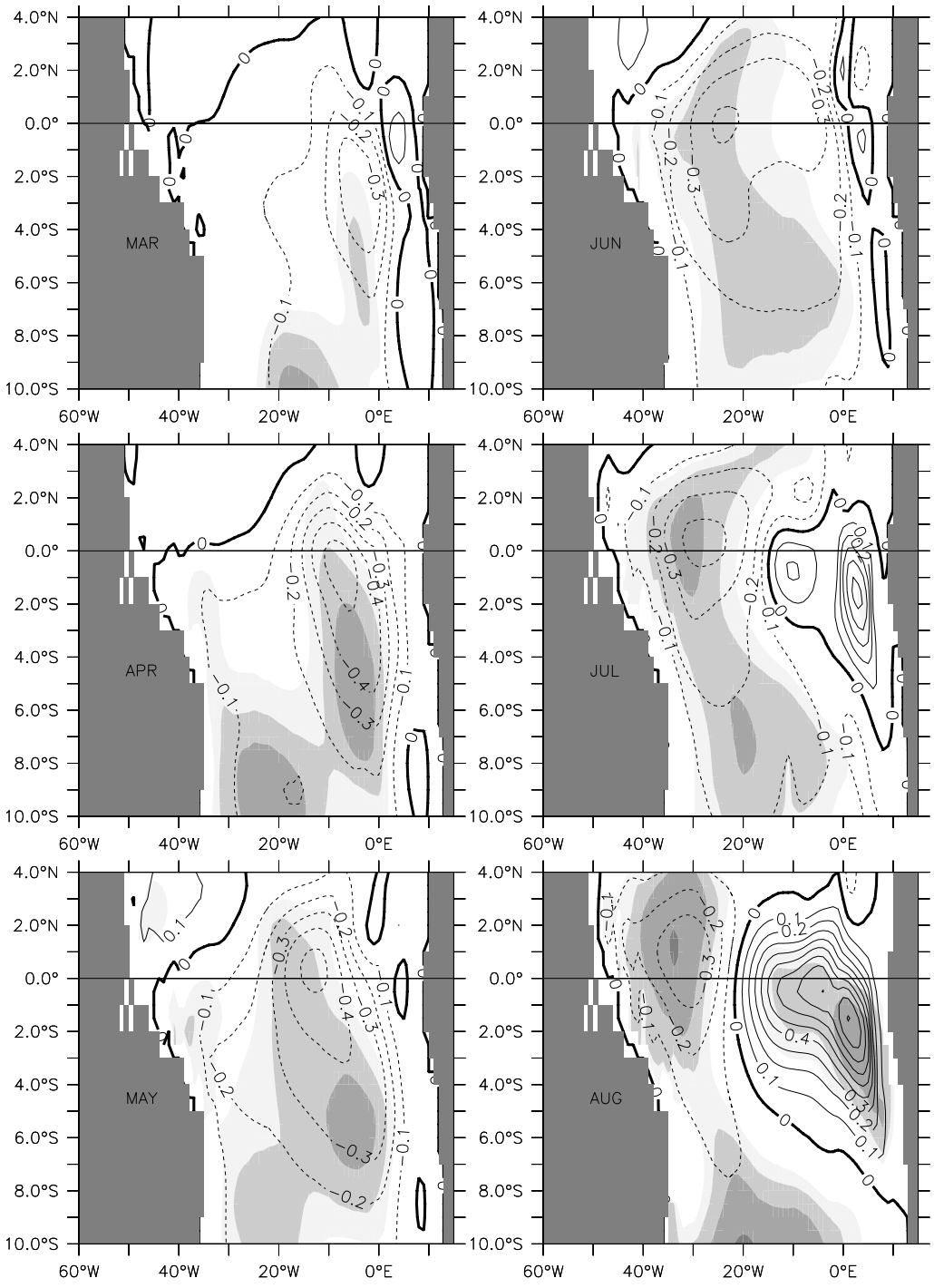

Fig. 4.11a. Temperature anomaly due to anomalous upwelling regressed on ODA summer PC1. Shaded areas denote the 95% significance level.

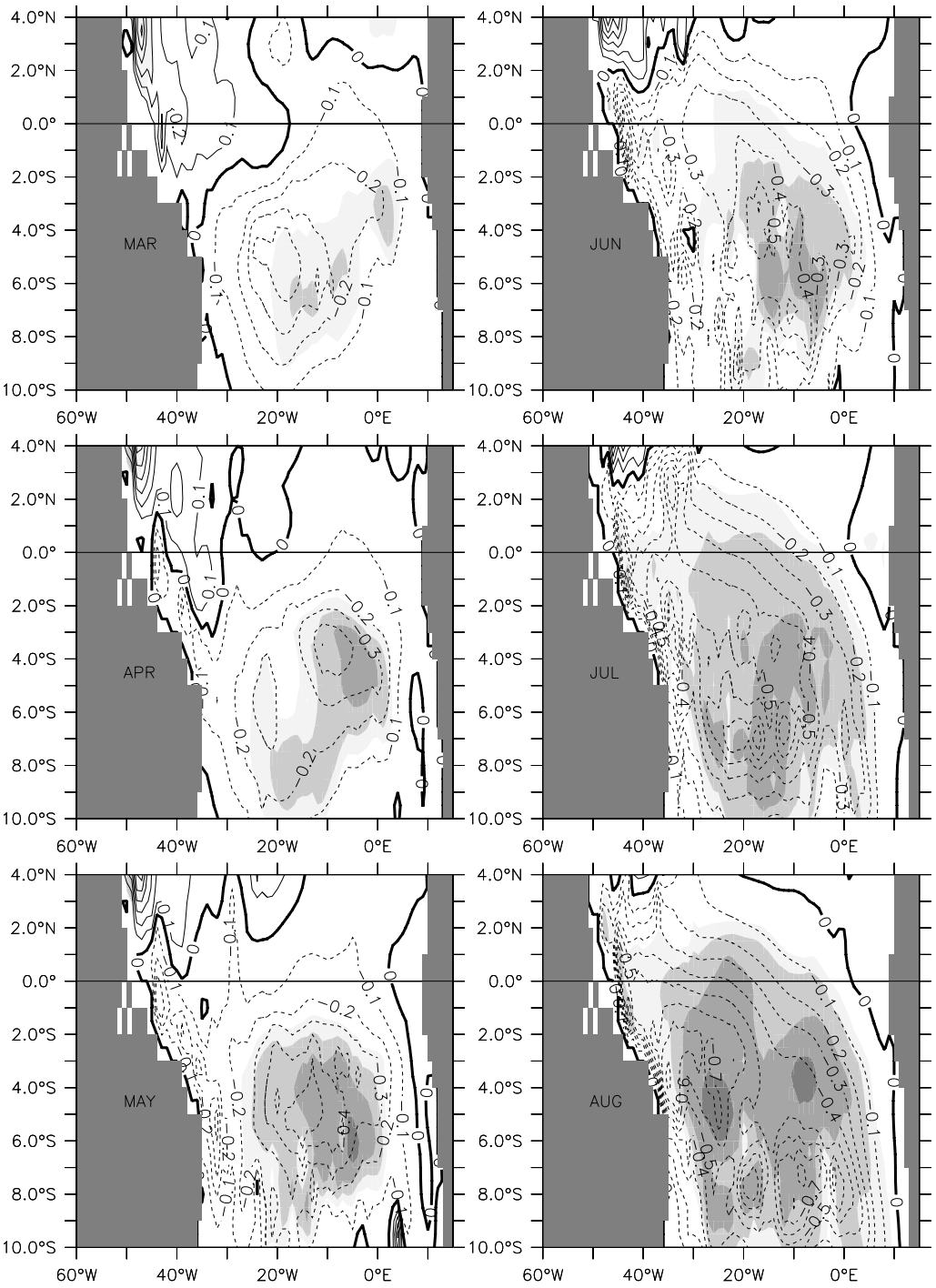

Fig. 4.11b. Same as Figure 4.11a except for mean upwelling.

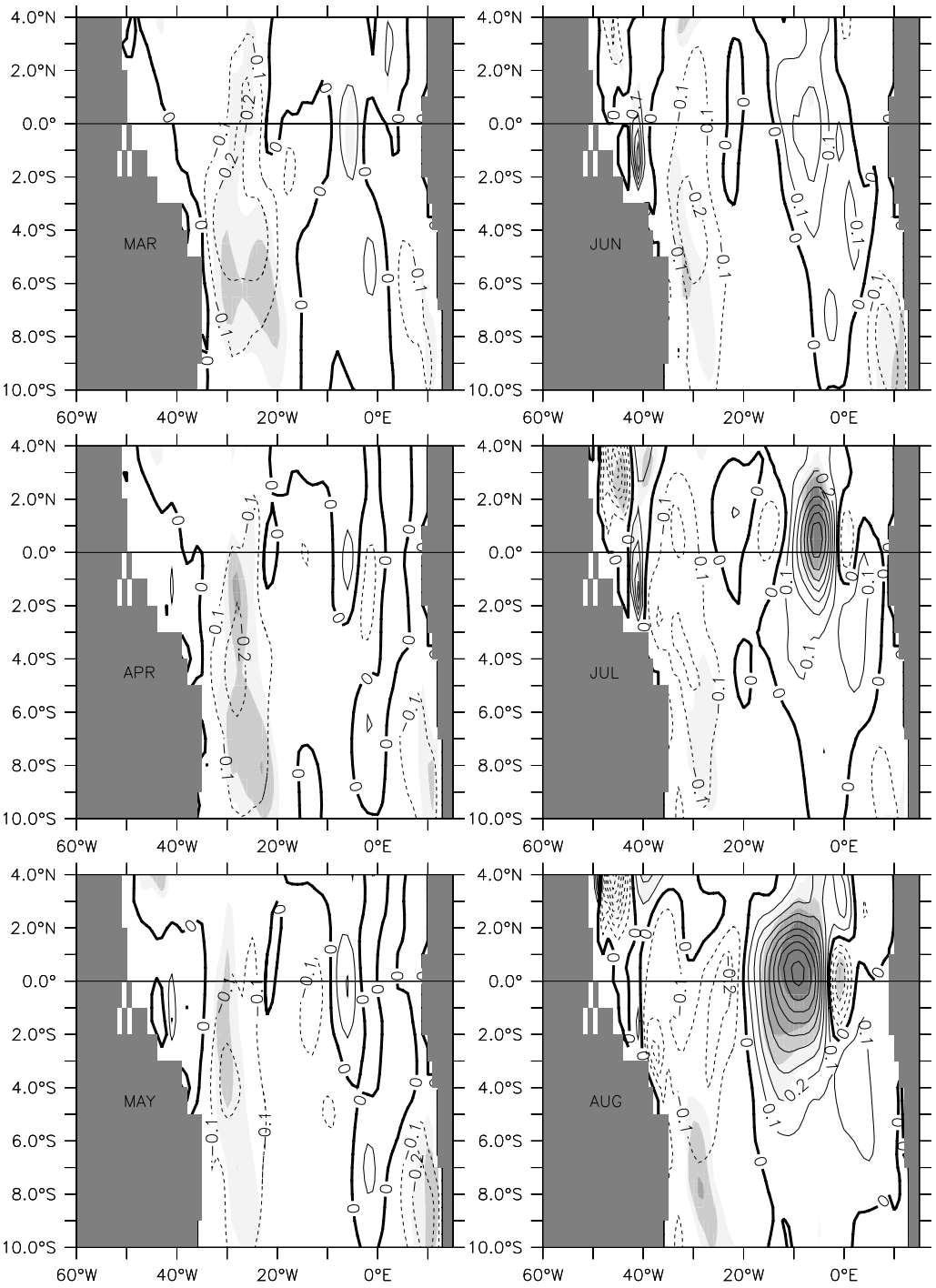

Fig. 4.11c. Same as Figure 4.11a except for advection by mean zonal currents.

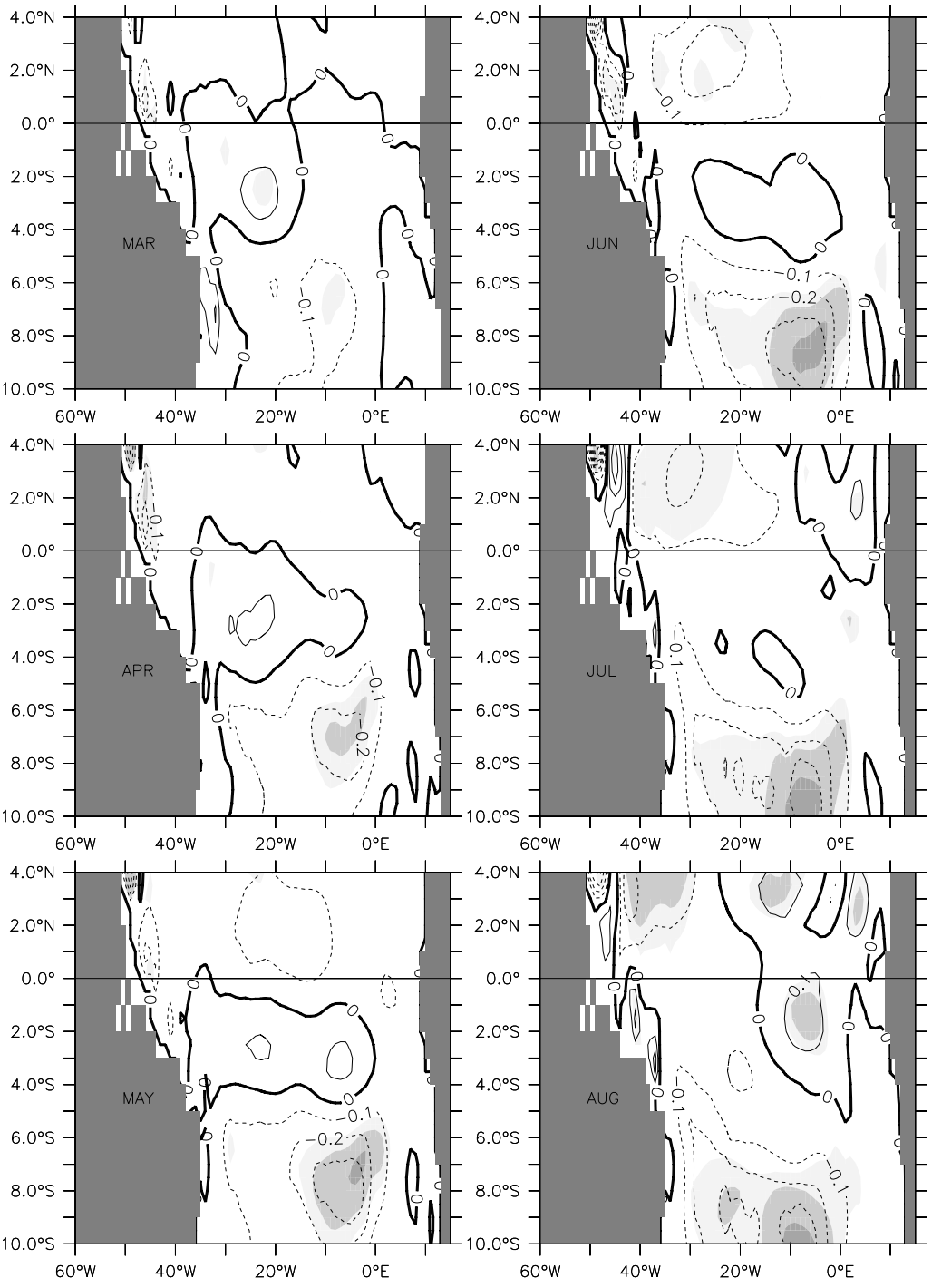

Fig. 4.11d. Same as Figure 4.11a except for advection by mean meridional currents.

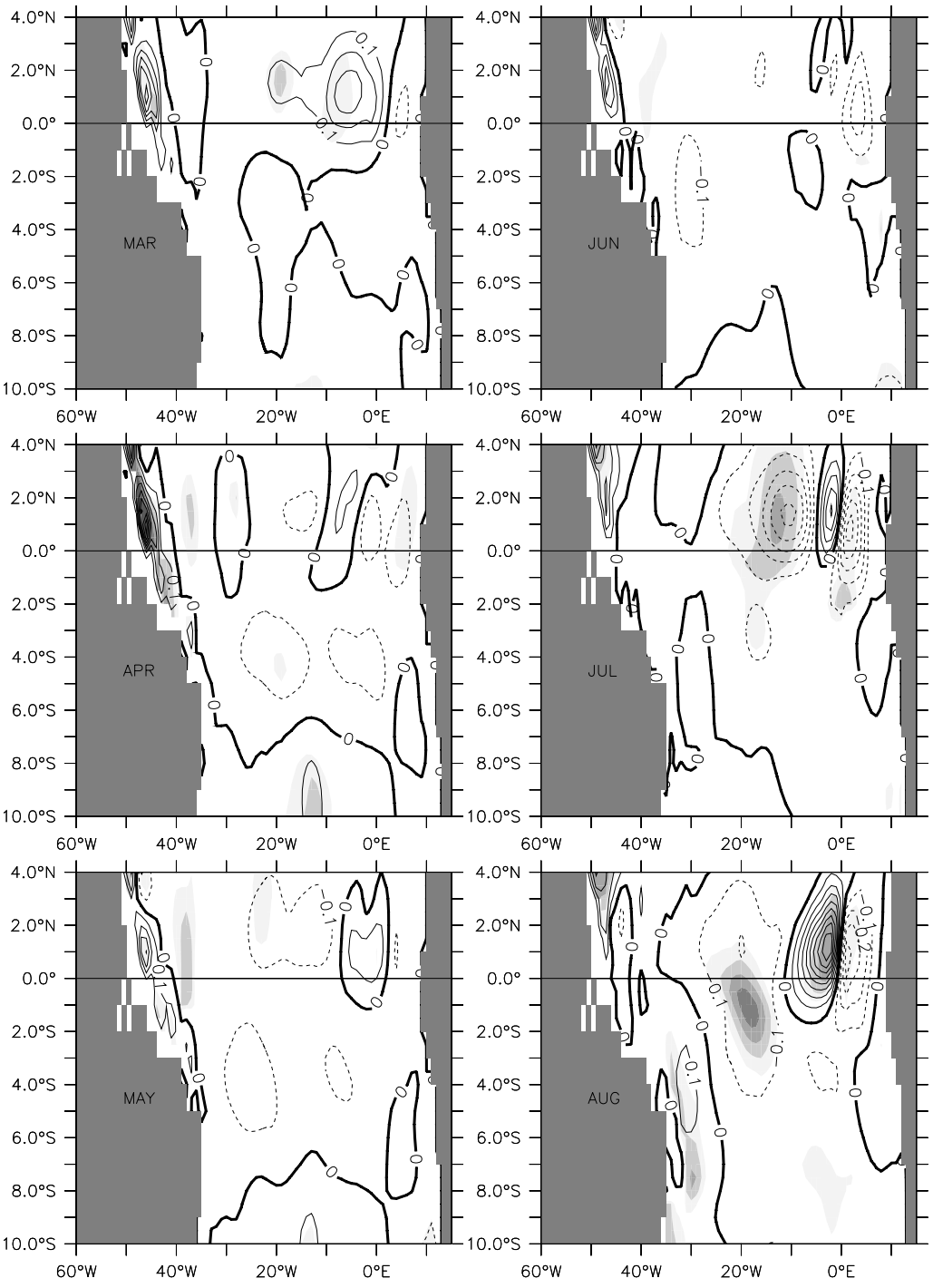

Fig. 4.11e. Same as Figure 4.11a except for advection by anomalous meridional currents.

c. The Role of Heat Flux in Boreal Spring

So far, attention has been given to the understanding of the evolution of the zonal mode in the experiments. Unlike the meridional mode, heat flux basically plays a role of damping SST anomaly in the zonal mode as shown in the previous section. However, there are some questions that need to be examined, for instance, why is the meridional mode in the CEXP different from the assimilation? In this section, we compare the role of heat flux in the ODA and CEXP by performing a similar analysis to Section 3.2. That is the evolution of the temperature anomaly due to net heat flux from ODA and CEXP is computed and regressed onto the respective spring PC1 time series.

Figure 4.12 shows regression maps for ODA (left panel) and CEXP (right panel). These maps indicate that in both ODA and CEXP during spring heat flux acts to enhance SST variability in the deep tropics and damps SST variability in the equatorial region. Note that the SST anomalies have an “apparent” migration towards the equator. Observation and coupled model results have shown a similar feature which has been taken as evidence of a positive feedback between wind-induced heat flux and SST, the so called WES feedback [*Chang et al.,* 1997; *Xie,* 1999].

There are, however, some interesting differences in the role played by the heat flux between the experiments. In the spring the intensity of the forcing in the ODA is much stronger than that in the CEXP, which helps to explain why the spring EOF of the CEXP does not capture very well the spatial pattern associated with the meridional mode. Another difference is that in the CEXP heat flux is strongly damping the SST anomaly south of the equator, while in the ODA the regression in the same area is not significant. This may indicate that in the 3-d flux corrected model, the ocean dynamics tend to generate “too much” SST variability so that the flux is trying to reduce it.

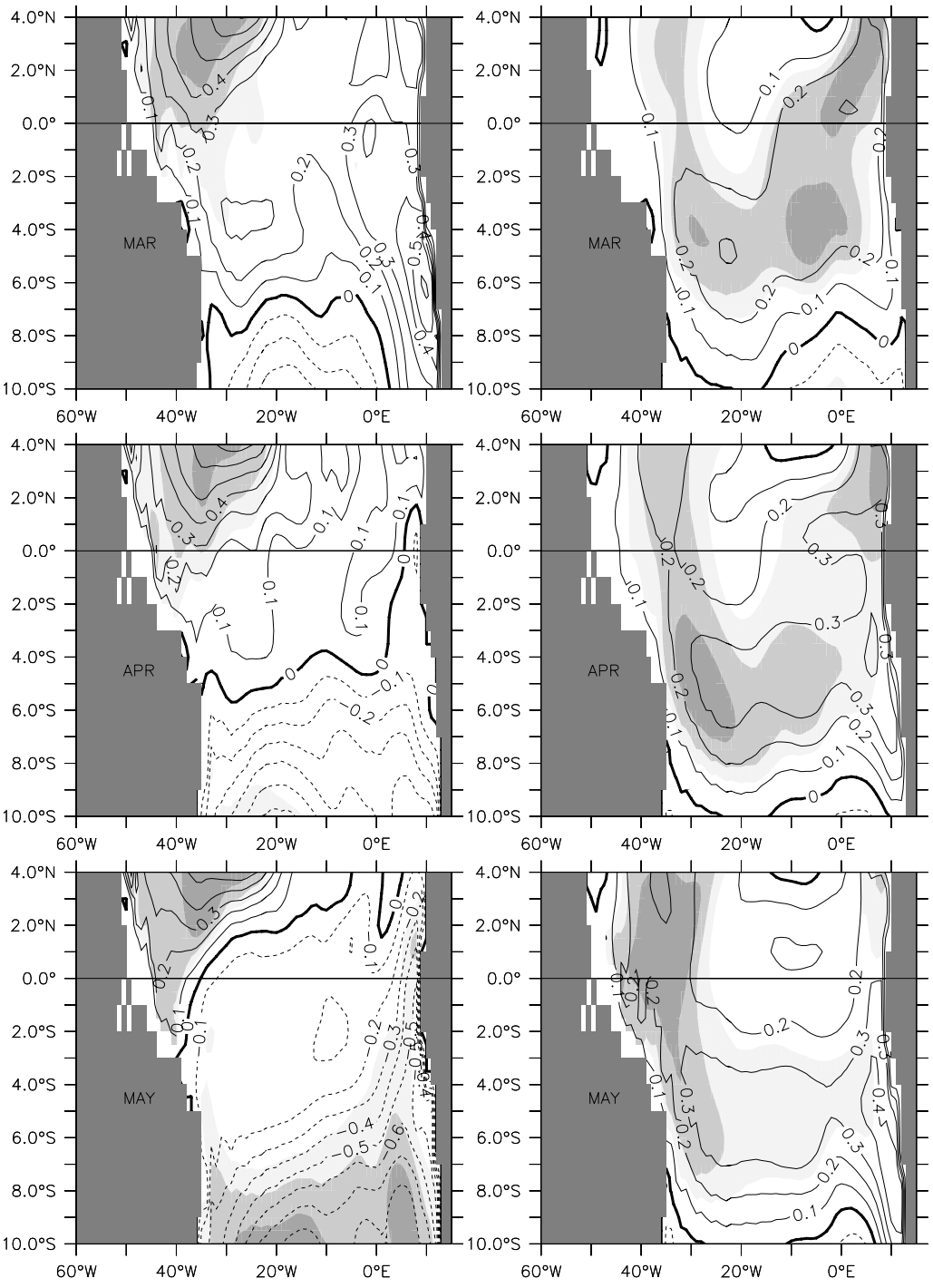

Fig. 4.12. The left panel represents temperature anomaly due to net heat flux from ODA regressed on ODA spring PC1. The right panel represents temperature anomaly due to net heat flux from CEXP regressed on CEXP spring PC1. Shaded areas denote the 95% significance level.

Another open issue which has been speculated on the previous section is the relationship between the zonal and the meridional modes. Although the high correlation between these two modes of variability seems to hold only for the period after the 80's [*Murtugudde et al.,* 2002], it is interesting to consider the potential mechanisms involved. Of particular interest is the spring to summer transition when the onset of the zonal mode coincides with the decay of meridional mode. To investigate the role played by the ocean dynamics in these seasons, the SST anomaly evolution given by each of the advective terms in equation (4.2) is computed using SM_WEXP experiment and then regressed onto the ODA spring PC1.

Figure 4.13 shows the regression maps for anomalous upwelling (left panels) and mean upwelling (right panels). Both anomalous and mean upwelling act to enhance SST variability south of 4^{o}N during spring, giving support to the assumption that the ODA spring EOF is partly forced by ocean dynamics, and that explains why even without heat flux the WEXP is able to capture some of the SST variability in this season (see Table 4.1). From March to May the anomalies generated by the anomalous upwelling term strengthen and the region of highest correlation shifts equatorward and westward. Although the anomalies associated with the mean upwelling also amplifies towards the end of the spring, there is not much evidence of propagation.

This result seems somewhat contradictory because modeling studies [*Chiang and Sobel,* 2002; *Sterl and Hazeleger,* 2003; *Seager et al.,* 2001] suggest that the role of the ocean in the tropical Atlantic is mainly damping, thereby providing a negative feedback to counteract the WES feedback. Thus, if upwelling is forcing the meridional gradient another mechanism should be responsible for the decay which occurs in the transition from spring to summer. According to recent numerical study by *Jochum et al.* [2004] nonlinear heat transport induced by Tropical Instability Waves (TIWs) can make a significant contribution to the mixed layer heat flux and may play a role of

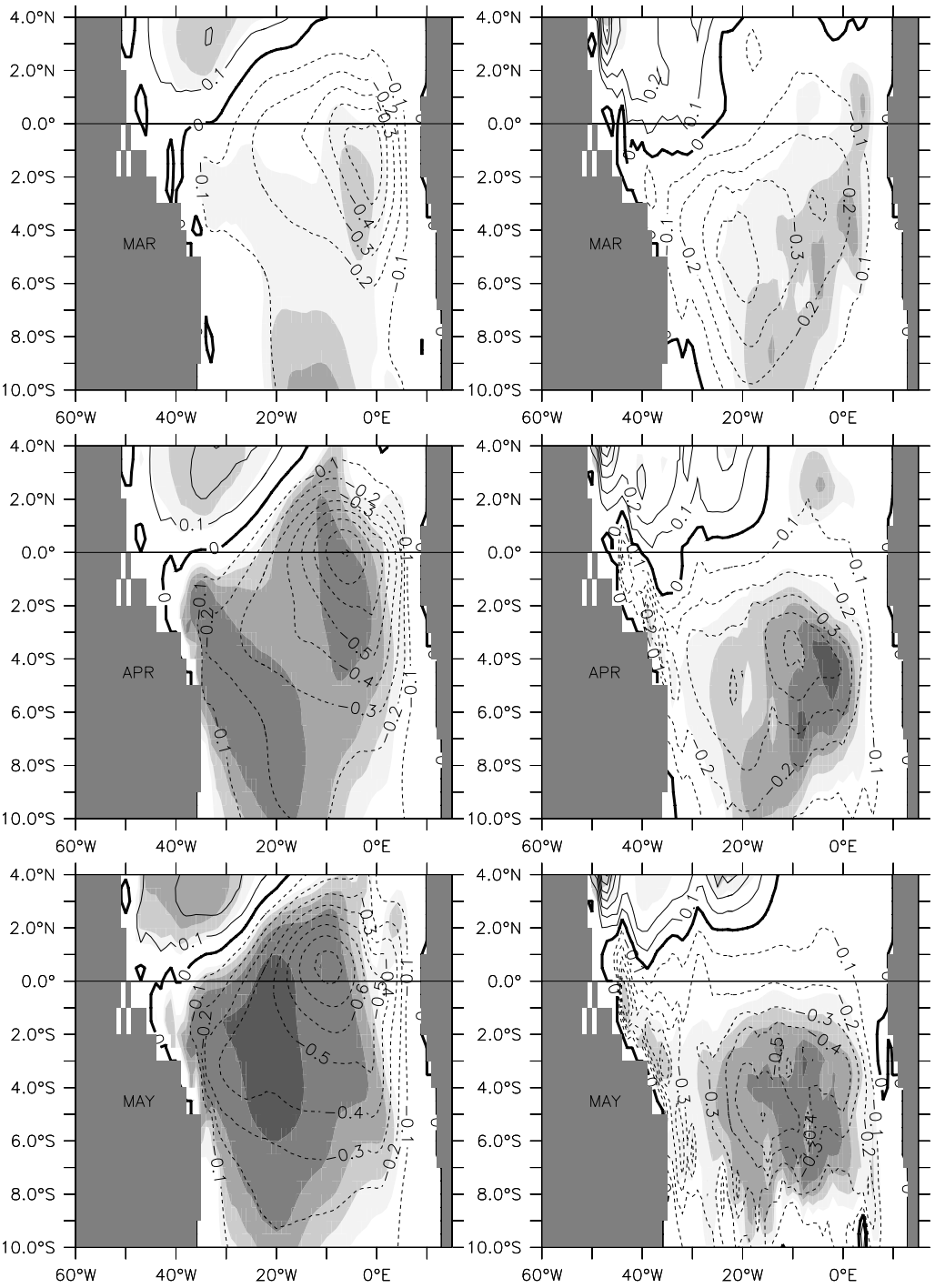

Fig. 4.13. Temperature anomaly due to anomalous upwelling (left panel) and mean upwelling (right panel) regressed on ODA spring PC1. Shaded areas denote the 95% significance level.

negative feedback to the meridional mode. They further suggest that the northward temperature gradient anomaly during boreal spring would lead to strong TIW activity (mainly from May to January), which in turn would lead to an enhanced southward heat flux, diffusing the initial northward temperature gradient. The 3-d flux corrected model used here does not have sufficient horizontal resolution to resolve nonlinear processes such as TIWs and the NBC and thus present low skill in reproducing the SST evolution in the regions where these processes are important (see Figs. 4.4a and 4.4b).

That been said, it is still necessary to formulate a plausible scenario in the framework of the model to explain the contribution of the upwelling terms to enhance the SST variability during the spring season that lead to the development of the zonal mode in the next season. Based on the results presented in this and previous sections we offer the following an explanation: The development of anomalous gradient begins during boreal winter/spring by WES feedback, this would be the favored mechanism since the weak entrainment and shallow mixed layer makes SST very sensitive to surface heat flux perturbations [*Chang et al*., 2004].

As spring progresses, the mixed layer starts to deepen and the spatially uniform warm climatological SST condition makes the winds very sensitive to perturbations in SST. These conditions are perfect for the development of an Ekman feedback, as described in the first section of this chapter, in which anomalous divergence of meridional winds reinforce the original gradient. Figure 4.13 tend to support this idea by showing that in March the correlation between the ODA spring PC1 and the anomalous upwelling term is more significant in the off equatorial region and in the following months gradually migrates towards the equator.

In the spring/summer transition, seasonal entrainment starts to increase and the thermocline to shallow. This ocean setting makes it highly favorable for dynamic interaction between the zonal wind and SST along the equator. At first

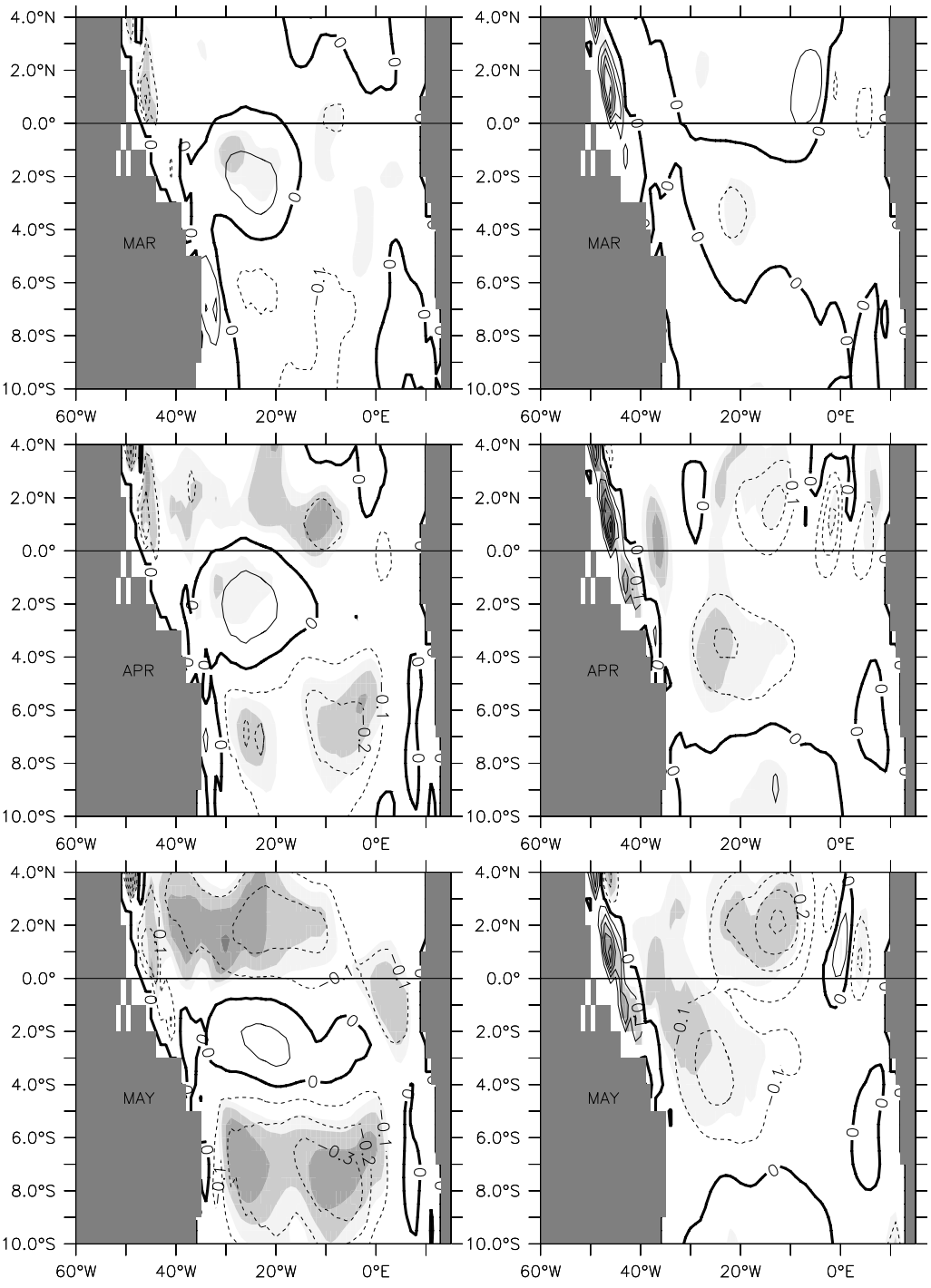

Fig. 4.14. Temperature anomaly due to advection by mean meridional currents (left panel) and anomalous meridional currents (right panel) regressed on ODA spring PC1. Shaded areas denote the 95% significance level.

this interaction primarily manifests itself as Ekman feedback in which the zonal winds are mainly responsible for the anomalous upwelling. Figures 4.11a, 4.13 and 4.14 show that the anomalous upwelling is not only the most important term forcing SST anomalies at the equator in April and May, but together with the advection by mean and anomalous meridional currents it also helps to damp SST anomalies in the northern equatorial region, contributing in this way to the decay of the meridional mode. As summer progresses, the thermocline reaches its shallowest position in July and August, and thus Bjerknes feedback appears to be more important. From Figure 4.11b, it is evident that SST anomalies associated with the mean upwelling term has strongest amplitude during this period.

4. Summary and Conclusions

The aim of this chapter was to elucidate key physical mechanisms by which the SST variability associated with the zonal mode may be driven. Based on two sets of OGCM experiments, analyses of the mixed layer heat budget in the tropical Atlantic were performed. The methodology used is somewhat novel in the sense that usually the terms of the temperature equation are computed during the model integration. However, that was not the case here and the output variables from the OGCM experiments were used to estimate the terms in the mixed layer heat budget and then to reconstruct the original temperature. Although this methodology is not perfect since it involves several assumptions and simplifications, it is shown that the reconstructed temperature is consistent, for the most part, with the SST variability of the original simulation, with the exception in the eastern tropical region close to the African coast. Where the OGCM is not able to reproduce very well the observed SST variability and the reconstructed temperature shows even large systematic error.

One key finding of this analysis is that both Bjerknes and Ekman feedbacks are important for the zonal mode. However, their relative importance is different in different regions and seasons. During the onset of the zonal mode, the largest contribution in the equatorial region comes from anomalous upwelling, primarily induced by the Ekman divergence of the zonal winds. The mean upwelling also contributes to forcing SST anomalies, but the largest contribution from this term comes during the peak phase (JJA) of the zonal mode in the southern equatorial region. Therefore, while Bjerknes feedback is the principal mechanism controlling the Pacific SST variability related to ENSO, both Bjerknes and Ekman feedback contribute to the evolution of the zonal mode in the Atlantic. Since Ekman feedback may also play a role in the seasonal onset of the cold tongue [*Mitchell and Wallace,* 1992; *Chang and Philander,* 1994], this may help explain why interannual variability in the Atlantic is more modulated by the annual cycle, as already suggested by *Chang et al.* [2004].

Comparison between ODA and CEXP reveals that the importance of the dynamical response is overestimated in the model, which may be caused by the simple treatment of surface heat flux forcing and by realistic physics of the model. This bias seems not to greatly affect the summer SST variability, except by the fact that SST anomalies in the CEXP is displaced further westward and southward than in the ODA. Although short lived, the WEXP is able to simulate seven of ten events in the assimilation, indicating that ocean dynamics in the model are important for SST variability in the region. More important though, the results suggest that the interplay between heat flux and ocean dynamics is very important in capturing the observed SST variability in the western equatorial region. *Chang et al.* [2001] have shown that the WES feedback is more efficient between the equator and 5^{o}N, and *Barreiro* [2003] shows that without ocean dynamics the WES feedback is exaggerated and the model tends to produce too much of a dipole like SST pattern (i.e., the gradient mode persists too long). The

results presented here indicate that without the heat fluxes ocean dynamics create SST variability that is too strong in the west side of the basin. Therefore, the two mechanisms tend to work together to give the right SST variability.

We have been able to show that the interannual mixed layer heat budget in the tropical Atlantic is a complicated one, with the relative importance of the different terms changing with season and region. However, our results are valid only for the equatorial region south of 4^{o}N and west of 0^{o}W. The eastern region along the African coast, a region of high SST variability (see Fig. 4.7), could not be addressed due to biases in the OGCM used in this study. This seems to be a very common problem in the current generation of OGCMs [*Chang et al.,* 1994], suggesting that the ocean processes controlling the SST variability in the equatorial region are still far from being completely understood. The few existent observational studies [e.g. *Foltz et al.,* 2003; *Weingartner and Weisberg,* 1991] reveal a quite complex scenario with eddy advection, vertical eddy diffusion, meridional advection and entrainment all playing roles in the mixed layer heat budget. Thus, to realistically simulate the SST variability in the eastern equatorial and cold tongue regions it might be necessary to improve vertical mixing schemes and rely on ocean models with higher vertical and horizontal resolutions.

CHAPTER V
SUMMARY AND OPEN ISSUES

1. Implications for Tropical Atlantic Variability

In the first part of this study we investigate the potential impact of the seasonal changes of the ITCZ on the exchange pathways of the northern tropical Atlantic. The results suggest that seasonal variation of the zonal slope of the thermal ridge along the boundary between the NECC and NEC in response to the seasonal variation of the ITCZ controls to a large extent the seasonal variation of the southward meridional transport towards the equator. The meridional southward flow has relatively high transports from July to September, when the zonal slope is well developed. Low transports occur from February to April when the zonal slope relaxes. More north Atlantic water flows into the equatorial region during the period when the total southward flow is strong. However, the time it takes for the water parcel to complete its journey varies from 9 month to 2 years. Thus, seasonal changes in the tropical circulation may modulate changes in the low-latitude stratification in interannual time scale.

Are such changes in the stratification capable of modulating TAV? Previous modeling studies indicate that ocean dynamics-induced SST changes are important only in the equatorial region (± 7^{o}) and in the two coastal zones off the coastal of Africa where the Guinea and Angola Domes reside [*Carton et al.,* 1996; *Carton and Zhou,* 1997]. Within the two former areas it is likely that waters from the northern subtropics will return to the surface and interact with the atmosphere. Although the equatorial thermocline is fed predominantly from the south, the changes in the northern tropical circulation have potential to cause a relatively large impact in the low latitude stratification since the circulation in the Southern Hemisphere is nearly steady [*Stramma et al,* 2003].

North Atlantic Deep Water (NADW) is formed in high latitudes of the Atlantic Ocean and exported southward into the Southern Ocean. The loss of NADW from the basin is compensated by the northward inflow of warm thermocline and intermediate waters across the equator. This so-called Meridional Overturning Circulation (MOC) return flow interacts with the low latitude wind-driven circulation and water mass transformations. *Fratantoni et al.* [2000] investigate the pathways of the MOC return flow and its effect on the wind driven circulation. Their results show that due to the presence of the MOC, the equatorward thermocline transport is highly nonsymmetrical with mass being supplied mostly from the south through the NBC retroflection. In the pure wind driven circulation case water is supplied in almost equal amount by both hemispheres, with a southward western boundary current being responsible for most of the transport from the north.

Thus, it is valid to wonder if seasonal changes in the wind driven circulation can affect the pathways of the MOC return flow. Since the integrated northward transport along 15^{o}N is relatively steady [*Philander and Pacanowski*, 1986], the seasonal changes in wind driven circulation are more likely to have a impact in the partition of the return flow among the pathways: surface and intermediate layers, interior and western boundary. The results presented in Chapter III indicate that southward flow of thermocline water coincides with the period of minimum northward heat flow at surface layer. Therefore, to maintain the relatively steady northward heat transport the northward intermediate flow should increase to accommodate the changes in the upper layers.

In terms of predictability, the work developed in the first part of this thesis is similar to research studies that try to understand ocean dynamics and its role in establishing the ocean mean state in order to improve ocean models and build simulation system capable of improving skill of climate models. Only with an OGCM capable of simulating realistically both the wind driven and the MOC circulations, the coupled climate model will be able to understand the

implications of the changes of ocean circulation in the regional climate variability at seasonal to interannual timescales, as well as the role of the tropical Atlantic in the global oceanic heat budget that is crucial for our understanding of long-term climate variability.

Although, seasonal and intraseasonal (not addressed in this work) ocean variability are important in explaining some features of the large scale circulation it remains to be determined how much of an impact they may have on TAV. It will be also interesting to compare the results presented in Chapter III with other ocean data assimilation systems and models forced with different wind stress forcing. Since *Inui et al.* [2002] have shown that the exchange pathways between tropics and subtropics are sensitive to the choice of wind stress product.

The aim of the second part of this study was to elucidate the physical mechanisms by which wind-driven ocean dynamics cause interannual variability in the equatorial Atlantic. In particular, we focused on the mechanisms at work during onset and mature phases of the zonal mode. Previous observational and modeling studies have suggested that SST variability associated with the Atlantic zonal mode, in contrast to the SST variability associated with Pacific ENSO, does not rely only on subsurface temperature changes induced by thermocline variability. Our results tend to confirm these earlier findings by indicating that both Bjerknes and Ekman feedbacks act together to force the zonal mode, although their relative importance and dominance depend on season and location.

During the onset of the zonal mode (AM) SST anomalies in the central equatorial Atlantic are mainly forced by anomalous upwelling acting in the mean vertical stratification. The anomalous upwelling is driven by local Ekman divergence of zonal winds and does not involve thermocline displacement. In the mature phase of the zonal mode (JJ), mean upwelling acting on the anomalous stratification is the largest term in generating SST anomalies in the eastern

equatorial region south of the equator. During this period the coupling between surface winds and SST requires thermocline changes similar to those involved in ENSO.

If these modeling results hold, it would mean that the predictable dynamics of the Atlantic zonal mode depend on a surface as well as a subsurface memory mechanism. This has mixed implications for the forecasting of TAV. On the positive side, the identification of the specific ocean processes required in the prediction of SST anomalies would lead to a more intensified effort to develop correction and assimilation schemes to maximally extract the information in the ocean. Results by *Barreiro* [2003] show that the SST and precipitation predictive skill of an AGCM coupled with slab ocean is improved when ocean dynamics are introduced through a statistical correction.

On the negative side, the fact that for most of the events analyzed here the onset of SST anomalies is driven by local Ekman feedback means that the memory of these climate anomalies may be short. Therefore, the potential for forecasting these events is relatively low since the response of the surface currents to the wind forcing is shorter than that associated with the propagation speeds of planetary waves, as required in the Bjerknes feedback. *Seidel et al.* [2005b] recently carried out sets of prediction experiments using an OGCM model coupled to a statistical atmosphere for the period from 1980 to 1999. Their results show that the predicted SSTs in the equatorial region have correlation skill higher than 0.4 for lead time up to six months. Since the model has no skill to simulate thermocline depth in this region, it is suggested that the limited model skill does not come from subsurface ocean dynamics. This notion is further supported by the findings that experiments with correcting subsurface temperature biases do not lead to any significant improvement in predictive skill.

On the other hand, the link between zonal and meridional mode may lead to an enhanced forecast potential because if in boreal spring the tropical Atlantic is evolving to a positive meridional gradient, negative SST anomalies in the

equatorial region associated with the zonal mode would be expected in boreal summer, and vice-versa. However, as mentioned in the previous chapter, observational [*Murtugudde et al.,* 2002] and modeling results [*Fang,* 2005, personal communication] suggest that the connection between zonal and meridional modes is stronger in some decades and weaker in others. The potential for predictability will depend also in finding a robust precursor to allow advanced-lead prediction.

As final remark we would like to point out the need for observational studies in the equatorial region to validate the model results and to establish the main ocean processes necessary to improve model physics in the problematic regions. Concentrated efforts should be placed in the boreal spring to summer transition when ocean dynamics play a crucial role in TAV. Of particular interest is to quantify the relative importance of anomalous versus mean upwelling in the mixed layer heat budget, to quantify the roles of mesoscale features and vertical turbulent diffusion in the eastern equatorial and cold tongue regions.

REFERENCES

Barreiro, M., Understanding seasonal climate predictability in the Atlantic sector, Ph.D. dissertation, Texas A&M University, College Station, 2003.

Bjerknes, J., Atmospheric teleconnections from the equatorial Pacific. *Mon. Weather Rev., 97,* 163-172, 1969.

Bryan, K., and L. J. Lewis, A water mass model of the world ocean, *J. Geophys. Res.*, *84*, 2503-2517, 1979.

Bryden, H. L., and E. C. Brady, Diagnostic model of the three-dimensional circulation in the upper equatorial Pacific Ocean, *J. Phys. Oceanogr., 15,* 1255-12773, 1985.

Cabosnarvaez, W., F. A. García, and M. J. Ortizbeviá, Generation of equatorial Atlantic warm and cold events in a coupled general circulation model simulation, *Tellus, 54A,* 426-438, 2002.

Carton, J.A., and B. Huang, Warm events in the tropical Atlantic, *J. Phys. Oceanogr., 24,* 888-903, 1994.

Carton, J.A., and Z.X. Zhou, Annual cycle of sea surface temperature in the tropical Atlantic Ocean, *J. Geophys. Res., 102,* 27,813-27,824, 1997.

Carton, J.A., X. Cao, B.S. Giese, and A.M. da Silva, Decadal and interannual SST variability in the tropical Atlantic Ocean. *J. Phys. Oceanogr., 26,* 1165-1175, 1996.

Chang, P., and S. G. H. Philander, Rossby wave packets in baroclinic currents, *Deep Sea Res., 36,* 17-37, 1988.

Chang, P., and S. G. H. Philander, A coupled ocean-atmosphere instability of relevance to the seasonal cycle*, J. Atmos. Sci., 51,* 3627-3648, 1994.

Chang, P., L. Ji, and H. Li, A decadal climate variation in the tropical Atlantic Ocean from thermodynamic air-sea interactions, *Nature, 385,* 516-518, 1997.

Chang, P., L. Ji, and H. Li, A hybrid coupled model study of the tropical Atlantic variability, *J. Clim., 14,* 361-390, 2001.

Chang, P., R. Saravanan, L. Ji, and G. C. Hegerl, The effects of local sea

surface temperatures on atmospheric circulation over the tropical Atlantic sector. *J. Clim., 13,* 2195-2216, 2000.

Chang, P., T. Yamagata, P. Schopf, S. K. Behera, J. Carton, W. S. Kessler, W. S. Kessler, G. Meyers, T. Qu, F. Schott, S. Shetye, and S.-P. Xie, Climate fluctuations of tropical coupled system - the role of ocean dynamics, *J. Clim.* (*submitted*), 2004.

Chelton, D. B., and M. G. Schlax, Global observations of oceanic Rossby waves, *Science, 272,* 234-238, 1996.

Chiang, J. C. H., and A. H. Sobel, Tropical tropospheric temperature variations caused by ENSO and their influence on the remote tropical climate. *J. Clim., 15,* 2616-2631, 2002.

Da Silva, M., and P. Chang, Seasonal variation of the subtropical/tropical pathways in the Atlantic Ocean from an ocean data assimilation experiment, in *Earth Climate: The Ocean-Atmosphere Interaction*, Geophys. Monogr. Ser., edited by C. Wang, S.-P. Xie and J. A. Carton, pp. 305-318, AGU, Washington, D. C., 2004.

Delecluse, P., J. Servain, C. Levy, K. Arpe, and L. Bengtsson, On the connection between the 1984 Atlantic warm event and the 1982-83 ENSO, *Tellus, 46A,* 448-464, 1994.

Derber, J., and A. Rosati, A global oceanic data assimilation system. *J. Phys. Oceanogr.,19,* 1333-1347, 1989.

Dommenget, D., and M. Latif, Interannual to decadal variability in the tropical Atlantic, *J. Clim., 13,* 777-792, 2000.

Foltz, G. R., S. A. Grodsky, J. A. Carton, and M. J. McPhaden, Seasonal mixed layer heat budget of the tropical Atlantic Ocean, *J. Geophys. Res., 108*(C5), 15,1-15,13, 2003.

Fratantoni, D. M., W. E. Johns, T. L. Townsend, and H. E. Hulburt, Low-latitude circulation and mass transport pathways in a model of the tropical Atlantic ocean, *J. Phys. Oceanogr., 3,* 1944-1966, 2000.

Galanti, E., E. Tziperman, M. Harrison, A. Rosati, and Z. Sirkes, A study of ENSO prediction using a hybrid coupled model and the adjoint method for data assimilation, *Mon. Weather Rev., 131*(11)*,* 2748-2764, 2003.

Garzoli, S. L., and E. J. Katz, The forced annual reversal of the Atlantic north equatorial countercurrent, *J. Phys. Oceanogr., 13,* 2082-2090, 1983.

Gent, P. R., and J. C. McWilliams, Isopycnal mixing in ocean circulation models, *J. Phys. Oceanogr., 20,* 150-155, 1990.

Giannini, A., Y. Kushnir, and M. A. Cane, Interannual variability of Caribbean rainfall, ENSO, and the Atlantic Ocean, *J. Clim., 13,* 297-311, 2000.

Harper, S., Thermocline ventilation and pathways of tropical-subtropical water mass exchange, *Tellus, 52A,* 330-345, 2000.

Hazeleger, W., P. de Fries, and Y. Fiocourt, Sources of the equatorial undercurrent in the Atlantic in a high resolution ocean model, *J. Phys. Oceanogr., 33,* 677-693, 2003.

Hisard, P., Observation de réponses de type « El Niño » dans l'Atlantique tropical oriental, Golfe de Guinée, *Oceanol. Act, 3,* 1,69-1,78, 1980.

Hisard, P., and C. Hénin, Response of equatorial Atlantic Ocean to the 1983-1984 wind from the Programme Français Océan et Climat Dans l'Atlantique Equatorial Cruise dataset, *J. Geophys. Res., 92*, 3759-3768, 1987.

Huang, B., and J. Shukla, Characteristics of the interannual and decadal variability in a general circulation model of the tropical Atlantic Ocean, *J. Phys. Oceanogr., 27,* 1693-1712, 1997.

Inui, T., P. Malanotte-Rizzoli, and A. Busalacchi, Wind stress effects on the Atlantic subtropical-tropical circulation, *J. Phys. Oceanogr., 32,* 2257-2276, 2002.

Jin, F.-F., J.-S. Kug, S.-I. An, and I.-S. Kang, A near-annual coupled ocean-atmosphere mode in the equatorial Pacific Ocean, *Geophys. Res. Lett., 30,* 52,1-52,4, 2003.

Jochum, M., and P. Malanotte-Rizzoli, Influence of the meridional overturning circulation on tropical/subtropical pathways, *J. Phys. Oceanogr., 31,* 1313-1323, 2001.

Jochum, M., P. Malanotte-Rizzoli, and A. Busalacchi, Tropical instability waves in the Atlantic Ocean, *Ocean Modelling, 7,* 145-163, 2004.

Johns, W. E., T. N. Lee, R. C. Beardsley, J. Candela, R. Limeburner, and B. Castro, Annual cycle and variability of the North Brazil current, *J. Phys. Oceanogr., 28,* 103-128, 1998.

Katz, E. J., Seasonal response of the sea surface to the wind in the equatorial Atlantic, *J. Geophys. Res., 92,* 1885-1893, 1987.

Kessler, W. S., Interannual variability of the subsurface high salinity tongue south of the equator at 165^{o}E, *J. Phys. Oceanogr., 29,* 2038-2049, 1999.

Kessler, W. S., and J. P. McCreary, Observations of long Rossby wave in the nothern tropical Pacific, *J. Geophys. Res., 95,* 5183-5217, 1990.

Köberle, C., and S. G. H. Philander, On the processes that control seasonal variations of sea surface temperatures in the tropical Pacific Ocean, *Tellus, 46A,* 481-496, 1994.

Lazar, A., T. Inui, A. J. Busalacchi, P. Malanotte-Rizzoli, and L. Wang, Seasonality of the ventilation of the tropical Atlantic thermocline, *J. Geophys. Res., 107,* 18,1-18,17, 2002.

Levitus, S., and T. Boyer, World ocean atlas 1994, Vol. 4: Temperature, *NOAA Atlas NESDIS 4,* 117pp., U.S. Gov. Print. Off., Washington, D.C., 1994.

Liu, Z., A simple model of the mass exchange between the subtropical and tropical ocean, *J. Phys. Oceanogr., 24,* 1153-1165, 1994.

Liu, Z., and S. G. H. Philander, How different wind stress patterns affect the tropical-subtropical circulations of the upper ocean, *J. Phys. Oceanogr., 25,* 449-462, 1995.

Liu, Z., S. G. H. Philander, and R. Pacanowski, A GCM study of tropical-subtropical upper-ocean exchange, *J. Phys. Oceanogr., 24,* 2606-2623, 1994.

Lu, P., and J. P. McCreary, Influence of the ITCZ on the flow of thermohaline water from the subtropical to the equatorial Pacific Ocean, *J. Phys. Oceanogr., 25,* 3076-3088, 1995.

Lux, M., H. Mercier, and M. Arhan, Interhemispheric exchanges of mass and heat in the Atlantic Ocean in January-March 1993, *Deep Sea Res., 48,* 605-638, 2000.

Luyten, J. R., J. Pedlosky, and H. Stommel, The ventilated thermocline, *J. Phys. Oceanogr., 13,* 292-309, 1983.

Malanotte-Rizzoli, P. , K. Hedstrom, H. Arango and D. B. Haidvogel, Water mass pathways between the subtropical and tropical ocean in a climatological simulation of the North Atlantic ocean circulation, *Dyn. Atmos. Oceans, 32,* 331-371, 2000.

McCreary, J. P., and P. Lu, On the interaction between the subtropical and equatorial ocean circulation: the subtropical cell, *J. Phys. Oceanogr., 24,* 466-497, 1994.

Merle, J., Variabilité thermique annuelle et interannuelle de l'océan Atlantique équatorial Est. L'hypothèse d'un « El Niño » Atlantique, *Oceanol. Acta, 3,* 2,209-2,220, 1980.

Metcalf, W. G., and M. C. Stalcup, Origin of the Atlantic equatorial undercurrent, *J. Geophys. Res., 72,* 4959-4875, 1967.

Meyers, G., On the annual Rossby wave in the tropical North Pacific Ocean, *J. Phys. Oceanogr., 9,* 885-891, 1979.

Mitchell, T.P., and J.M. Wallace, The annual cycle in equatorial convection and sea surface temperature. *J. Clim., 10,* 1140-1156, 1992.

Monterey, G, and S. Levitus, Seasonal variability of mixed layer depth for the world ocean, *NOAA Atlas NESDIS 14,* 96pp., U.S. Gov. Print. Off., Washington, D.C., 1997.

Murtugudde, R., J. Ballabrera, J. Beauchamp, and A. Busalacchi, Relationship between zonal and meridional modes in the tropical Atlantic, *Geophys. Res. Lett., 22,* 4463-4466, 2002.

Neelin, J. D., D. S. Battisit, A. C. Hirst, F.-F. Jin, Y. Wakata, T. Yamagata, and S. E. Zebiak, ENSO theory, *J. Geophys. Res., 103,* 14,261-14,290, 1998.

Nobre, P., and J. Shukla, Variations of sea surface temperature, wind stress, and rainfall over the tropical Atlantic and South America, *J. Clim., 9,* 2464-2479, 1996.

O'Connor, B. M., Formation rates of subtropical underwater in the Pacific Ocean, *Deep Sea Res. Part I, 49,* 1571-1590, 2002.

Pacanowski, R. C., MOM 3.0 Manual, *The GFDL Ocean Group Technical Report,* 668 pp, Geophysical Fluid Dynamics Laboratory, Princeton, N. J., 1999.

Pedlosky, J., An inertial theory of the equatorial undercurrent, *J. Phys. Oceanogr., 17,* 1978-1985, 1987.

Philander, S. G. H., Oceanic adjustment: I, in *El Niño, La Niña, and the Southern Oscillation*, edited by R. Dmowska and J. R. Holton, pp. 103-157, Academic Press, London, 1990.

Philander, S. G. H., and R. C. Pacanowski, A model of the seasonal cycle in the tropical Atlantic Ocean, *J. Geophys. Res., 91,* 14,192-14,206, 1986.

Richardson, P. L., S. Arnault, S. Garzoli, and J. G. Bruce, Annual cycle of the Atlantic north equatorial countercurrent, *Deep Sea Res., 39,* 997-1014, 1992.

Rothstein, L. M., R. -H. Zhang, A. J. Busalacchi, and D. Chen, A numerical simulation of the mean water pathways in the subtropical and tropical Pacific Ocean, *J. Phys. Oceanogr., 11,* 794-812, 1998.

Schmitz, W. J., Jr., and M. S. McCartney, On the North Atlantic circulation, *Rev. Geophys., 31,* 29-49, 1993.

Schott, F. A., J. Fischer, and L. Stramma, Transports and pathways of the upper-layer circulation in the western tropical, *J. Phys. Oceanogr., 28,* 1904-1928, 1998.

Schott, F. A., J. Fischer, J. Reppin, and U. Send, On mean and seasonal currents and transports at the western boundary of the equatorial Atlantic, *J. Geophys. Res., 98,* 14,353-14,368, 1993.

Seager, R., Y. Kushnir, P. Chang, N. Naik, J. Miller, and W. Hazeleger, Looking for the role of the ocean in tropical Atlantic decadal climate variability, *J. Climate, 14,* 638-655, 2001.

Seidel, H. F., P. Chang, and S. Zebiak, A method for correcting the mean state of ocean general circulation models, *J. Clim.,* (submitted), 2005a.

Seidel, H. F., P. Chang, R. Saravanan, and D. Dewitt, A study of tropical Atlantic variability with a high-resolution regional coupled climate model, in *Proceedings of U. S. CLIVAR Atlantic Conference*, 2005b. (Available at http://www.usclivar.org/Atl05_agenda.html)

Servain, J., and S. Arnault, On forecasting abnormal climatic events in the tropical Atlantic Ocean, *Ann. Geophysicae, 13,* 995-1008, 1995.

Servain, J., I Wainer, H. L. Ayina and H. Roquet, The relationship between the

simulated climatic variability modes of the tropical Atlantic. *Int. J. Climatol., 20,* 939-953, 2000.

Smagorinsky, J., Some historical remarks on the use of nonlinear viscosities, in *Large Eddy Simulation of Complex Engineering and Geophysical Flows*, edited by B. Galperin and S. A. Orszag, pp 3-36, Cambridge University Press, New York, 1993.

Sterl, A. and W. Hazeleger, Coupled variability and air-sea interaction in the South Atlantic Ocean. *Climate Dyn., 21,* 559-571, 2003.

Stevenson, J. W., and P. P. Niiler, Upper ocean heat budget during Hawaii-to-Tahiti shuttle experiment, *J. Phys. Oceanogr., 13,* 1894-1907, 1983.

Stramma, L., and F. A. Schott, The mean flow field of the tropical Atlantic ocean, *Deep Sea Res.II, 46,* 279-303, 1999.

Stramma, L., J. Fischer, P. Brandt, and F. Schott, Circulation, variability and near-equatorial meridional flow in the central tropical Atlantic, in *Interhemispheric Water Exchange in the Atlantic Ocean*, *Elsevier Oceanographic Ser*. *68*, edited by G. Goni, and P. Malanotte-Rizzoli, pp. 1-22, 2003.

Weingartner, T. J., and R. H. Weisberg, On the annual cycle in sea surface temperature and upper ocean heat in the equatorial Atlantic, *J. Phys. Oceanogr., 21,* 83-96, 1991.

White, W. B., Design of a global observing system for gyre-scale upper ocean temperature variability, *Prog. Oceanogr., 36,* 169-217, 1995.

Vauclair, F. and Y. du Penhoat, Interannual variability of the upper layer of the tropical Atlantic Ocean from in situ data between 1979 and 1999, *Climate Dyn., 17,* 527-546, 2001.

Xie, S.-P., A dynamic ocean-atmosphere model of the tropical Atlantic decadal variability. *J. Clim., 12,* 64-70, 1999.

Yamagata, T., and S. Iizuka, Simulation of the tropical thermal domes in the Atlantic: a seasonal cycle, *J. Phys. Oceanogr., 25,* 2129-2140, 1995.

Zebiak, S. E., Air-sea interaction in the equatorial Atlantic region, *J. Climate, 6,* 1567-158, 1993.

Zebiak, S. E., and M. A. Cane, A model El Nino-Southern Oscillation, *Mon. Weather Rev., 115,* 2262-2278, 1987.

APPENDIX A
HEAT BUDGET ANALYSIS

The mixed layer temperature equation under the assumptions of vertically uniform mixed layer, incompressibility ($\nabla \cdot U = 0$) can be written as:

$$\frac{\partial T}{\partial t} + \frac{\partial}{\partial x}(uT) + \frac{\partial}{\partial y}(vT) + \frac{\partial}{\partial z}(wT) = K\nabla^2 T + \frac{\partial}{\partial z}(K_v \frac{\partial T}{\partial z}) \quad \text{(A.1)}$$

Vertically integrating (A1) from $z = 0$ to $z = -h_{mix}(x, y, t)$, where h_{mix} is the depth of the mixed layer, gives

$$h_{mix}\frac{\partial T}{\partial t} + h_{mix}\left(\frac{\partial}{\partial x}(uT) + \frac{\partial}{\partial y}(vT)\right) + wT_{(0)} - wT_{(-h_{mix})} = h_{mix}K\nabla^2 T + K_v \frac{\partial T}{\partial z}_{(0)} - K_v \frac{\partial T}{\partial z}_{(-h_{mix})} \quad \text{(A.2)}$$

Let the surface radiative and turbulent heat flux be Q, then

$$-wT_{(0)} + K_v \frac{\partial T}{\partial z}_{(0)} = Q \big/ Cp\rho_0 ,$$

where C_p is the thermal expansion coefficient and ρ_0 is the density of seawater. Therefore, (A.2) becomes:

$$h_{mix}\frac{\partial T}{\partial t} + h_{mix}\left(\frac{\partial}{\partial x}(uT) + \frac{\partial}{\partial y}(vT)\right) - wT_{(-h_{mix})} = \frac{Q}{\rho_0 C_p} - K_v \frac{\partial T}{\partial z}_{(-h_{mix})} + h_{mix}K\nabla^2 T$$

or

$$\frac{\partial T}{\partial t}+\frac{\partial}{\partial x}(uT)+\frac{\partial}{\partial y}(vT)-\frac{wT_{(-h_{mix})}}{h_{mix}}=\frac{Q}{\rho_0 C_p h_{mix}}-K_v\frac{\overline{\partial T}}{\partial z}_{(-h_{mix})}+K\nabla^2 T \quad \text{(A.3)}$$

Let $wT_{(-h_{mix})}-K_v\frac{\partial T}{\partial z}_{(-h_{mix})}=w_e H(w_e)(T-T_{sub})$, where H(x) is the Heaviside step function (H(x) = 1 if x > 0, H(x) =0 if x < 0); w_e represents the entrainment velocity at the base of the mixed layer; and T_{sub} is the temperature of entrained water beneath the base of the mixed layer. Then (A.3) becomes:

$$\frac{\partial T}{\partial t}+\frac{\partial}{\partial x}(uT)+\frac{\partial}{\partial y}(vT)-w_e H(w_e)\frac{T-T_{sub}}{h_{mix}}=\frac{Q}{\rho_0 C_p h_{mix}}+K\nabla^2 T \quad \text{(A.4)}$$

The terms in (A.4) represent from left to right the temperature tendency; zonal and meridional advection; entrainment cooling across the base of the mixed layer; the net surface flux into the mixed layer and horizontal diffusion.

Usually, to perform the mixed layer heat budget the terms in (A.4) are computed during the model integration. Unfortunately, this was not the case for the CEXP and WEXP. Therefore the alternative method described below was used to estimate the terms in (A.4) from the above experiments. Using u, v, w_e, h_{mix}, T_{sub}, and Q from CEXP and WEXP averaged over the mixed layer, given K and initial T = T_0, the equation (A.4) was integrated to find temperature T. The equation (A.4) was solved numerically using a leap-frog scheme with a time step Δt = 8 days and spatial resolution Δx = 1°, Δy = 0.5°. The following relaxation term of the surface heat is added:

$$Q_{rel}=dQ/dT(T_{MOD}-T_{EXP}),$$

where T_{EXP} is the CEXP or WEXP mean SST and T_{MOD} is the model SST. Here dQ/dT is set -35 W m^{-2} K. This term correct for systematic errors introduced in the formulation of the simple model. During integration monthly mean of each term in (A.4) is saved for posterior heat budget analysis.

VITA

Meyre P. Da Silva was born in Campo Grande, Brazil, on April 4, 1967. She received her B.S. degree in oceanography in 1990 from Fundação Universidade do R. Grande, and her M.S. degree in physical oceanography in 1995 at Instituto Oceanográfico da Universidade de São Paulo, both in Brazil. From 1996 to 1998 she worked at Fundação Universidade do R. Grande as Research Associate. In 1999 she started her Ph.D program in oceanography at Texas A&M University. She graduated in May 2005.

She can be reached at R. Arthur Jorge 198, Campo Grande, MS, 79002-440, Brazil.